T-1238

ELECTRICAL RESISTIVITY AND HALL-EFFECT IN GOLD DITELLURIDE

By

Millard M. Judy

ProQuest Number: 10795970

All rights reserved

INFORMATION TO ALL USERS
The quality of this reproduction is dependent upon the quality of the copy submitted.

In the unlikely event that the author did not send a complete manuscript
and there are missing pages, these will be noted. Also, if material had to be removed,
a note will indicate the deletion.

ProQuest 10795970

Published by ProQuest LLC (2019). Copyright of the Dissertation is held by the Author.

All rights reserved.
This work is protected against unauthorized copying under Title 17, United States Code
Microform Edition © ProQuest LLC.

ProQuest LLC.
789 East Eisenhower Parkway
P.O. Box 1346
Ann Arbor, MI 48106 – 1346

A Thesis submitted to the Faculty and the Board of Trustees of the Colorado School of Mines in partial fulfillment of the requirements for the degree of Doctor of Philosophy.

Signed: _____
Student

Golden, Colorado

Date: May 16, 1969

Approved: _____
Thesis Advisor

_____
Head of the Department
of Physics

_____
Head of the Department
of Metallurgical
Engineering

Golden, Colorado

Date: May 16, 1969

ABSTRACT

With samples grown from melts containing 1.5-wt-percent excess Au and Te, respectively, the four nonzero components of the zero-magnetic-field resistivity tensor, ρ^{o}_{ik}, were determined for monoclinic $AuTe_2$ between 80° and 300°K. From Hall-effect measurements, at 290°K, three components of the Hall tensor (five nonzero components) were also calculated. All electrical measurements were determined with D.C. potentiometric techniques.

At 290°K the data show the dominant band (or bands) to be n-type and indicate little change in relative charge-carrier concentrations or mobility over the apparently very narrow compositional range of the compound. Moreover, small differences in magnitudes of corresponding components of $\rho_{ik}(B)$ at 290°K suggest only limited changes in relative charge-carrier densities and mobilities with the Au:Te ratio.

Phase transformations at 136° and 216°K and temperature-dependent changes in relative carrier populations of the bands responsible for electrical conduction are suggested by the resistivity data for $80° \leq T \leq 300°K$. The suspected phase transformations associated with abrupt breaks in the temperature dependence of the ρ^{o}_{ik} may involve only changes in the lattice constants. This condition is suggested because no lattice symmetry changes were detected in a low-temperature X-ray diffractometry study in previous work.

Relative band motion or impurity ionization causing carrier-population changes may explain the nonlinearities observed in the temperature curves of the ρ^{o}_{ik} between 80° and 300°K.

CONTENTS

CONTENTS--Cont.

CONTENTS--Cont.

LIST OF ILLUSTRATIONS, FIGURES AND TABLES

LIST OF ILLUSTRATIONS, FIGURES
AND TABLES--Cont.

Dedicated to

my wife

Alice I. Judy

Her devotion and patient understanding

are invaluable to me.

ACKNOWLEDGMENTS

For their guidance and advice during the graduate program, the author wishes to express his deep gratitude to the members of his Doctoral committee:

Professor Ralph B. Bowersox, Chairman,

Assistant Professor C. Samuel Miller,

Professor Paul G. Herold,

Professor Donald B. Marsh,

Professor Anton G. Pegis.

The interest and guidance of Dr. Ralph B. Bowersox during the thesis research are gratefully acknowledged.

In appreciation of the education he received from this institution, the author sincerely acknowledges his debt to the faculty members of the departments of Physics, Metallurgical Engineering, and Mathematics of the Colorado School of Mines. Particular acknowledgment is made to Professors Paul F. Bartunek, John V. Kline, Robert W. Allister, William B. Law, F. Richard Yeatts, and Arthur Y. Sakakura of the Physics Department and to Professor D. Cyril Schieltz of the Department of Metallurgical Engineering.

The construction of the sample cells used in this work by Mr. Jack P. Kintner and construction of some of the electronic equipment by Mr. Roy Yoshida are acknowledged with gratitude.

The author also thanks Professor Anton G. Pegis for his critical review of the manuscript.

The financial support of a part of this research by the Colorado School of Mines Research Foundation, Inc. is also gratefully acknowledged.

INTRODUCTION

Electrical transport properties of the monoclinic C2/m compound $AuTe_2$ have been the subject of two previous investigations[1,2].

Harman[1] determined values of the electrical conductivity, Hall constant, and thermoelectric power at 77° and 298°K for a monocrystalline sample cut from an ingot which had been grown from a melt containing excess Te. The orientation of the crystal used by Harman was determined by Judy during the investigation comprising Reference 2, to be approximately parallel to < 201 >.

In Reference 2, the author of this paper determined values of the electrical resistivity and absolute thermoelectric power at temperatures between 77° and 298°K (Table 2). Single crystals cut from an ingot grown from a melt containing 1.5-wt-percent excess Te and having nominal orientations corresponding to the crystallographic a-, b-, and c-axes were used. Recent vapor-pressure measurements of Veale and Barrett[3] indicate that the maximum excess Te content of the samples used in References 1 and 2 relative to stoiciometric composition, 66.666 atomic percent Te, was of the order of 10^{-2} atomic percent.

As shown in Tables 1 and 2, the electrical resistivity and thermoelectric power of the compound containing a small quantity of excess Te are anisotropic. Examination of the temperature behavior of the electrical resistivity and absolute thermoelectric power in Reference 2 demonstrated these properties to have positive temperature coefficients between 80° and 300°K. However, the experimentally determined resistivity versus temperature curves for the samples of nominal b- and c-orientation

TABLE 1

VALUES OF SELECTED TRANSPORT PROPERTIES OF $AuTe_2$ DETERMINED FOR A CRYSTAL OF NOMINAL < 201 > ORIENTATION[1]

Property	Temperature (Deg. K)	
	77	298
Electrical Resistivity (Ω : cm)	3.38×10^{-5}	1.65×10^{-4}
Hall Constant (cm^3/coul)	-5.1×10^{-2}	-1.8×10^{-2}
Thermoelectric Power (microvolts/deg. K)	----------	5.5×10^{1}

TABLE 2

ANISOTROPY OF THE ELECTRICAL RESISTIVITY AND THERMOELECTRIC POWER OF $AuTe_2$ CONTAINING EXCESS Te[2]

A. THE ELECTRICAL RESISTIVITY (Ω : cm)		
Nominal sample orientation	Temperature	
	77°K	298°K
a-axis	3.974×10^{-5}	1.550×10^{-4}
b-axis	7.765×10^{-5}	2.466×10^{-4}
c-axis	5.969×10^{-5}	2.924×10^{-4}
B. THE THERMOELECTRIC POWER (μv/Deg. K)		
Nominal sample orientation	Temperature	
	80°K	298°K
a-axis	-29.7*	-80.4
b-axis	-10.5	-29.1
c-axis	-26.4	-51.2

* Value at 120°K.

do not increase uniformly with temperature, as does the curve for the sample of a-orientation; rather, these curves exhibit changes in slope at about 150°K. Above this temperature, the slope of each of the curves determined for the samples of b- and c-orientation decreases relative to values typical of lower temperatures (Figure 9). Also the resistivity of each sample demonstrated hysteresis upon temperature cycling. The resistivity values of the samples at room temperature increased 10 to 20 percent after cooling to 77°K and warming to room temperature.

To ascertain whether the changes in the slopes of the resistivity curves and the resistivity hysteresis were associated with a crystalline structural change, an X-ray diffraction study at 125°K was conducted[1/].

[1/] This research was performed after completion of the work comprising Reference 2 by R. J. Barton and the author of this paper.

The sample was held at this temperature for 12 hours before the measurements were begun. This time was greater by a factor of two than that necessary to cool the samples from room temperature to 150°K during the resistivity runs. No evidence of changes in the crystal structure was detected. This negative result was considered to exclude the presence of any gross change in the crystal structure being associated with the temperature behavior of the resistivity. This behavior, therefore, is related to more subtle changes within the crystal.

The following considerations motivated the present study. Although the previous two investigations demonstrate anisotropy of the electrical resistivity and absolute thermoelectric power, each is limited in that the data determined in each investigation are too few to allow calculation of the complete transport property tensors. Combination of the thermoelectric power data of both papers does not allow determination of the complete tensor because data for at least five samples of different orientation must be known. Unfortunately, calculation of the resistivity tensor cannot proceed with confidence from the data of both papers because knowledge of resistivity values for four samples of different orientation, while allowing calculation of the tensor, does not include the desired redundancy of the data to allow checking the results. Also, Harman did not investigate the anisotropy of the Hall-effect.

In the previous investigations, only the electrical properties of the phase containing excess Te are determined. Frequently in compounds, changes in the cation-anion ratio alters either, or both, the charge-carrier density and mobility of the carriers in the bands contributing to electrical conduction. Because the macroscopic electrical transport properties are related directly to these parameters, studies of these properties using material containing excess Au or an increased Au:Te ratio are desirable for illuminating the effect of the presence of excess cation on the conduction process.

Knowledge of the values of all components of the resistivity tensor as functions of temperature between 80° and 300°K is a desirable step towards understanding the causes of the changes in temperature dependence of the resistivity discovered in Reference 2.

In the present study the electrical resistivity tensor through terms linear in the magnetic field is investigated. The complete zero-magnetic field resistivity tensor for materials grown from melts containing excess Au and Te, respectively, is determined at temperatures between 80° and 300°K from measurements on single crystals of different orientations. Also, Hall-effect measurements in a weak magnetic field are performed at 290°K on samples of the two materials. From these data the components ρ_{123}, ρ_{231}, and ρ_{132}, and the sum of the components, ρ_{131} and ρ_{322}, of the Hall tensor at 290°K are calculated.

The first section of this study is a discussion of the phenomenological theory of the galvanomagnetic effects and consideration of the effects upon the resistivity tensor $\rho_{ik}(B)$ arising from the imposition of the monoclinic C2/m symmetry of $AuTe_2$ and application of the Onsager relations which insist that $\rho_{ik}(B) = \rho_{ki}(-B)$. The resulting equations linking the measurable electric field, current density, and magnetic field allow solution of experimentally determined resistivities for the components of the tensors. A discussion of the experimental techniques used in this investigation then follows. Results are then presented and discussed.

PHENOMENOLOGICAL THEORY OF THE GALVANOMAGNETIC EFFECTS

Presented initially is a general treatment of electrical and thermal transport in an anisotropic crystalline medium. The effects of an external magnetic field upon the transport equations are considered. Isothermal conditions are then specified and, under the assumption of small magnitudes of the magnetic field, the electrical resistivity is expanded in powers of the magnetic field. Identification of the zero-magnetic field resistivity tensor ρ^{o}_{ik} and Hall tensor ρ_{ikl} follows. Relations between the components of each of the tensors are demonstrated to arise from application of Onsager's relations.

In the second section, effects of the imposition of the monoclinic C2/m symmetry of $AuTe_2$ on the tensors ρ^{o}_{ik} and ρ_{ikl} are analyzed. Simplified forms of the tensors in which some components are identically zero result.

The last section is devoted to development of expressions for the longitudinal and transverse electric field in a crystal of arbitrary orientation as functions of the external magnetic field and current density. Use of these expressions allows solution of experimental data for the nonzero components of ρ^{o}_{ik} and ρ_{ikl}.

THE GENERAL TRANSPORT EQUATIONS

The phenomenological transport equations for crystalline media may be written in the Einstein tensor notation, where the repeated index k in adjacent terms implies summation over k = 1, 2, 3, as[4]

$$E_i = \rho_{ik} J_k - Q_{ik} \partial T/\partial X_k,$$

and

$$q_i = -P_{ik} J_k - K_{ik} \partial T/\partial X_k, \qquad (1)$$

where E_i, q_i, J_k, $\partial T/\partial X_k$ are, respectively, the i-th components of the electric field and the heat flux and the k-th components of the current density and the temperature gradient. Thus, the coefficients of the components of the current density and the temperature gradient are themselves components of second-rank tensors. These tensors are defined as

ρ_{ik} = electrical resistivity tensor,

K_{ik} = thermal conductivity tensor,

Q_{ik} = thermoelectric power or,
Seebeck effect tensor,

P_{ik} = Peltier effect tensor.

Furthermore, the Onsager relations of the thermodynamics of irreversible processes dictate that the matrix of the coefficients of an interrelated set of transport equations as equations 1 must be symmetric[5]. Thus,

$$\rho_{ik} = \rho_{ki}; \quad K_{ik} = K_{ki};$$

$$P_{ik} = Q_{ik} T.$$

In the presence of a magnetic field, equations 1 hold; however, the coefficient tensors are to be regarded as functions of the magnetic field B. Then, for a crystalline medium in a magnetic field equations 1 become

$$E_i = \rho_{ik}(B)\ J_k - Q_{ik}(B)\ \partial T/\partial X_k,$$

and

$$q_i = -P_{ik}(B)\ J_k - K_{ik}(B)\ \partial T/\partial X_k, \tag{2}$$

where application of the Onsager relations modified for the presence of a magnetic field results in

$$\rho_{ik}(B) = \rho_{ki}(-B),$$

$$K_{ik}(B) = K_{ki}(-B),$$

$$P_{ik}(B) = Q_{ki}(B)\ T. \tag{3}$$

Thus, the resistivity tensor $\rho_{ik}(B)$ and thermal-conductivity tensor $K_{ik}(B)$ are no longer symmetric. Because any second-rank tensor can be expressed as the sum of symmetric and antisymmetric parts, the resistivity tensor may be written as

$$\rho_{ik}(B) = s_{ik}(B) + a_{ik}(B) \tag{4}$$

where $s_{ik}(B)$ and $a_{ik}(B)$ are, respectively, the symmetric and antisymmetric parts. By definition

$$s_{ik}(B) = s_{ki}(B)$$

and

$$a_{ik}(B) = -a_{ki}(B). \tag{5}$$

From equations 3 and 4, it follows that

$$s_{ik}(B) = s_{ki}(-B) = s_{ik}(-B),$$

and

$$a_{ik}(B) = a_{ki}(-B) = -a_{ik}(-B). \tag{6}$$

Thus, $s_{ik}(B)$, the symmetric part, is an even function of B and $a_{ik}(B)$; the antisymmetric part, is an odd function of B.

Effect of Isothermal Conditions

If isothermal conditions are specified, the first of equations 2 becomes simply Ohm's Law, or

$$E_i = \rho_{ik}(B)\ J_k = s_{ik}(B)\ J_k + a_{ik}(B)\ J_k. \qquad (7)$$

According to Casimir[6], the direction of the electric field defined by equations 7 exhibits the following specific relationship to that of the current density J. The symmetric part of E generally possesses components parallel and perpendicular to J, whereas the antisymmetric part of E is always perpendicular to J, but is not necessarily perpendicular to B.

Power-Series Expansion of $\rho_{ik}(B)$

Most galvanomagnetic measurements suggest that $\rho_{ik}(B)$ in equations 7 may be expanded as a series in powers of the components B_j[7]. Assumption of the validity of the power-series expansion implies the absence of oscillatory terms in $\rho_{ik}(B)$ appearing at low temperatures and large values of B which are proportional to $B \sin(B_o/B)$. These terms cannot be included in the power-series expansion because they do not possess a derivative at $B = 0$. Expansion of $\rho_{ik}(B)$ through terms of second power results in

$$\rho_{ik}(B) = \rho^{o}_{ik} + \rho_{ikl}\ B_l + \rho_{iklm}\ B_l\ B_m. \qquad (8)$$

Then, as $s_{ik}(B)$ and $a_{ik}(B)$ are respectively even and odd functions of B_j,

$$s_{ik}(B) = \rho^{o}_{ik} + \rho_{iklm} B_l B_m, \tag{9}$$

and

$$a_{ik}(B) = \rho_{ikl} B_l. \tag{10}$$

The tensors ρ^{o}_{ik}; the zero-magnetic field-resistivity tensor; and ρ_{iklm}, the magnetoresistivity tensor, are symmetrical polar tensors[8], so that by equations 6

$$\rho^{o}_{ik} = \rho^{o}_{ki}$$

$$\rho_{iklm} = \rho_{kilm} \tag{11}$$

The tensor ρ_{ikl}, called the Hall tensor, is an antisymmetric axial tensor[9].

From equations 6

$$\rho_{ikl} = -\rho_{kil} \tag{12}$$

THE EFFECTS OF MONOCLINIC C2/m SYMMETRY ON THE TENSORS

Requirements placed on the transport property tensors by various crystal symmetries have been examined by a number of authors[10,11,12,13,14,15]. In particular, Nye[11] and Bhagavantam[12] list the four nonzero independent components of the zero-magnetic-field resistivity tensor appropriate to the C/2m symmetry. Kohler[10] derived 13 nonzero components for the Hall tensor of a crystal of C2/m symmetry. However, these components are not all independent nor nonzero. Application of Onsager's relations[5]

(discovered after Kohler's work) results in (using the notation of Kohler) $R_{113} = R_{223} = R_{333} = 0$, the remaining ten being related in pairs so that only five nonzero independent components remain.

For completeness in the discussion of the phenomenological theory, the effects of the requirements of the C2/m symmetry on the tensors ρ^{o}_{ik} and ρ_{ikl} are now explicitly demonstrated.

According to Neumann's principle[16], any physical-property tensor must be invariant under all permissable symmetry operations appropriate to the particular crystal class. Thus, if $S^{(n)}$ is the matrix of an allowable symmetry operation and $|S^{(n)}|$ is its determinant, the transformation[17]

$$d'_{ijk...n} = S^{(n)}_{ip} S^{(n)}_{jq} S^{(n)}_{kr} ... S^{(n)}_{nu} d_{pqr...u} \tag{13}$$

of the polar tensor $d_{pqr...u}$ and the transformation[18]

$$c'_{ijk...n} = \left|S^{(n)}\right| S^{(n)}_{ip} S^{(n)}_{jq} S^{(n)}_{kr} ... S^{(n)}_{nu} c_{pqr...u} \tag{14}$$

of the axial tensor $c_{pqr...u}$ must result in

$$d' = d \tag{15}$$

and

$$c' = c. \tag{16}$$

Any given crystal class is characterized completely by its generating matrices; all other permissable symmetry operations are accomplished by multiplication of the appropriate generating matrices[19]. Then, for any crystal class, equations 13 and 15 for any polar physical-property tensor $d_{ijk...n}$ and equations 14 and 16 for any axial

physical-property tensor $c_{ijk...n}$ must be satisfied for the appropriate generating matrices.

The monoclinic centrosymmetric crystal class C2/m is characterized by the generating matrices[20],

$$S^{(1)} = \begin{pmatrix} -1 & 0 & 0 \\ 0 & -1 & 0 \\ 0 & 0 & -1 \end{pmatrix} \tag{17}$$

and

$$S^{(3)} = \begin{pmatrix} -1 & 0 & 0 \\ 0 & -1 & 0 \\ 0 & 0 & 1 \end{pmatrix}; \tag{18}$$

the crystal coordinate axes X_k, i = 1, 2, 3, are chosen so that the three axes comprise a right-handed orthogonal axial system. Figure 1 shows the relationships between these crystal coordinate axes and the crystallographic a-, b-, and c-axes.

Inversion through the origin is represented by the matrix $S^{(1)}$. Therefore, the monoclinic C2/m crystal system is centrosymmetric. Because the matrix $S^{(3)}$ represents a rotation of π about the X_3-axis, the crystallographic b-axis which coincides with the X_3-axis is an axis of binary rotational symmetry.

The zero and nonzero components of ρ^{o}_{ik}, ρ_{ikl}, and ρ_{iklm} can now be determined and the simplified form of each of these tensors be presented for monoclinic $AuTe_2$.

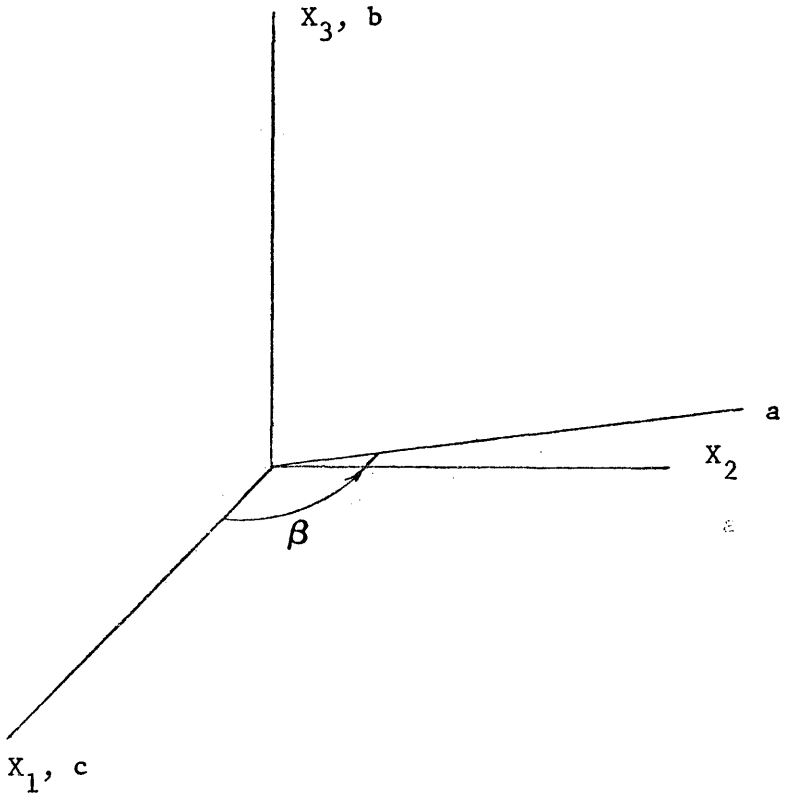

Figure 1. Relationships between the orthogonal crystal coordinates, X_i, i = 1, 2, 3, and the crystallographic a-, b-, and c-axes. Axes X_1, X_2, a, and c are all coplanar and perpendicular to the X_3 and b axes. In $AuTe_2$[49], the monoclinic angle β is 90°13'±10' (Appendix 1).

The Form of ρ^o_{ik} for Gold Ditelluride

Equation 13 applied to ρ^o_{ik}, a polar second-rank tensor, yields

$$\rho'^o_{ik} = S^{(n)}_{ip}\, S^{(n)}_{kq}\, \rho^o_{pq}. \tag{19}$$

In $S^{(1)}$, equation 17, all off-diagonal terms are equal to zero; for the three diagonal terms, each of which is equal to -1, $i = p$ and $k = q$. Therefore, for all p and q, substitution of $S^{(1)}$ into equation 19 results in

$$\rho'^o_{ik} = S^{(1)}_{ii}\, S^{(1)}_{kk}\, \rho^o_{ik},$$

or

$$\rho'^o_{ik} = (-1)(-1)\, \rho^o_{ik};$$

so that,

$$\rho'^o_{ik} = \rho^o_{ik}.$$

Then, imposition of centrosymmetry upon ρ^o_{ik} results in none of the nine components becoming identically equal to zero. However, as will be seen, considerable simplification of this tensor occurs when $S^{(3)}$ is substituted into equation 19. Examination of $S^{(3)}$, equation 18, shows that only the diagonal terms are nonzero; thus, in equation 18, $i = p$ and $k = q$. Furthermore, $S^{(3)}_{11} = S^{(3)}_{22} = -1$, but $S^{(3)}_{33} = 1$. Accordingly, only the components ρ^o_{11}, ρ^o_{22}, ρ^o_{33}, ρ^o_{12}, ρ^o_{21} are different from zero; because for these indices, equation 13 yields upon substitution of equation 18,

$$\rho'^o_{ik} = \rho^o_{ik};$$

whereas, for the indices 13 and 23, the resulting expression is

$$\rho'^{o}_{ik} = -\rho^{o}_{ik},$$

which can only be satisfied for $\rho^{o}_{ik} = 0$, $i = 1, 2$, $k = 3$.

The final simplified form of ρ^{o}_{ik} for $AuTe_2$ can now be written as the symmetric matrix

$$\rho^{o}_{ik} = \begin{Bmatrix} \rho^{o}_{11} & \rho^{o}_{12} & 0 \\ \rho^{o}_{12} & \rho^{o}_{22} & 0 \\ 0 & 0 & \rho^{o}_{33} \end{Bmatrix}, \tag{20}$$

where $\rho^{o}_{21} = \rho^{o}_{12}$ by equations 11.

The Form of ρ_{ikl} for Gold Ditelluride

Because the Hall tensor ρ_{ikl} is an antisymmetric tensor, all terms for which $i = k$ are identically zero. Thus, only terms for which $i \neq k$ need be considered.

Because the determinant of $S^{(1)}$ equals -1 and each diagonal term equals -1 application of equation 14 using $S^{(1)}$ to ρ_{ikl}, with $i \neq k$, results in none of these components becoming identically equal to zero.

After substitution of $S^{(3)}$ into equation 14, the remaining nonzero components are ρ_{123}, ρ_{213}, ρ_{132}, ρ_{312}, ρ_{231}, ρ_{321}, ρ_{232}, ρ_{322}, ρ_{131}, and ρ_{311}. However, according to equation 12, $\rho_{ikl} = -\rho_{kil}$, so that the tensor possesses five independent nonzero components, say, ρ_{123}, ρ_{132}, ρ_{231}, ρ_{232}, and ρ_{131}. The Hall tensor ρ_{ikl} for $AuTe_2$ is then of the form:

$$\begin{Bmatrix} 0 & 0 & \rho_{131} & 0 & 0 & \rho_{132} & 0 & \rho_{123} & 0 \\ 0 & 0 & \rho_{231} & 0 & 0 & \rho_{232} & -\rho_{123} & 0 & 0 \\ -\rho_{131} & -\rho_{231} & 0 & -\rho_{132} & -\rho_{232} & 0 & 0 & 0 & 0 \end{Bmatrix} \quad (21)$$

Expression of $\rho_{ik}(B)$ Through Terms Linear In B For $AuTe_2$

According to equations 8, 9, and 10, the resistivity tensor $\rho_{ik}(B)$ through terms linear in the magnetic field B can be expressed as a function of the zero-magnetic field resistivity and Hall tensors, equations 20 and 21. Then with B_i, i = 1, 2, 3, being the components of B along the crystal coordinate axes X_i,

$$\rho_{ik}(B) =$$

$$\begin{Bmatrix} \rho^o_{11} & (\rho^o_{12} + \rho_{123} B_3) & (\rho_{131} B_1 + \rho_{132} B_2) \\ (\rho^o_{12} - \rho_{123} B_3) & \rho^o_{22} & (\rho_{231} B_1 + \rho_{232} B_2) \\ (-\rho_{131} B_1 - \rho_{132} B_2) & (-\rho_{231} B_1 - \rho_{232} B_2) & \rho^o_{33} \end{Bmatrix} \quad (22)$$

EXPRESSIONS FOR THE ELECTRIC FIELD IN CRYSTALS OF ARBITRARY ORIENTATION

For the development of equations expressing the electric field in crystals of arbitrary crystallographic orientation, the laboratory coordinates X_α, α = 1, 2, 3 are defined to comprise a right-handed orthogonal axial system. The laboratory coordinates are related to the crystal coordinates X_i by the direction cosines L_i; i = 1, 2, 3;

α = 1, 2, 3. Furthermore, the current density J is always taken as parallel to X', i.e. $J \equiv J^1$

Ohm's law, equation 7 restated in laboratory coordinates, is

$$E^{\alpha} = \rho^{\alpha 1}(B)\ J^1, \tag{23}$$

where

$$\rho^{\alpha 1}(B) = L_i^{\alpha}\ L_k^1\ \rho_{ik}(B), \tag{24}$$

and, i, k = 1, 2, 3. For α = 1, these equations describe the longitudinal component of the electric field; for α = 2 or 3, they describe the transverse components.

Two particular conditions of measurement to be applied to equations 23 and 24 are of interest in this research:

(1) The longitudinal electric field E^1 is determined with B = 0. Thus, the only terms in equation 24 are those corresponding to the ρ_{ik}^{o} appropriate to $AuTe_2$ (monoclinic C2/m symmetry).

(2) The part of the total transverse field E^2, which is odd or antisymmetric in the magnetic field B, E_a^2 is determined. This is the definition[21] of the Hall effect used in this work. Then, the only terms in equation 24 are those corresponding to the nonzero ρ_{ikl}.

The expressions for E^1 and E_a^2 which result from substitution of equation 20 into equations 23 and 24 and application of the special cases 1 and 2 are, for samples of arbitrary orientation:

$$E^1 = \rho^{11}(B = 0)\ J^1$$

or

$$E^1 = \left[\left(L_1^1\right)^2 \rho_{11}^o + \left(L_2^1\right)^2 \rho_{22}^o + \left(L_3^1\right)^2 \rho_{33}^o + 2\ L_1^1\ L_2^1\ \rho_{12}^o\right] J^1, \quad (27)$$

and

$$E_a^2 = \rho_a^{21}(B)\ J^1$$

or

$$\begin{aligned} E_a^2 = \Big[& L_1^2\ L_2^1\ \rho_{123}\ B_3 + L_1^2\ L_3^1\ \rho_{131}\ B_1 + L_1^2\ L_3^1\ \rho_{132}\ B_2 \\ & - L_2^2\ L_1^1\ \rho_{123}\ B_3 + L_2^2\ L_3^1\ \rho_{231}\ B_1 + L_2^2\ L_3^1\ \rho_{232}\ B_2 \\ & - L_3^2\ L_1^1\ \rho_{131}\ B_1 - L_3^2\ L_1^1\ \rho_{132}\ B_2 - L_3^2\ L_2^1\ \rho_{231}\ B_1 \\ & - L_3^2\ L_2^1\ \rho_{232}\ B_2\Big] J^1. \end{aligned} \quad (28)$$

If B is parallel to X^3, equation 24 becomes

$$\begin{aligned} E_a^2 = \Big[& \left(L_1^2\ L_2^1 - L_2^2\ L_1^1\right) L_3^3\ \rho_{123} + \left(L_1^2\ L_3^1 - L_3^2\ L_1^1\right) L_2^3\ \rho_{132} \\ & + \left(L_2^2\ L_3^1 - L_3^2\ L_2^1\right) L_1^3\ \rho_{231} + \left(L_1^2\ L_3^1 - L_3^2\ L_1^1\right) L_1^3\ \rho_{131} \\ & + \left(L_2^2\ L_3^1 - L_3^2\ L_2^1\right) L_2^3\ \rho_{232}\Big]\ B\ J^1. \end{aligned} \quad (29)$$

Furthermore, as the X^{α} are related to the X_i through a rigid-axis rotation, each of the nine L_i^{α} is equal to its cofactor in the determinant L_i; and equation 27 can be simplified to

$$E_a^2 = \left[- \left(L_3^3\right)^2 \rho_{123} + \left(L_2^3\right)^2 \rho_{132} - \left(L_1^3\right)^2 \rho_{231} + L_1^3 L_2^3 \left(\rho_{131} - \rho_{232}\right)\right] B J^1. \quad (30)$$

Examination of equations 27, 28, 29, and 30 shows that:

(1) determination of values of ρ^{11} from electrical measurements on at least four crystals of different orientation L_i is necessary and sufficient to determine the four nonzero components ρ^o_{ik} for $AuTe_2$;

(2) knowledge of ρ_a^{21} from Hall-effect measurements on at least five crystals of different L_i suffices to determine the five nonzero components ρ_{ikl} of the Hall tensor of $AuTe_2$, if the sample can be rotated relative to B. If B is always maintained parallel to X^3, the three components ρ_{123}, ρ_{132}, and ρ_{231} and the sum $(\rho_{131} + \rho_{322})$ can be determined.

EXPERIMENTAL DETAILS

The sample preparation and electrical measurements are considered separately.

SAMPLE PREPARATION

Comprising the procedures used to prepare samples for the electrical measurements were synthesis of the compound, crystal growth, sample cutting and lapping, measurement of each sample's dimensions, and determination of the orientation of each sample. These procedures and an explanation of the sample designation are presented in the following sections.

Compound Synthesis

Although the ingot from which the samples containing excess Te were obtained for the present study was that grown for the previous research (Reference 2), the compound synthesis and growth of this ingot is described for completeness.

Because $AuTe_2$ forms readily upon solidification of a melt containing gold and tellurium[22], synthesis of the compound was easily achieved by reacting the constituents at a temperature greater than the melting point of the compound[23], 464°C, and then allowing the melt to cool. The melt oxidizes rapidly in air; accordingly, the synthesis was performed under a dry reducing atmosphere.

Gold and tellurium, each of 99.999 percent purity and obtained from the American Smelting and Refining Company, were used in the synthesis of the compound from both the gold-rich and tellurium-rich

melts. The supplier's analyses of these materials are presented in Appendix 2. Gold and tellurium, in weights corresponding to stoichiometric composition (43.59 wt percent Au and 56.41 wt percent Te), plus 1.5 weight percent of either excess Te or Au, were placed in pointed silica crucibles which had been cleaned in a manner described by Lawson and Nielsen[24]. The inside of each crucible was etched with a solution of 50-percent concentrated HNO_3 and 50-percent concentrated HF, rinsed repeatedly in distilled water, and then rinsed repeatedly with reagent-grade methanol.

Evacuated to approximately 1×10^{-6} Torr and then backfilled with dry H_2, the filled crucibles were sealed off under approximately one-third of an atmosphere of the gas.

The crucibles containing the constituents were heated to approximately 510°C and then held at this temperature for 72 hours. During this time the furnaces were gently shaken to promote adequate mixing of the constituents. The crucibles and contents were then slowly cooled to room temperature.

Identity of the compound in the crucibles was firmly established in each case by comparison of the θ-values calculated from X-ray powder photographs with standard values[25]. Details are presented in Appendix 3.

Crystal Growth

Crystal growth from the melts of both compositions was accomplished through use of a modified Stockbarger technique[26]. For both melts, two-zone furnaces were used, with the upper zone held at 510°C and the lower at 430°C. Crystal growth from the Te-rich melt was accomplished by raising the furnace at a rate of 0.5 cm/hr relative to the crucible so that a liquid-solid interface passed upward through the ingot. Motion was maintained until the solid ingot was located entirely within the lower (cooler) zone. The power input to the furnaces in the two zones was then slowly decreased to zero over a 12-hour period. Growth from the Au-rich melt was the same as that from the Te-rich melt, except that the crucible was lowered relative to the furnace at a rate of 0.2 cm/hr. Both ingots were grown in the crucibles in which the compound synthesis had been accomplished.

Each ingot exhibited lower, middle, and upper monocrystalline portions which were separated by zones of coarse lamallae approximately 1 mm wide. These zones appeared to be regions of polysynthetic twinning. Through microscopic examination at 500x, the monocrystalline portions, clean and bright, exhibited no evidence of twinning. These portions yielded the samples used for the electrical measurements.

Sample Cutting and Lapping

The ingot was sectioned and blanks cut for lapping by wire-sawing, a method used in cutting brittle semiconductor materials[27]. An abrasive, 600-mesh SiC suspended in petroleum jelly, served as the

cutting agent. A 24-gauge stainless-steel wire attached to a slowly moving reciprocating frame dragged the abrasive along the surface being cut. The sample, waxed in a cradle located on the end of a lever-arm, was positively fed towards the wire by very slight imbalance introduced by adjusting the position of a counterweight. Care was taken to maintain small bearing pressures between wire and sample to minimize damage introduced by the sawing. By careful lapping of the crude blanks obtained by wire-sawing, samples were obtained for the resistivity and Hall-effect measurements in the form of rectangular parallelepipeds. Approximately 2 to 3 mm of material was removed in the directions normal to the four lateral sample faces during the procedure. This procedure removed any portions of the crude slabs damaged by wire-sawing.

Lapping was done by hand. During the procedure, the sample was affixed with black-wax to the flat-faced end of a metal cylinder. The cylinder rested with an easy-sliding fit in a cylindrical hole milled in the center of a rectangular slide, the axis of the hole being perpendicular to a flat face of the slide. Slow motion of this slide face along two mutually parallel rails, both of which were parallel to a piece of plate-glass, resulted in motion of the sample along the surface of the glass. A suitable abrasive was placed on the surface of the plate glass. As the cylinder was constrained to be perpendicular to the glass surface, flat surfaces resulted from lapping. Parallel lateral surfaces were obtained by first lapping one flat surface. The

sample was then reaffixed so that the lapped surface was in contact with the end of the cylinder. Subsequent lapping resulted in a face parallel with the initially lapped surface. Parallel faces perpendicular to those initially lapped were attained through use of small metal shims of rectangular cross section. The sample was held between these shim blocks during lapping so that the two initially lapped surfaces were held perpendicularly to the end of the cylinder.

During the initial stages of lapping, 600-mesh SiC was used as the abrasive. Final lapping of each lateral surface of the samples was done with 4-0 paper (approximately 10μ particle size). This final procedure produced a semi-polished surface upon which no traces of the initial lapping were visually detectable.

Measurement of the Sample Dimensions

The width w and thickness t of the zero-magnetic-field resistivity samples and the thickness t of the Hall-effect samples were determined with a traveling microscope. Each of the values reported in Table 3 is the arithmetic mean of six separate determinations. Uncertainty in positioning the hair-line relative to an edge and an instrument least-count of 5×10^{-4} cm resulted in an estimated error of 1×10^{-3} cm in each dimension reported in the table.

TABLE 3

SAMPLE DIMENSIONS

A. ZERO-MAGNETIC FIELD RESISTIVITY SAMPLES			
Sample	Width, w (10^{-1} cm)	Thickness, t (10^{-1} cm)	Cross-sectional Area A (10^{-2} cm^2)
R-1-Te	2.321	0.961	2.23
R-2-Te	1.958	1.090	2.13
R-3-Te	2.364	1.300	3.07
R-4-Te	2.779	1.519	4.22
R-5-Te	2.168	1.104	2.39
R-1-Au	2.802	2.073	5.81
R-2-Au	2.554	1.967	5.02
R-3-Au	2.206	1.759	3.88
R-4-Au	3.121	2.052	6.40
R-5-Au	3.176	1.717	5.45
R-6-Au	2.843	1.274	3.62
R-7-Au	3.034	2.157	6.54
R-8-Au	2.060	2.169	4.46
R-9-Au	3.815	0.091	3.47

TABLE 3--Cont.

B. HALL-EFFECT SAMPLES	
Sample	Thickness, t (10^{-1} cm)
H-1-Te	0.960
H-2-Te	1.300
H-3-Te	1.519
H-4-Te	1.104
H-5-Te	1.172
H-6-Te	1.119
H-7-Te	1.418
H-1-Au	1.052
H-2-Au	0.974
H-3-Au	1.403
H-4-Au	0.704
H-5-Au	0.906
H-6-Au	0.955
H-7-Au	0.656
H-8-Au	0.698

Sample Orientation

X-ray techniques were used to determine the relative angular orientation of the crystal coordinates X_i, $i = 1, 2, 3$ and laboratory coordinates X^{α}, $\alpha = 1, 2, 3$; both coordinate systems are defined in the discussion of the phenomenological theory of the galvanomagnetic effects. The laboratory coordinates X^1, X^2, and X^3 were taken parallel to the length, width, and thickness, respectively, of each sample.

Orientations were determined by use of the back-reflection-Laue technique developed by Forest, Barton, and Schieltz[28], a method in which a cylindrical rotation-camera replaces the conventional flat-plate camera. This method has the advantage over the conventional one in that many more Laue spots and prominent zones are recorded per exposure. The angular orientations given in Table 4 are probably correct to within $\pm 1°$. This error arises from the estimation of the location of a spot on the X-ray film and the plotting and reading of angles on a 30-cm-diameter Wulff net. The angular orientations in the table are given as the θ_i^{α}; $i = 1, 2, 3$, with $\alpha = 1$ for the zero-magnetic-field resistivity samples and $\alpha = 3$ for the Hall-effect samples.

Designation of the Samples

Samples designated by R and H are resistivity and Hall samples, respectively. The suffixes Au or Te indicate the excess constituent in the parent melt. Numbering is in order of the proximity of the sample's original location to the first part of the ingot to

TABLE 4

SAMPLE ORIENTATIONS

A. ZERO-MAGNETIC-FIELD RESISTIVITY SAMPLES			
Sample	θ_1^1 (deg.)	θ_2^1 (deg.)	θ_3^1 (deg.)
R-1-Au	28	76	66
R-2-Au	30	78	62
R-3-Au	31	72	62
R-4-Au	24	68	80
R-5-Au	18	83	72
R-6-Au	14	84	76
R-7-Au	44	72	51
R-8-Au	8	86	87
R-9-Au	29	78	64
R-1-Te	16	91	74
R-2-Te	43	64	58
R-3-Te	4	97	98
R-4-Te	100	10	90
R-5-Te	80	37	55

TABLE 4--Cont.

B. HALL-EFFECT SAMPLES			
Sample	θ_1^3 (deg.)	θ_2^3 (deg.)	θ_3^3 (deg.)
H-1-Au	87	24	64
H-2-Au	70	158	100
H-3-Au	106	56	39
H-4-Au	48	116	127
H-5-Au	63	93	152
H-6-Au	69	154	75
H-7-Au	66	151	105
H-8-Au	77	141	54
H-1-Te	89	3	93
H-2-Te	93	4	88
H-3-Te	87	89	3
H-4-Te	21	95	110
H-5-Te	162	77	78
H-6-Te	86	7	85
H-7-Te	74	85	16

solidify. Samples R-1-Au through R-9-Au and H-1-Au through H-8-Au were cut from the lower and middle one-third part of the ingot. Samples R-1-Te and R-3-Te through R-5-Te, also used in the Hall measurements, were cut from the middle one-third part of the ingot. The upper one-third of the parent ingot was cut to yield the Hall samples H-5-Te, H-6-Te and H-7-Te, and the resistivity sample R-2-Te.

ELECTRICAL MEASUREMENTS

Electrical and cryogenic equipment and the techniques used in the present study are discussed in this section.

Zero-Magnetic-Field Resistivity Measurements

As shown in Equations 27, calculation of the four independent components ρ^{o}_{ik} of the zero-magnetic-field resistivity tensor requires resistivity values, ρ^{11}, of at least four samples (preferably more to establish redundancy) of different orientations.

In the present study, the temperature dependence of ρ^{11} for each sample was obtained from values of the resistance R^{11}, determined under essentially isothermal conditions at temperatures between 80° and 300°K. The resistance values were obtained by use of the comparison technique, in which the potential difference across a gauge length l of the sample and that across a standard resistor R_s in series with the sample, are measured and the sample resistance calculated from

$$R^{11} = R_s \, (V^{11}/V_s). \tag{31}$$

The potential differences V^{11} and V_s are measured across the sample and standard resistor, respectively. The current flowing through both the sample and standard resistor must remain constant during the measurements. In practice, satisfactory results are obtained if no differences are noted in values of V_s, taken immediately before and after measuring V^{11}.

The electrical circuitry

The potential differences V^{11} and V_s were determined by standard potentiometric technique. A Leeds and Northrup K-3 potentiometer, used in conjunction with an Eppley standard cell and a Minneapolis-Honeywell galvonometer, Model 3131, constituted the measuring system. An uncertainty of ±(0.015 percent of the reading + 0.5 μv) in any reading with the potentiometer on the low scale (0 to 0.016 v) was specified by the manufacturer. The sensitivity of the galvanometer was stated to be 7×10^{-3} μa/mm at a meter. The series combination of 38 ohms internal resistance of the galvanometer and 100 ohms within a part of the potentiometer included in the galvanometer circuit resulted in a voltage sensitivity of 0.1 μv/mm at a meter. Thus, the overall accuracy of the measurement system was essentially dictated by that of the potentiometer. A 0.01-ohm precision resistor with maximum error in the resistance value of ±0.01 percent was used as the resistance standard.

The sample cell

The design of the sample cell, Figure 2, reflects a number of features directed towards minimizing errors in the voltage measurements.

The current density must be uniform over the gauge length 1. Accordingly, 1, made considerably smaller than the total sample length, was located symmetrically with respect to the midpoint of the sample length. Also, large rectangular copper blocks comprised the current leads at the ends of the sample. Good electrical contact between the ends of these blocks and the ends of the sample was attained by use of In-Hg amalgam.

The use of knife-edged potential probes provided a well-defined gauge length, easily measured with a traveling microscope. These lengths are recorded in Table 5. The probes were constrained to move with an easy-sliding fit in parallel slots milled in the Bakelite block. Coaxial coil springs housed within the block served to press the probes gently against the sample. This design provided a stable gauge length at all temperatures. The linear contraction of Bakelite upon cooling from 300° to 80°K is listed[29] as 0.6 percent. No correction in the gauge length was made.

Use of the phenomenological equation, Equation 27, to describe the relationship between E^{11} and J^{1}, necessitates measurement under isothermal conditions. Accordingly, thermal anchoring of the sample and of all electrical leads to the body of the cell was provided. The sample was thermally anchored to the large copper block which comprised the body of the cell via a thin ($\simeq 5 \times 10^{-4}$ cm thick) mica sheet. This

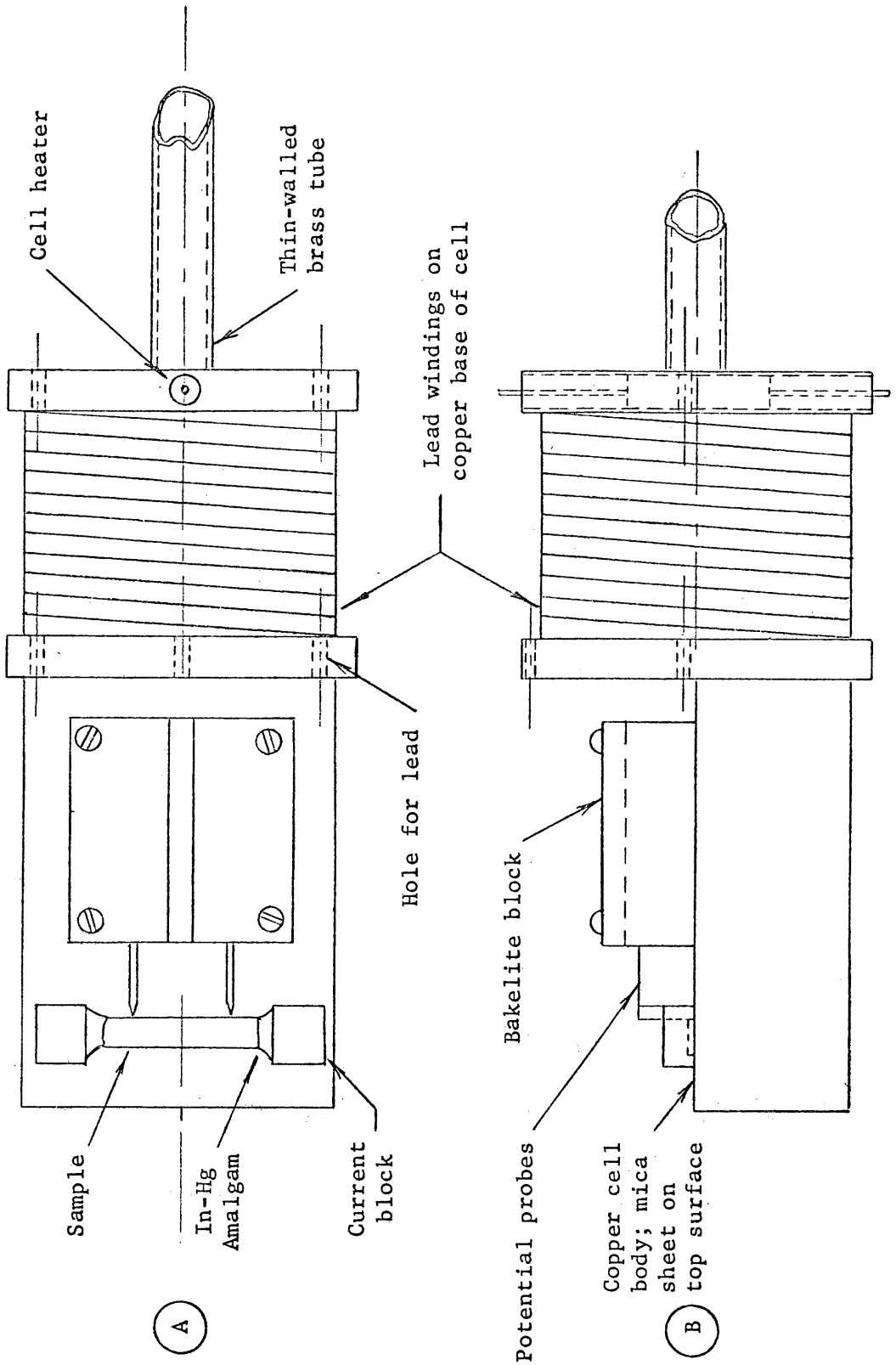

Figure 2. Top (A) and side (B) views of the sample cell used in the zero-magnetic-field resistivity measurements. The cylindrical cover which fits over the cell body and the electrical leads are not shown.

TABLE 5

SAMPLE GAUGE LENGTHS

Sample	Gauge length, l (cm)
R-1-Au	1.027
R-2-Au	1.014
R-3-Au	1.031
R-4-Au	1.003
R-5-Au	1.016
R-6-Au	1.010
R-7-Au	0.940
R-8-Au	0.5103
R-9-Au	1.001
R-1-Te	0.510
R-2-Te	0.510
R-3-Te	0.509
R-4-Te	0.511
R-5-Te	0.513

sheet electrically insulated the sample from the cell. Glyptal varnish served to anchor the sample to the cell. Further thermal anchoring was provided by use of the copper current-blocks; these made establishment of a temperature gradient within the sample difficult. The In-Hg analgam provided a good thermal link between the sample and lead blocks. Each wire entering or leaving the cell was thermally anchored to the base of the cell. Approximately 6 feet of each lead wire was wound around the base and varnished in place with glyptal.

Good heat exchange between the sample and cell was further enhanced by the presence of 1 atm of He exchange gas within the system. A thick-walled cylindrical cover, placed around the top of the cell, served to keep convective currents in the exchange gas to a minimum and to isolate the interior of the cell from direct radiative heat exchange with the rest of the cryogenic system.

Cryogenic system

For the measurements below room temperature, a cryostat patterned after the design of Ure[30] was used. The cryostat, Figure 3, was so constructed that very stable temperatures between 80° and 300°K were attained. Solid CO_2 and liquid N_2 were used as coolants. Stable temperatures above the equilibrium points of the coolants were attained by supplying a very stable electrical current to a heater (a 2.5-watt 2,500-Ω carbon resistor) located within the base of the cell. A Hewlett-Packard power supply, Model HO 1-722AR, served as the heater power supply.

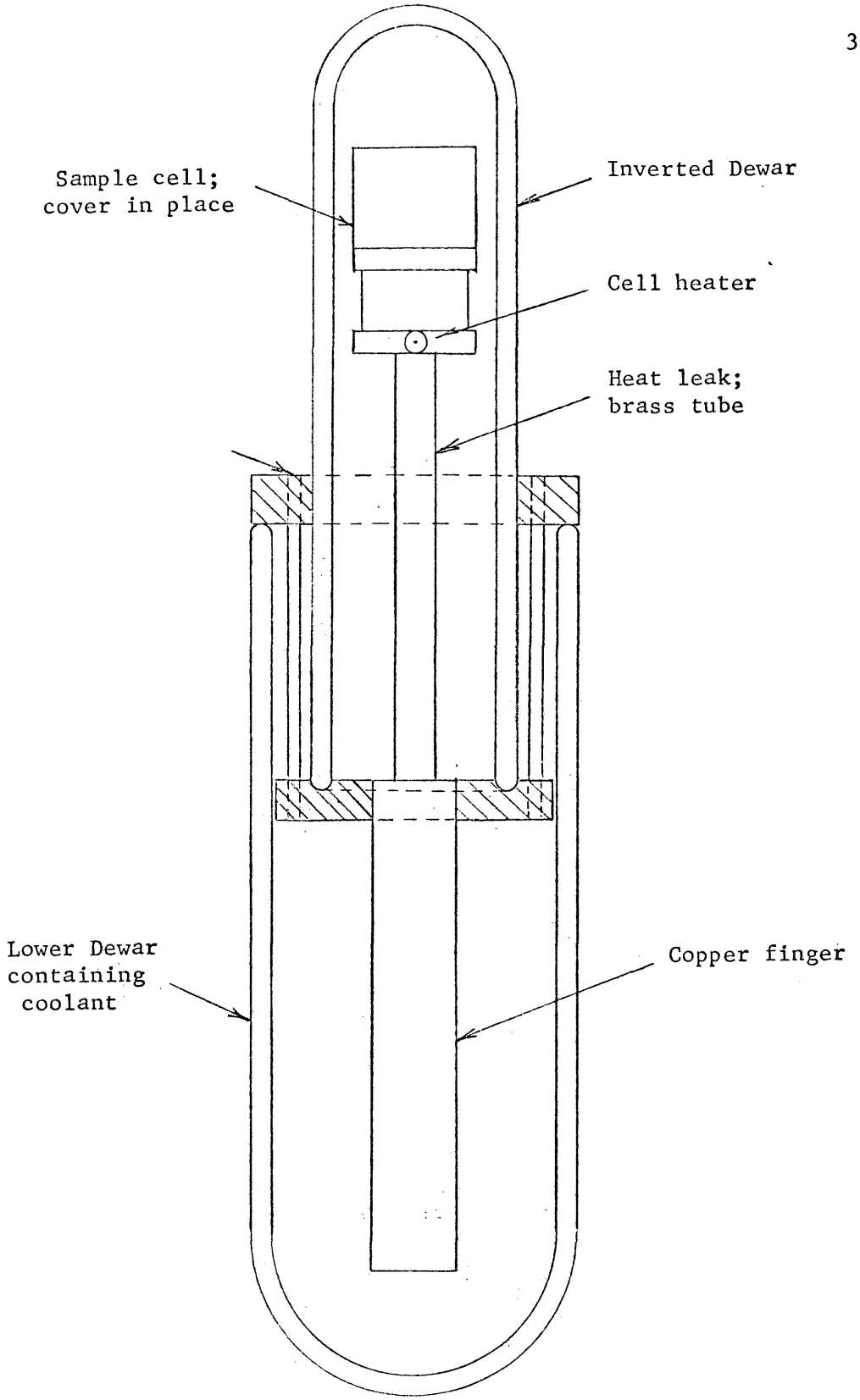

Figure 3. Cryostat used in electrical resistivity measurements between 80° and 300°K. Electrical leads to the cell are not shown.

With the lower dewar filled with either coolant to the level of the micarta support for the upper inverted dewar (Figure 3), cooling rates of approximately 0.3°K/min were achieved.

The temperature of the sample was determined by use of a copper-constantan thermocouple. So as to be located directly underneath the sample, the bead of the thermocouple was placed just below the under-surface of the mica insulating sheet. A stirred ice-bath (273.16°K) served as the reference junction cryostat.

The thermocouple was constructed of wires which had been previously checked[2] against tables with ice-point reference temperature constructed from the thermocouple emf versus temperature data of Powell, Bunch, and Corruccini[31]. During this procedure, the thermocouple emf was determined at the sublimation point of solid CO_2 and boiling point of liquid N_2. No correction terms were found necessary. These tables were used in the present work; however, the thermocouple emf was checked at the boiling point of liquid N_2. The emf of the thermocouple was determined with the entire cell immersed in stirred liquid N_2, boiling at 608 mm Hg and 75.95°K. A measured emf of 5554.0±10 μv was in excellent agreement with the tabular value of 5552.2 μv.

A Leeds and Northrup model 7645 potentiometer was used to read the thermocouple emf. A limit of error of ±10 μv as reported by the manufacturer led to possible error in measured temperatures of ±0.24°K and 0.60°K at 300° and 80°K, respectively. These uncertainties constitute relative error in the determined temperatures of less than 0.8 percent over the entire range used in this work.

Measurement procedure

Potential-difference measurements on each sample were made at from 15 to 30 temperatures between 300° and 80°K during descent from room temperature. Measurements were normally taken at a much smaller number of temperatures during temperature ascent.

A rigid measurement procedure was followed at each temperature within a run. The thermocouple emf was determined to establish the presence of temperature equilibrium. An emf constant to within ±3 μv over a 3-minute interval was considered to indicate establishment of an equilibrium temperature. A series of potential-difference measurements across sample and standard resistor immediately was begun using a sample current of approximately 100 to 150 ma. First, the potential difference across the sample, V^{11}, was measured for both directions of the current. Immediately afterward, V_s, the emf across the standard resistor, was determined for both directions of the current. At least five such sets of measurements were made of the potential difference across both sample and standard. For each direction of current flow, values of the sample and standard potential differences were reproducible to within a few fractions of a μv. Also, the values of V^{11} and V_s determined for positive direction of current flow differed from those obtained with reversed direction of the current by at most one to four μv. Furthermore, these differences remained constant to within a few fractions of a μv during any set of measurements. Therefore, current drift and any influence of extraneous emfs on the measured values of V^{11} and V_s

was felt to be negligible. A typical measurement set, performed in 5 minutes, was followed immediately by a measurement of the thermocouple emf.

Hall-Effect Measurements

The components of the Hall tensor are related to the resistivity ρ_a^{21} in Equations 28. In the present work, the value of this resistivity for each sample is determined from the value of R_a^{21}, calculated from the Hall-voltage measurements. The Hall-voltage, V_a^{21}, arising from the antisymmetric part, E_a^2, of the total transverse field, E^2, was measured with a magnetic field directed along the X^3-axis. The quantity R_a^{21} is related to the Hall voltage, current, and magnetic field by

$$V_a^{21} = IR_a^{21} B. \tag{32}$$

Unfortunately, measurement of V_a^{21} is frequently complicated by parasitic emfs arising from the presence of the Nernst, Righi-Leduc and Ettinghausen effects. Correction for these emfs is commonly made by measuring V_a^{21} for both directions of current flow and combining the results algebraically to give

$$4\, V_a^{21} = \Big[V_a^{21}\,(I, H) - V_a^{21}\,(-I, H) \\ V_a^{21}\,(-I, -H) - V_a^{21}\,(I, -H)\Big]. \tag{33}$$

Moreover, this practice eliminates from V_a^{21} that contribution arising from longitudinal probe misalignment[32]. This procedure, however, will

not eliminate any parasitic emf that may be present because of the Ettinghausen effect which is antisymmetric in the magnetic field. Fortunately, the time necessary to establish this emf can be made large by adequate thermal anchoring of the sample and the Hall-voltage measurement performed before the build-up of this emf occurs. Furthermore, thermal anchoring helps to minimize the build-up of emfs due to the Nernst and Righi-Leduc effects.

Not only must the effects of parasitic emfs on the measured value of V_a^{21} be minimized, but the effects due to shorting of the Hall field by the current contacts and of a possibly inhomogeneous magnetic field must be considered. Corrections to the measured Hall voltage for the presence of both shorting by the current contacts and an inhomogeneous magnetic field have been developed by Flanagan, et al.[33]. It is sufficient to indicate here that, for the magnetic field B uniform over a homogeneous sample of length to width ratio $1/w \geq 4$ and the Hall probes located at $1/2$, the shorting effect is essentially negligible. Under these conditions, the ratio of the measured to the actual Hall-voltage lies between 0.996 and 1.000.

Electrical circuitry

The Hall-electrode configuration shown in Figure 4 deserves special mention. The position of the contact on the slidewire R can be adjusted with the normal working current and $B = 0$ to make the transverse voltage between points a and b approximately equal to zero. This procedure prevents large voltages because of probe misalignment

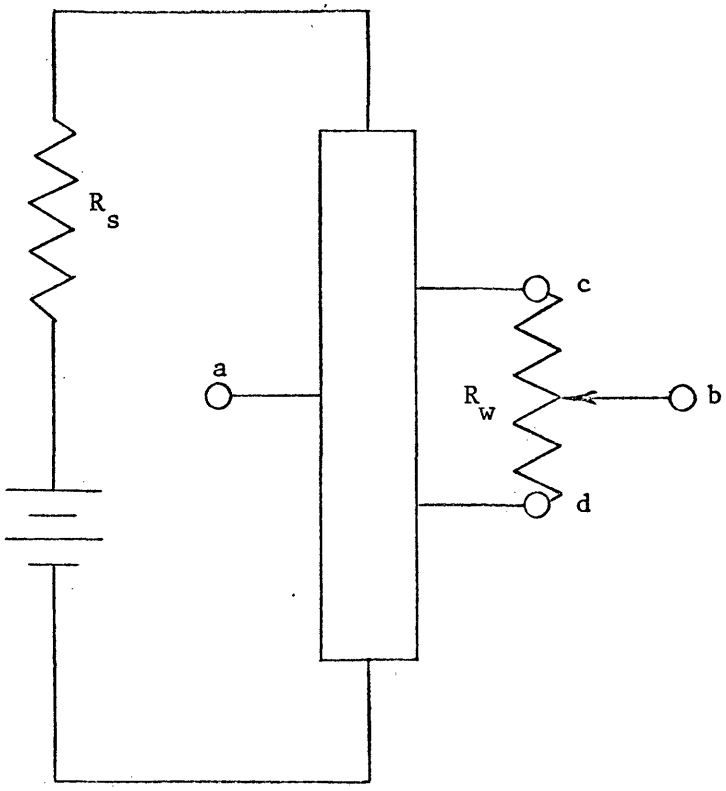

Figure 4. Schematic representation of electrical circuit used in the Hall-effect measurements. The Hall voltage was read across points a and b and the occasionally-read magnetoresistance data were taken across c and d. R_s and R_w were a 1 X 10^{-3}-Ω-standard resistor and 100-Ω-copper slidewire, respectively.

in the X^1 direction from swamping the small voltages arising from the Hall effect. Then, error associated with the algebraic combination of large quantities to obtain much smaller numbers (Equation 33) is minimized.

The Hall voltages were read potentiometrically under conditions of constant sample current of 1 amp and a homogeneous and steady magnetic field. The same Leeds and Northrup K-3 potentiometer used in the measurements for the determination of the zero-magnetic-field resistivity tensor was used. Although the absolute uncertainty in reading the potentiometer in the measurement of small Hall voltages was approximately ± 0.5 μv, the resolution of the system was about 0.1 μv. This value is consistent with the sensitivity of the galvanometer, 0.1 μv/mm at a meter, and interpolation to 0.1 μv on the potentiometer dial.

A Hewlett-Packard power supply, the same one used to power the heater in the determination of ρ^{11} at low temperatures, functioned as a source of constant sample current. After 30 minutes warm up, the sample current of 1 amp was observed to vary at most $\pm 5 \times 10^{-4}$ amp during an entire run of approximately 3 hours. Nevertheless, for each set of Hall-voltage determinations at a given value of B, the sample current was determined by measuring the potential drop across a 1×10^{-3} ohm ± 0.01 percent resistor in series with the sample.

The sample cell

During the Hall-effect work, the sample was contained in the cell shown in Figure 5. Several design features of this cell are noteworthy.

The distance between the pair of electrodes located on the same side of the sample was either 1 or 1/2 cm, depending upon the length of the sample. The electrode spacing was then ≈1/3 of the total sample length. This feature, along with the use of area current contacts, served to minimize any inhomogeneity in the current density in the region of the Hall electrodes.

Shown in Figure 5 is the sample, thermally anchored to large current blocks at its ends and to the large copper block comprising the body of the cell. Thermal contact to the body of the cell was through a thin, $\approx 5 \times 10^{-4}$-cm-thick mica sheet which electrically insulated the sample from the cell body. This sheet was attached to the cell body with epoxy cement.

The rectangular cell fitted easily into a closely fitted slot milled in an aluminum positioning ring concentric with the poles of the electromagnet. This arrangement served to reproducibly position the cell for each run so that the center of each sample was located in the geometric center of the magnet gap.

Attainment and measurement of the magnetic field

Magnetic fields ranging from 0 to 13 kilogauss were achieved with an electromagnet (Alpha Scientific Laboratory) equipped with 6-inch-diameter flat-faced pole tips. The 50-ampere power supply

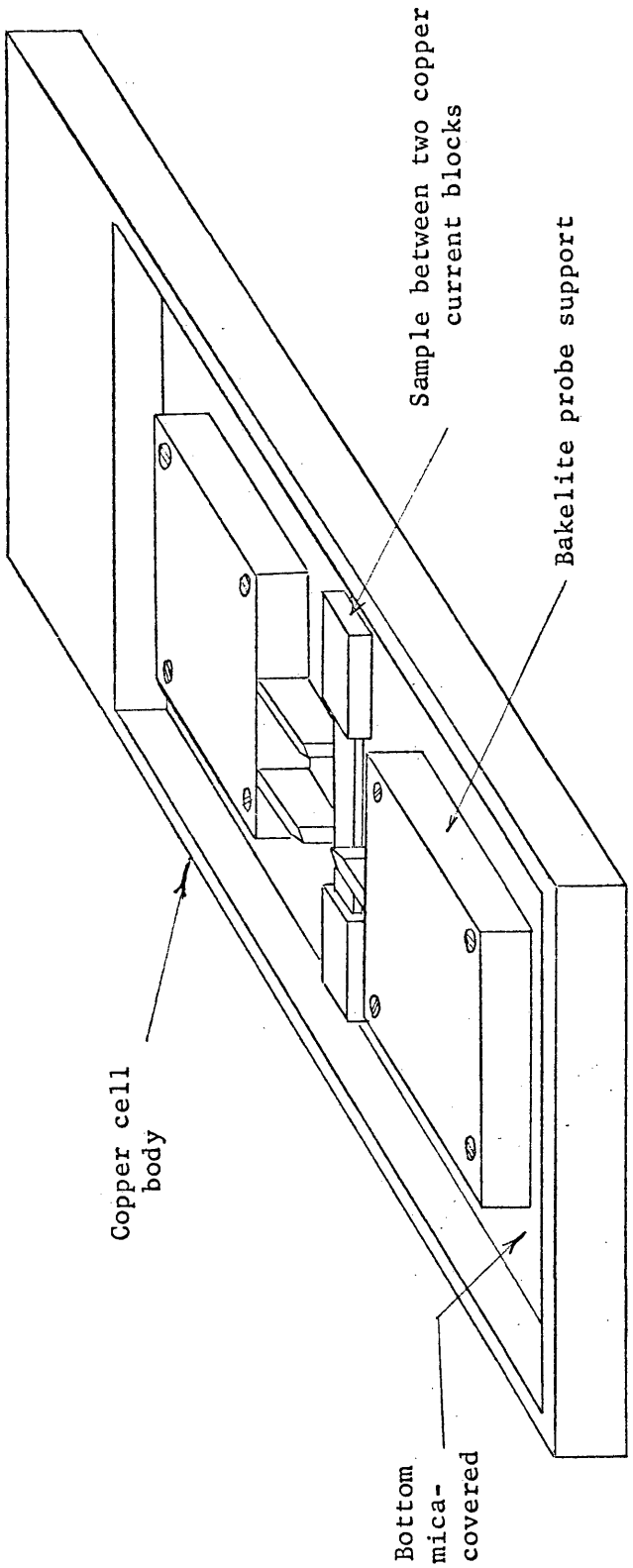

Figure 5. View of interior of sample cell used in Hall-effect measurements. Lid for cell and leads to current blocks and potential probes are not shown.

which powered the magnet was, according to the manufacturer, Alpha Scientific Laboratory, stable to within ±1 part in 10^4. During operation, the magnet coils were cooled with tap water; the average temperature of the pole tips and sample cell during any run was 290±5 deg. K. The magnitude of the field was observed to change as the coil temperature changed; however, the drift in field B during any one of the 10 to 15 sets of Hall measurements which comprised a run never exceeded 0.5 percent of the field.

In order to establish the homogeneity of the magnetic field, the radial variation in B within the air gap at maximum coil current was determined by the use of a calibrated Hall probe. Values of B were determined at various distances r_x and r_y from the cylindrical axis of the pole tips along two mutually perpendicular axes, x and y (Figure 6). Values of B at $r_y = r_x$, approximately equal, were averaged, as shown in Table 6 and the accompanying figure. To within a probe sensitivity of approximately 0.02 percent (25 gauss in 13 kilogauss), no variation in B was found over the range $0 \leq < r > \leq 2$ cm; $< r > = [r_x + r_y]/2$. Accordingly, the field was taken to be homogeneous over the volume of each sample because the length of any sample used in the study was 3.5 cm, and each sample was centered at $r = 0$ during the measurements.

A Halltron Model 31 Hall probe, manufactured by the Ohio Semiconductor Company, was used after calibration to determine the magnitude of the magnetic field during the Hall-effect measurements. Details of the calibration are in Appendix 4. During the runs, the probe sensing area was located at a

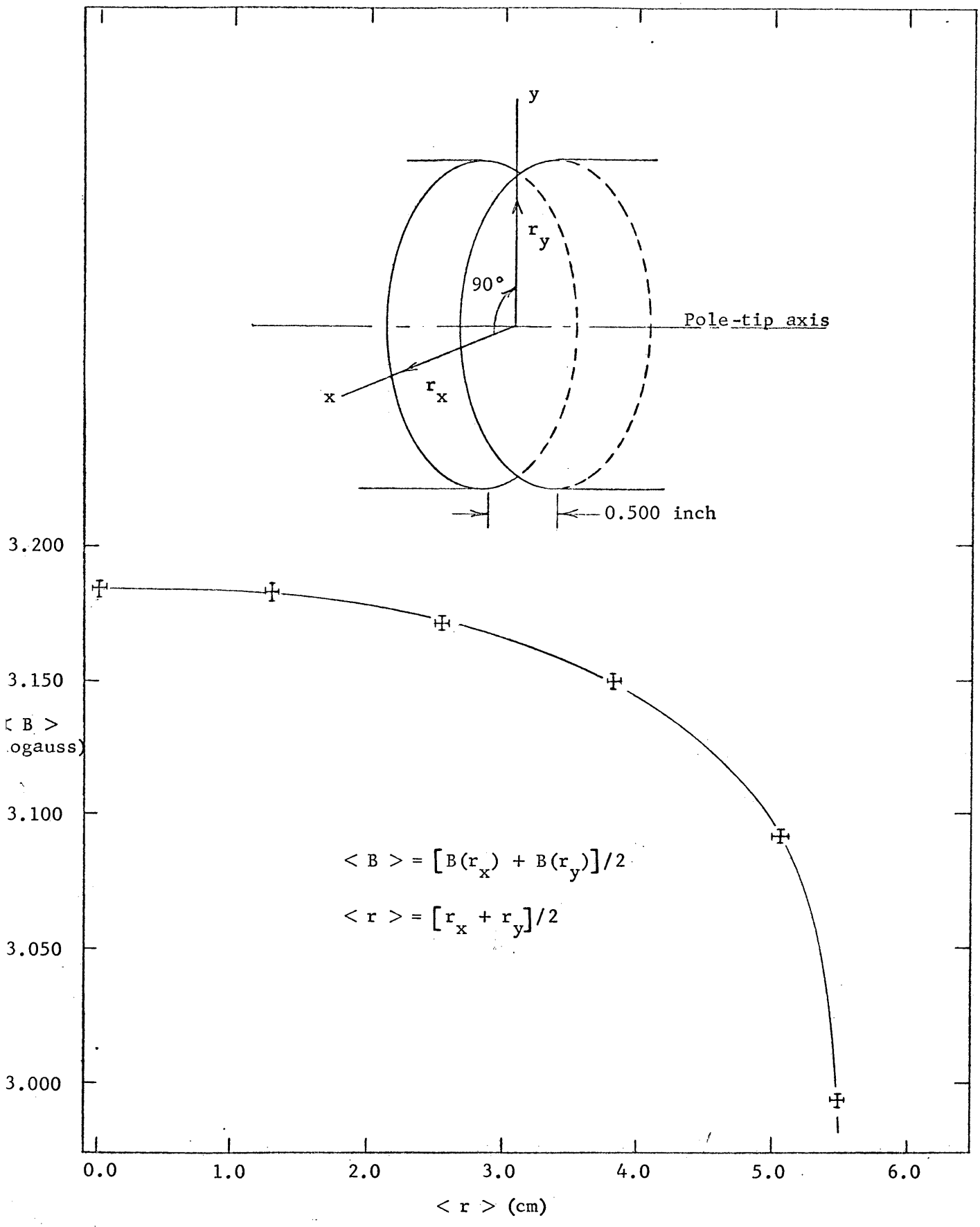

re 6. Radial variation of < B > in the air gap of the magnet used in the Hall-effect asurements.

TABLE 6

THE RADIAL VARIATION OF THE MAGNETIC FIELD

r_x (cm)	r_y (cm)	$< r >^*$ (cm)	$B(r_x)$	$B(r_y)$ (kilogauss)	$< B >^{**}$
0	0		13.182	13.208	
					13.193
0	0	0	13.185	13.200	
1.27	1.27	1.27	13.180	13.185	13.182
2.54	2.54	2.54	13.170	13.185	13.177
3.80	3.80	3.80	13.150	13.147	13.148
5.08	5.08	5.08	13.092	13.095	13.094
5.48	5.48	5.48	12.929	12.936	12.932
6.67	6.67	6.67	7.269	7.266	7.267
6.99	6.99	6.99	5.661	5.670	5.665
7.62	7.62	7.62	3.770	3.770	3.770
8.26	8.26	8.26	2.495	2.490	2.492
8.89	8.89	8.89	2.209	2.215	2.212
9.53	9.53	9.53	1.835	1.835	1.835
10.16	10.16	10.16	1.560	1.550	1.555

$^*< r > = [r_x + r_y]/2$ $^{**}< B > = [B(r_x) + B(r_y)]/2$

distance of $r = 4.6$ cm from the cylindrical axis of the pole tips. The value of B at this location differed from that at $r = 0$ by only 0.5 percent. Therefore, the value of the field at the sample was taken equal to the value determined with the probe.

A Leeds and Northrup potentiometer, Model 7645, was used to read the output emf of the probe and an operating current of 16 ma was supplied to the probe by a Lambda power supply, Model C-480. All probe output emf values were normalized to output at an operating current of 16 ma and 290°K temperature. Thus, the probe temperature and input current were measured each time the probe emf was read. The magnitude of the input current to the probe was monitored by measuring the potential difference across a 0.01-ohm resistor in series with the probe. In conjunction with the same potentiometer used to measure the probe emf, a copper-constantan thermocouple served to determine the probe temperature.

The overall sensitivity of the system appears to be limited by an uncertainty of ± 10 μv in the magnitude of any potentiometer reading. Estimated error in the measured magnetic field arising from this uncertainty ranges from approximately 0.02 percent at 13 kilogauss to 0.2 percent at 1 kilogauss.

Measurement procedure

Hall-voltage measurements were made on each sample at from 10 to 15 different values of the magnetic held in the range $0 \leq B \leq 13$ kilogauss.

Initially, the contact on the copper slidewire was adjusted at $B = 0$ to yield approximately zero potential-difference between points a and b in Figure 4. A magnetic field was established in the positive direction, and its magnitude determined. Immediately afterward, the magnitude of the sample current of 1.0000 amp was checked by measuring the potential difference across standard resistor in series with the sample; the Hall voltages were determined for both directions of the sample current. The direction of the field was then reversed, and the Hall voltages again were determined for both directions of the current. This procedure, in which the Hall voltage is determined for each of the four possible combinations of $\pm I$, $\pm B$, was repeated at least four more times. Thus, a typical set of Hall-voltage measurements at each magnitude of B chosen for measurement comprised at least 20 measured potential differences from which five corrected values of V_a^{21} were obtained by use of equation 33. After completion of the Hall-voltage measurements, the magnitudes of the sample current and magnetic field were again determined.

Transverse magnetoresistance data were taken only infrequently. The potential differences were read between points c and d (Figure 4) for both directions of the current. The magnetic field was not reversed because the magnetoresistance was known to be an even function of B.

TABLE 7

COMPARISON OF RESISTIVITIES, ρ^{11}, AT ROOM TEMPERATURE BEFORE AND AFTER DESCENT TO 80°K

Sample	ρ_1^{11*} (10^{-4} Ω · cm)	ρ_2^{11**} (10^{-4} Ω · cm)	$\frac{\rho_2^{11} - \rho_1^{11}}{\rho_1^{11}}$ (percent)
R-1-Au	2.697	2.926	8.5
R-2-Au	2.646	2.903	9.7
R-3-Au	2.529	2.795	10.5
R-4-Au	2.616	2.959	13.15
R-5-Au	2.498	2.773	11.0
R-6-Au	2.541	2.895	12.1
R-7-Au	2.495	2.739	8.9
R-8-Au	1.273	1.637	28.6
R-1-Te	2.368	2.752	16.2
R-2-Te	2.615	3.014	15.3
R-3-Te	2.345	2.829	20.7
R-4-Te	1.074	1.358	26.5
R-5-Te	1.731	2.192	26.6

*Resistivity at 298°K before temperature descent.

**Resistivity at 298°K after temperature descent.

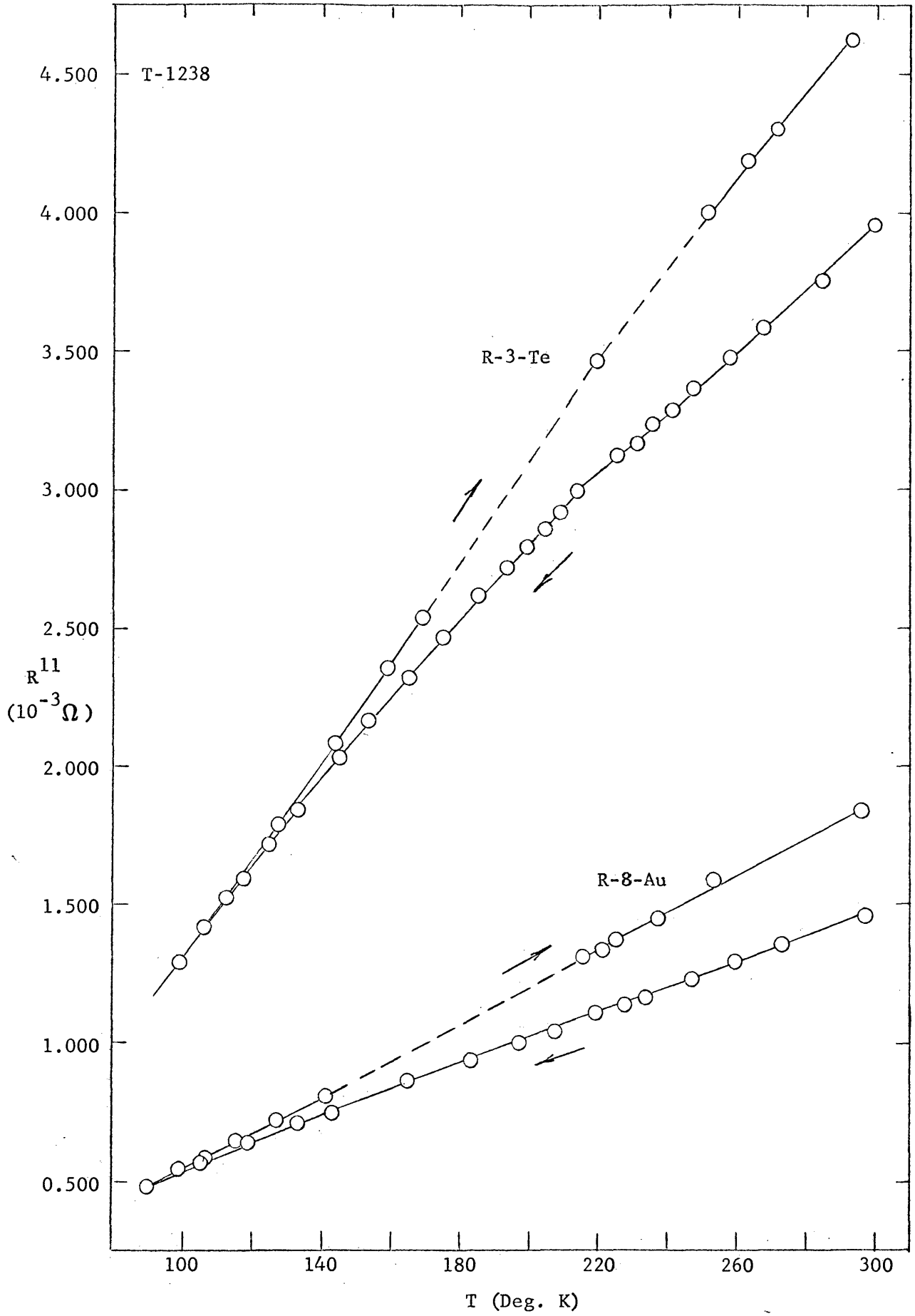

Figure 7. Resistance values determined for samples R-8-Au and R-3-Te during temperature descent and ascent. Arrows indicate the direction of the temperature change.

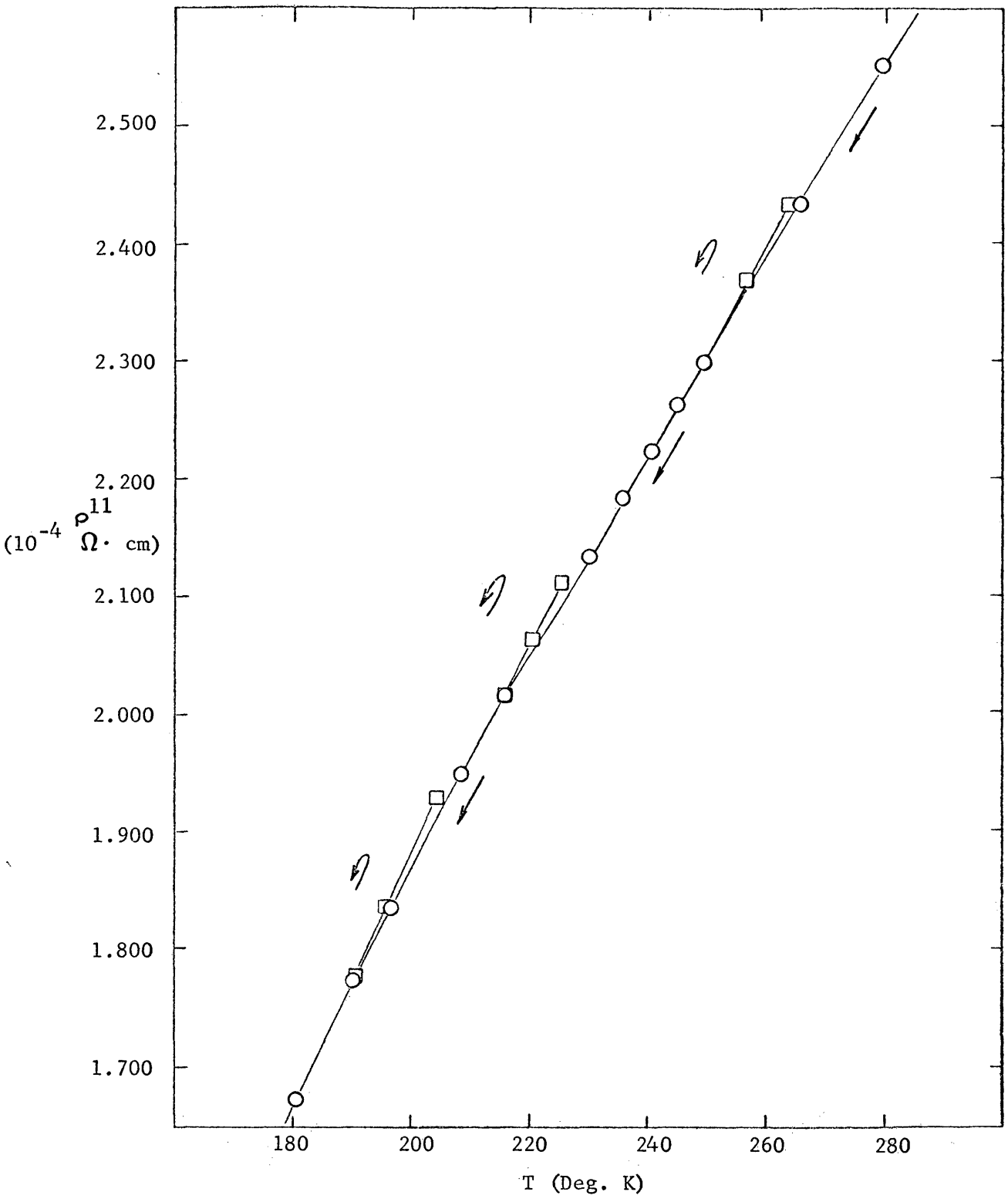

Figure 8. Hysteresis in the resistivity ρ^{11} of sample R-9-Au induced by temperature cycling. The run was begun at T = 294.4°K. Arrows show the direction of changes in temperature; circles and squares denote data taken after temperature descent and ascent, respectively. Uncertainties in ρ^{11} and T are less than $0.004 \times 10^{-4}\ \Omega \cdot cm$ and 0.33°K, respectively, over $160° \leq T \leq 300°K$.

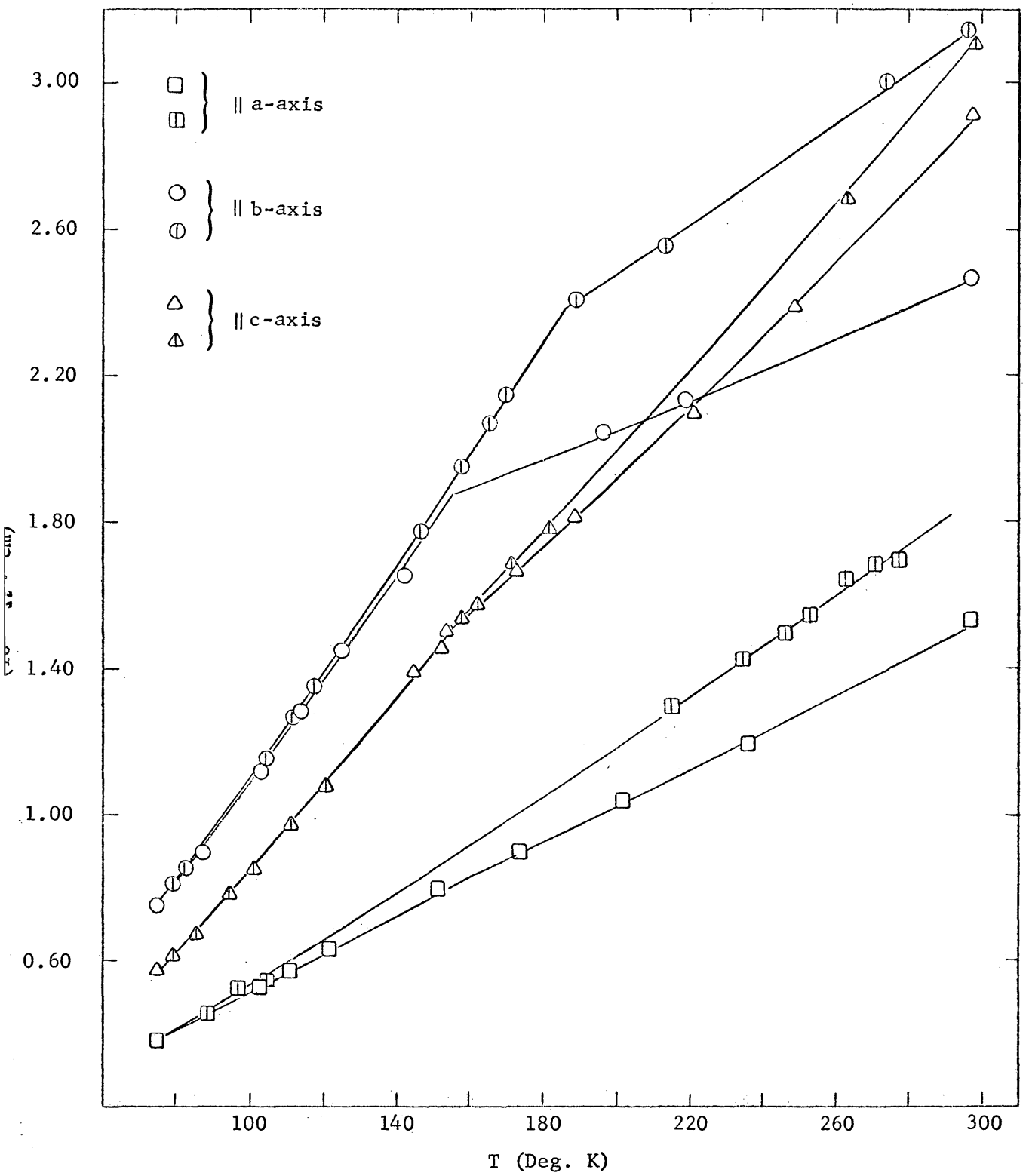

Figure 9. Resistivity values obtained in Reference 2 for samples with nominal orientations corresponding to the crystallographic a-, b-, and c-axes. Results obtained during temperature descent (open symbols) and ascent (barred symbols) are shown.

DATA REDUCTION AND PRESENTATION OF RESULTS

Described in the following sections are methods of calculating the four nonzero components of the zero-magnetic-field resistivity tensor and the components ρ_{123}, ρ_{231}, and ρ_{132} of the Hall-tensor, along with results. The calculation of the transverse magnetoresistance from data which were taken for a few samples are also presented. Because of the limited quantity of these data, no calculation of any of the 12 components, ρ_{iklm}, of the magnetoresistivity tensor can be made.

ZERO-MAGNETIC-FIELD RESISTIVITY DATA

The calculation of the four independent components of this tensor for both types of materials (Au-rich and Te-rich) at equally spaced temperatures (intervals of 4°K) followed a rather complex course. Because of hysteresis in the values of sample resistance evidenced on temperature cycling (Table 7 and Figures 7 and 8), only the data taken during descent from room temperature were used in the calculations. Details of the calculations used to obtain the values of ρ^{o}_{ik}--Tables 8 and 9 and graphically shown in Figures 10 and 11--are given below. Quantities obtained in the intermediate calculations are presented in the tables of Appendix 5. A CDC 8090 computor was used in all the calculations.

Treatment of V^{11} and V_s

Treatment of these data obtained at each measurement temperature (V^{11} and V_s are the potential differences across the sample and standard resistor, respectively) followed conventional methods. The five values of V^{11} measured for positive current direction and the five corresponding values obtained for the opposite current direction were first averaged in pairs to eliminate parasitic thermoelectric emfs; the five resulting values were then averaged. Standard deviations of any of these sets were typically less than the uncertainty in reading the potentiometer, approximately 0.5 μv. The V_s data in each set of data were treated in the same way. Because these potential differences ranged between 1,000 and 1,500 μv, standard deviation of ± 1 μv were considered acceptable in these averaged sets. The values of the potential differences obtained from these averaging procedures, labeled V^{11} and V_s, are contained in Tables A 5.1 through A 5.13.

Least-Square Fit to the R^{11}

By use of $R^{11} = (V^{11}/V_s)R_s$, (Equation 31) and the averaged values of V^{11} and V_s, the sample resistance R^{11} at each measurement temperature was calculated. Polynomials of best fit, $R^{11} = f(T)$, were fitted to the R^{11} data over intermediate temperature ranges by the method of least-squares. The criterion of minimum variance was used to select the approximating polynomials of best fit. Also, at the common boundary point of the temperature ranges of definition of two polynomials, the two values of R^{11} calculated by use of the polynomials

and the experimentally derived R^{11} were required to agree to within $\pm\Delta R^{11}$, the propogated error or uncertainty in the experimental R^{11}.

The uncertainties, ΔR^{11}, typically $\pm 5 \times 10^{-6}\ \Omega\cdot cm$, were calculated from values of experimental uncertainties in V^{11} and V_s of approximately 0.5 and 1 μv, respectively. The calculation of ΔR^{11} proceeded according to the theory[35] of the propogation of error or uncertainty in functions of the form $f(x_1, x_2, \ldots, x_n)$. The propogated error or uncertainty, $\Delta f(x_1, x_2, \ldots, x_n)$, in the function arising from the Δx_i, or errors (assumed to be mutually independent) in the x_i, is given by

$$[\Delta f(x_1, x_2, \ldots, x_n)]^2 = \sum_{i=1}^{n} \left[\frac{\partial f}{\partial x_i}\right]^2 (\Delta x_i)^2. \qquad (34)$$

For each sample, experimentally determined values of R^{11} and calculated uncertainties ΔR^{11} are contained in Appendix 5. Presented also in this appendix are the approximating polynomials and the residuals calculated during the fitting procedure. Calculated values of R^{11} and the curves derived from the fitted polynomials are presented graphically for two samples, R-3-Te and R-8-Au in Figure 7.

Calculation of the ρ^{11}

For each sample, values of ρ^{11} were calculated at evenly spaced temperatures (4°K increments) through use of the approximating polynomials for R^{11} (Appendix 5) and the geometric constants.

The error in ρ^{11}, $\Delta\rho^{11}$, arising from uncertainties in R^{11} and in the geometric constants were calculated from data appropriate to 80° and 300°K using Equation 34. These values of $\Delta\rho^{11}$ (Tables A 6.1 and A 6.2) are, respectively, the minimum and maximum values of the uncertainty in the appropriate ρ^{11} over the temperature range.

Determination of the Resistivity-Tensor Components

The ρ^{o}_{ik} are linearly related to ρ^{11} for a sample of arbitrary orientation through Equation 27. Thus, the eight and five calculated values of ρ^{11} for the different samples of the Au- and Te-excess materials constitute sets of overdetermined equations at each of the equally spaced temperatures. These sets of equations were solved by the method of least-squares[36,37] for the components ρ^{o}_{ik} for each material as functions of temperature. The results are given in Tables 8 and 9 and Figures 10 and 11.

An estimate of the error in each determined ρ^{o}_{ik}, that is, the standard deviation[37], δ_{ik}, was calculated for the temperatures, 80°, 136°, 216°, and 300°K. The temperatures 80° and 300°K bound the temperature range investigated and, as will be seen, 136° and 216°K are temperatures at which the ρ^{o}_{ik} exhibit breaks in their temperature behavior. The values of δ_{ik} are listed at the end of Tables 8 and 9.

TABLE 8

VALUES OF THE ρ^{o}_{ik} AND δ_{ik} DETERMINED FOR THE Te-EXCESS MATERIAL

Temperature (Deg. K)	ρ^{o}_{11} (10^{-4} Ω · cm)	ρ^{o}_{22} (10^{-4} Ω · cm)	ρ^{o}_{33} (10^{-4} Ω · cm)	ρ^{o}_{12} (10^{-4} Ω · cm)
300	2.51	1.31	2.47	0.71
296	2.47	1.29	2.43	0.69
292	2.44	1.26	2.39	0.69
288	2.41	1.25	2.35	0.68
284	2.38	1.23	2.32	0.67
280	2.35	1.21	2.29	0.66
276	2.32	1.20	2.26	0.65
272	2.29	1.18	2.24	0.64
268	2.26	1.16	2.21	0.63
264	2.23	1.14	2.18	0.61
260	2.20	1.13	2.16	0.60
256	2.16	1.11	2.13	0.59
252	2.13	1.10	2.11	0.57
248	2.11	1.08	2.10	0.56
244	2.07	1.06	2.09	0.54
240	2.04	1.05	2.07	0.53
236	2.01	1.03	2.05	0.51
232	1.98	1.01	2.03	0.50
228	1.95	1.00	2.02	0.48
224	1.91	0.98	2.01	0.46
220	1.88	0.96	2.01	0.45
216	1.86	0.94	2.00	0.43
212	1.83	0.92	1.97	0.41
208	1.79	0.91	1.94	0.40
204	1.76	0.89	1.90	0.39
200	1.73	0.88	1.86	0.38

TABLE 8--Cont.

Temperature (Deg. K)	ρ^{o}_{11} (10^{-4} Ω · cm)	ρ^{o}_{22} (10^{-4} Ω · cm)	ρ^{o}_{33} (10^{-4} Ω · cm)	ρ^{o}_{12} (10^{-4} Ω · cm)
196	1.69	0.86	1.83	0.37
192	1.66	0.84	1.80	0.36
188	1.62	0.83	1.77	0.35
184	1.59	0.81	1.73	0.34
180	1.55	0.80	1.70	0.33
176	1.52	0.78	1.66	0.32
172	1.48	0.76	1.62	0.31
168	1.45	0.75	1.59	0.31
164	1.41	0.73	1.55	0.30
160	1.37	0.72	1.51	0.30
156	1.34	0.70	1.47	0.29
152	1.30	0.69	1.44	0.29
148	1.27	0.67	1.39	0.29
144	1.23	0.66	1.35	0.29
140	1.19	0.64	1.30	0.29
136	1.16	0.63	1.25	0.29
132	1.12	0.61	1.21	0.28
128	1.08	0.60	1.16	0.28
124	1.04	0.58	1.13	0.26
120	1.00	0.56	1.08	0.25
116	0.96	0.54	1.04	0.24
112	0.91	0.52	0.99	0.23
108	0.87	0.50	0.96	0.22
104	0.83	0.48	0.92	0.21
100	0.79	0.46	0.87	0.20
96	0.75	0.45	0.82	0.19
92	0.70	0.43	0.78	0.18
88	0.66	0.41	0.74	0.17

TABLE 8--Cont.

Temperature (Deg. K)	ρ^{o}_{11} (10^{-4} Ω · cm)	ρ^{o}_{22} (10^{-4} Ω · cm)	ρ^{o}_{33} (10^{-4} Ω · cm)	ρ^{o}_{12} (10^{-4} Ω · cm)
84	0.62	0.39	0.70	0.16
80	0.58	0.37	0.65	0.15
Temperature (Deg. K)	δ_{11} (10^{-4} Ω · cm)	δ_{22} (10^{-4} Ω · cm)	δ_{33} (10^{-4} Ω · cm)	δ_{12} (10^{-4} Ω · cm)
300	0.06	0.09	0.04	0.10
216	0.06	0.09	0.04	0.06
136	0.04	0.04	0.03	0.03
80	0.02	0.02	0.02	0.03

TABLE 9

VALUES OF THE ρ^{o}_{ik} AND δ_{ik} DETERMINED FOR THE Au-EXCESS MATERIAL

Temperature (Deg. K)	ρ^{o}_{11} (10^{-4} $\Omega \cdot$ cm)	ρ^{o}_{22} (10^{-4} $\Omega \cdot$ cm)	ρ^{o}_{33} (10^{-4} $\Omega \cdot$ cm)	ρ^{o}_{12} (10^{-4} $\Omega \cdot$ cm)
300	2.51	1.31	2.39	0.43
296	2.48	1.29	2.36	0.44
292	2.44	1.26	2.33	0.45
288	2.40	1.25	2.30	0.45
284	2.38	1.23	2.28	0.45
280	2.35	1.21	2.26	0.45
276	2.32	1.19	2.24	0.44
272	2.29	1.17	2.22	0.44
268	2.27	1.15	2.21	0.43
264	2.24	1.13	2.19	0.42
260	2.22	1.11	2.18	0.40
256	2.19	1.09	2.16	0.39
252	2.17	1.07	2.15	0.38
248	2.15	1.05	2.13	0.36
244	2.12	1.03	2.12	0.35
240	2.09	1.01	2.10	0.34
236	2.07	0.99	2.09	0.32
232	2.04	0.98	2.08	0.31
228	2.02	0.98	2.08	0.29
224	1.99	0.96	2.06	0.28
220	1.97	0.95	2.06	0.26
216	1.94	0.94	2.04	0.26
212	1.90	0.92	2.01	0.26
208	1.86	0.90	1.98	0.25
204	1.83	0.88	1.95	0.25
200	1.79	0.87	1.91	0.25

TABLE 9--Cont.

Temperature (Deg. K)	ρ^{o}_{11} (10^{-4} Ω · cm)	ρ^{o}_{22} (10^{-4} Ω · cm)	ρ^{o}_{33} (10^{-4} Ω · cm)	ρ^{o}_{12} (10^{-4} Ω · cm)
196	1.75	0.85	1.87	0.25
192	1.72	0.84	1.82	0.25
188	1.68	0.82	1.78	0.25
184	1.64	0.80	1.73	0.26
180	1.60	0.79	1.68	0.26
176	1.56	0.77	1.62	0.26
172	1.52	0.75	1.57	0.27
168	1.47	0.74	1.51	0.27
164	1.43	0.72	1.46	0.27
160	1.39	0.70	1.40	0.27
156	1.35	0.69	1.34	0.28
152	1.30	0.67	1.29	0.28
148	1.26	0.65	1.24	0.28
144	1.22	0.64	1.19	0.28
140	1.17	0.62	1.14	0.29
136	1.13	0.60	1.09	0.29
132	1.09	0.59	1.04	0.27
128	1.07	0.58	0.98	0.26
124	1.00	0.55	0.95	0.26
120	0.96	0.54	0.90	0.25
116	0.91	0.52	0.86	0.25
112	0.87	0.51	0.81	0.24
108	0.83	0.49	0.77	0.23
104	0.78	0.48	0.73	0.22
100	0.75	0.46	0.68	0.22
96	0.70	0.44	0.63	0.21
92	0.66	0.42	0.59	0.20
88	0.62	0.40	0.55	0.19

TABLE 9--Cont.

Temperature (Deg. K)	ρ^{o}_{11} (10^{-4} Ω · cm)	ρ^{o}_{22} (10^{-4} Ω · cm)	ρ^{o}_{33} (10^{-4} Ω · cm)	ρ^{o}_{12} (10^{-4} Ω · cm)
84	0.58	0.38	0.50	0.18
80	0.54	0.36	0.45	0.17
Temperature (Deg. K)	δ_{11} (10^{-4} Ω · cm)	δ_{22} (10^{-4} Ω · cm)	δ_{33} (10^{-4} Ω · cm)	δ_{12} (10^{-4} Ω · cm)
300	0.09	0.08	0.01	0.09
216	0.08	0.05	0.01	0.05
136	0.03	0.03	0.004	0.03
80	0.03	0.03	0.004	0.03

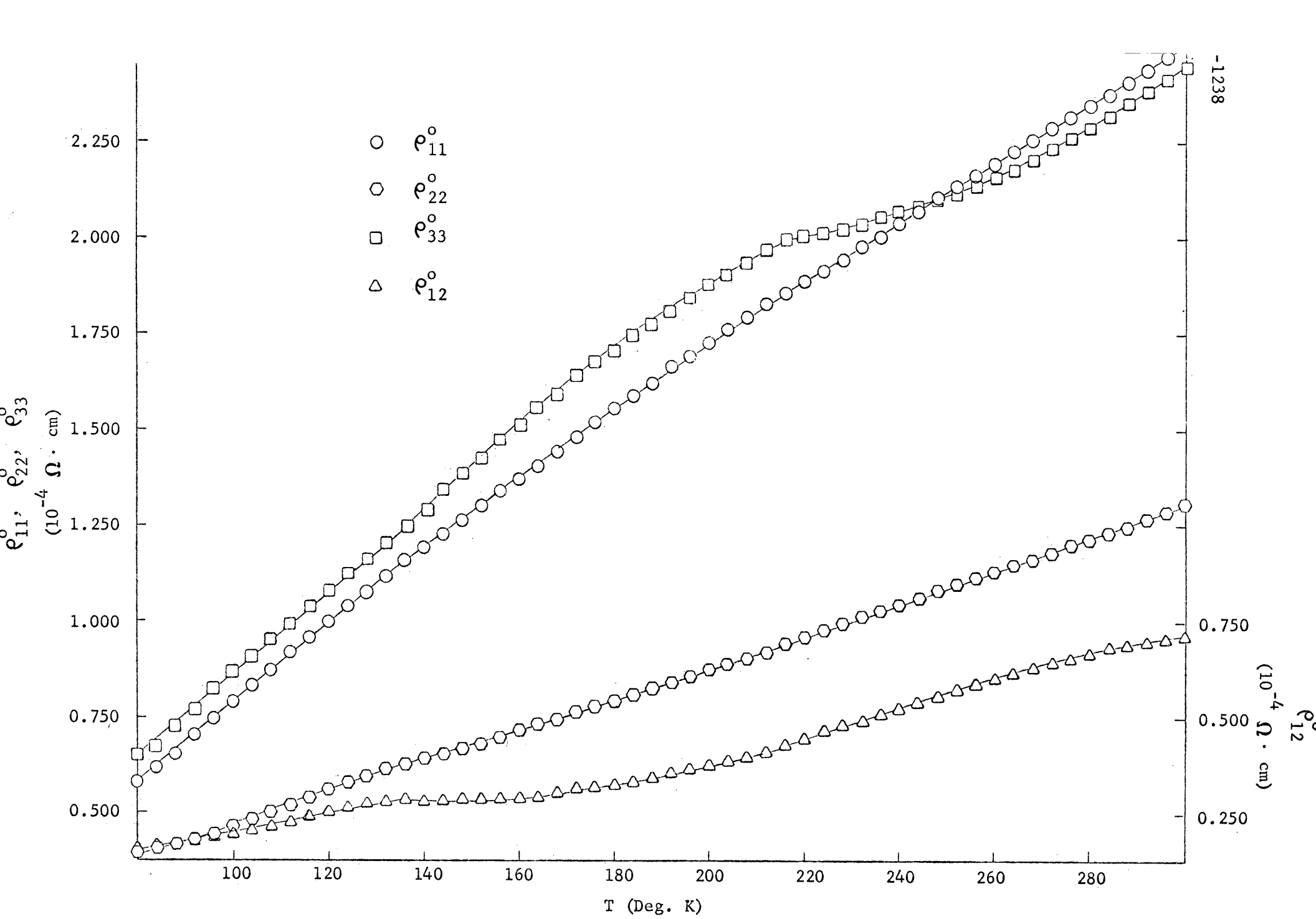

Figure 10. Values of the four nonzero ρ^o_{ik} for $AuTe_2$ containing excess Te.

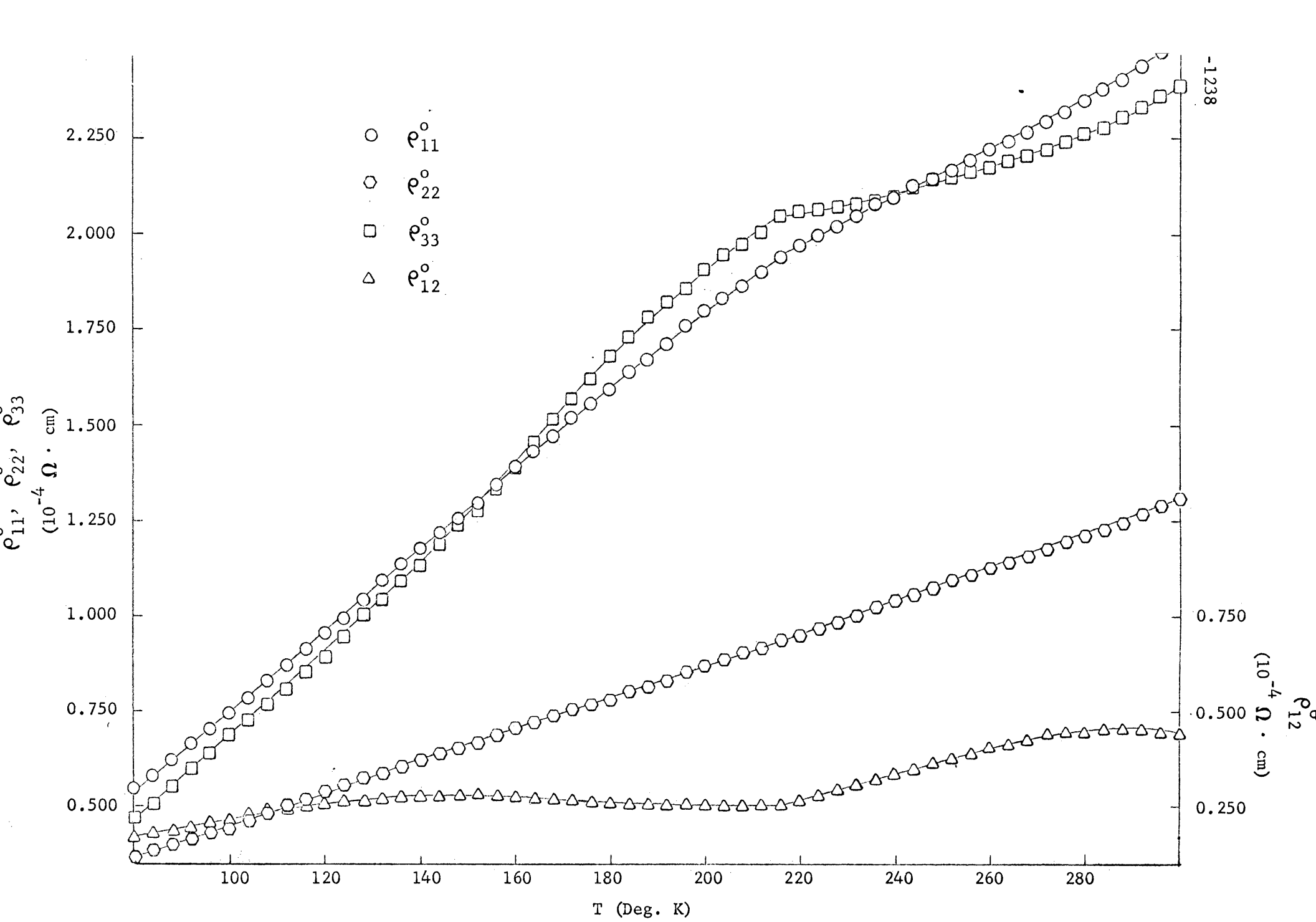

Figure 11. Values of the four nonzero ρ^o_{ik} for $AuTe_2$ containing excess Au.

HALL-EFFECT DATA

Three components of the Hall tensor, ρ_{123}, ρ_{231}, and ρ_{132}, for the materials obtained from both melts are calculated from the Hall-effect measurements. Because the samples, during the measurements, could not be rotated with respect to the magnetic field complete determination of the tensors could not be made (Equation 30).

Determination of the R_a^{21}

Before reduction of the Hall-effect data for the components of the tensor, preliminary steps were necessary. Each set of five values of the transverse potential difference, V_a^{21}, obtained from experimental data by use of Equation 33, was averaged to give the quantity $< V_a^{21} >$. Ten to fifteen such average values were determined for each sample. Each $< V_a^{21} >$ corresponds to a known value of the magnetic field, B, between 0 and 13 kilogauss. By least-square technique these data for each sample were fitted to a linear relation of the form,

$$< V_a^{21} >/I = A + R_a^{21} B. \tag{35}$$

Values of the constants A and R_a^{21} and of $< V_a^{21} >/I$ at measured values of B for each sample are given in Appendix 7. The uncertainty given for each of the constants is the standard deviation. The experimental quantities $< V_a^{21} >/I$ and the approximating linear function for the different samples are graphed in Figures 12 and 13.

Ideally, the intercept A should be identically zero for all samples. A number of samples have values of A and its standard deviation, δ_A, so that the origin is included in $A \pm \delta_A$; however, some samples have values of $A \pm \delta_A$ which exclude the origin. The nonzero intercept may indicate the presence of "systematic" errors arising from operator bias in determining small Hall voltages (in the range of 5 to 20 μv) with the K-3 potentiometer and the presence of small nonlinearites in the slide wire.

Calculation of ρ_a^{21}

The constants R_a^{21} and sample thickness t (Table 3) were used to obtain values of ρ_a^{21} for each of the samples of arbitrary orientation (Table 10). Values of the propogated error, ρ_a^{21}, in each of the ρ_a^{21} are also included in the table. For the error calculation the uncertainty in each R_a^{21} was taken to be the calculated standard deviation and a value of $\pm 1 \times 10^{-3}$ cm was used as the uncertainty in the sample thickness t. This value is believed to represent adequately the errors in positioning the hairline and those due to parallax.

Determination of Selected ρ_{ikl}

As a value of ρ_a^{21} was calculated for each Hall-effect sample of arbitrary orientation, sets of overdetermined equations of the form of Equation 30 were obtained for both materials used in this study.

The set of overdetermined equations for each of the two materials was solved for ρ_{123}, ρ_{231}, ρ_{132}, and $[\rho_{131} + \rho_{322}]$ by the same least-squares method used in the solution for the ρ^{o}_{ik}. Values of the ρ_{ikl} obtained by this method and the associated standard deviations[36] are listed in Table 11.

MAGNETORESISTANCE DATA

The transverse magnetoresistance change[39], that is, the change in ρ^{11} caused by a transverse magnetic field B, is calculated from

$$\delta\rho^{11} = \rho^{11}(B) - \rho^{11}(B = 0). \tag{36}$$

The resistivities are those determined parallel to the laboratory coordinate, X^1, with J parallel to this axis, and B parallel to X^3.

The results of the calculation for samples H-1-Au, H-2-Au, H-3-Au, and H-1-Te (the only samples for which data were taken) are given in Table 12. Values of uncertainty in the results calculated by use of equation 34 are also included.

TABLE 10

VALUES OF THE RESISTIVITY ρ_a^{21}

Sample	ρ_a^{21} $\left(\frac{10^{-11}\ \Omega \cdot \text{cm}}{\text{gauss}}\right)$	$\Delta\rho_a^{21}$ $\left(\frac{10^{-11}\ \Omega \cdot \text{cm}}{\text{gauss}}\right)$
H-1-Au	- 9.0	0.1
H-2-Au	- 3.61	0.05
H-3-Au	-10.42	0.08
H-4-Au	- 8.5	0.1
H-5-Au	-15.2	0.2
H-6-Au	- 3.31	0.08
H-7-Au	- 4.47	0.08
H-8-Au	- 4.74	0.07
H-1-Te	- 5.75	0.06
H-2-Te	- 4.72	0.09
H-3-Te	-11.4	0.09
H-4-Te	- 7.8	0.1
H-5-Te	- 5.9	0.1
H-6-Te	- 6.5	0.1
H-7-Te	-12.2	0.2

TABLE 11

DETERMINED ρ_{ikl} OF THE HALL TENSOR

Material	ρ_{123} 10^{-11} $\frac{\Omega \cdot cm}{gauss}$	ρ_{231} 10^{-11} $\frac{\Omega \cdot cm}{gauss}$	ρ_{132} 10^{-11} $\frac{\Omega \cdot cm}{gauss}$	$[\rho_{131} + \rho_{322}]$ 10^{-11} $\frac{\Omega \cdot cm}{gauss}$
Te-excess	+11.4±3	+9.3±0.5	-5.8±0.4	-19.3±5
Au-excess	+16.1±0.7	+9.6±2	-6.3±0.7	- 9.4±2

TABLE 12

MAGNETORESISTANCE CHANGES

Sample*	$\rho^{11}(B)$ (10^{-4} Ω · cm)	$\rho^{11}(B = 0)$ (10^{-4} Ω · cm)	$\rho^{11}(B) - \rho^{11}(B = 0)$ (10^{-8} Ω · cm)	B (kilogauss)
H-1-Au	2.431	2.429	22±6	13.13
H-2-Au	2.520	2.519	10±5	13.08
H-3-Au	2.463	2.461	18±5	13.05
H-1-Te	2.384	2.379	5±3	12.22

* Gauge length between points c and d of Figure 4 was 0.4905 cm for the first two samples and 1.012 cm for the latter two.

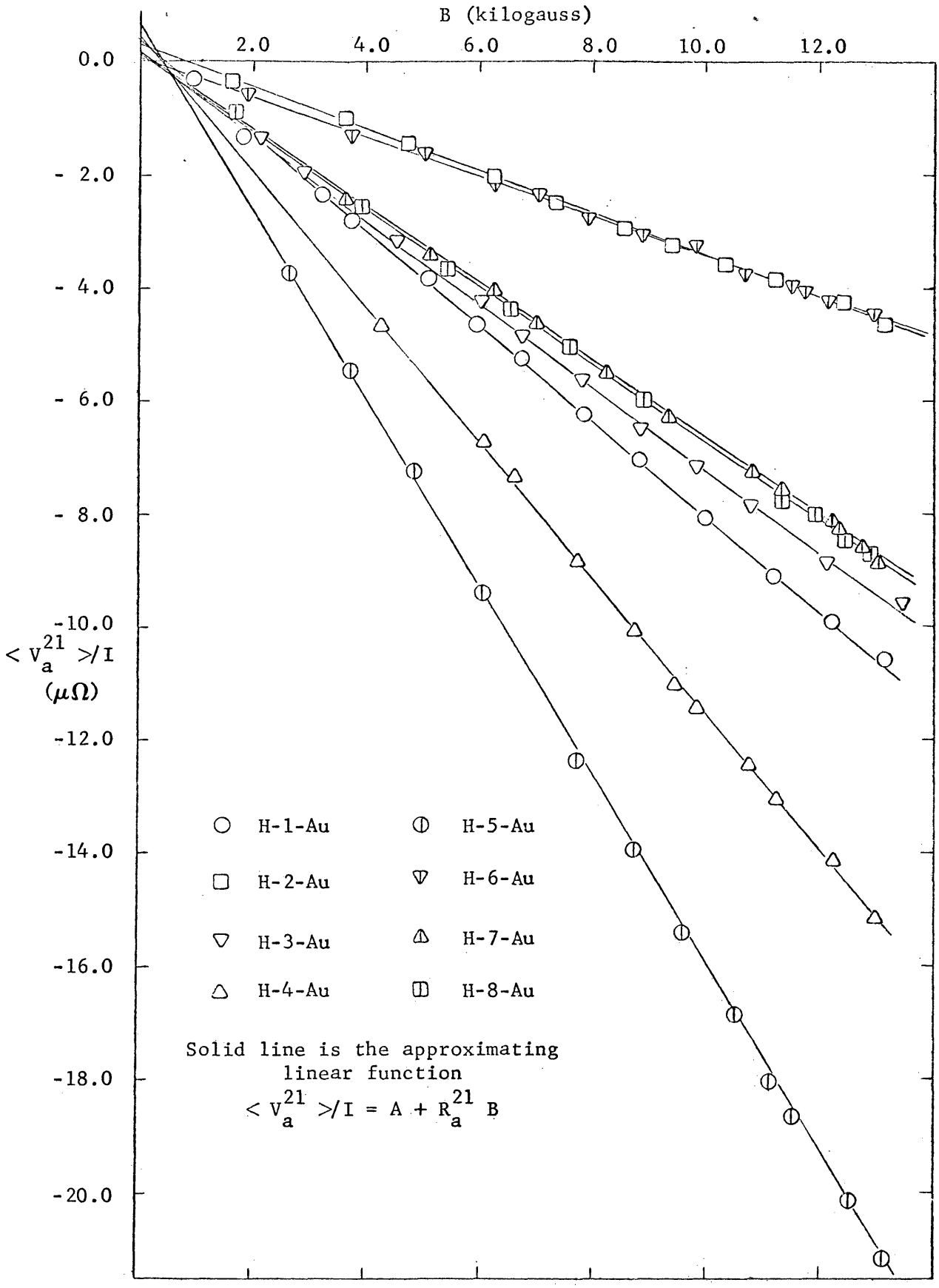

Figure 12. Hall-effect data for the samples containing excess Au.

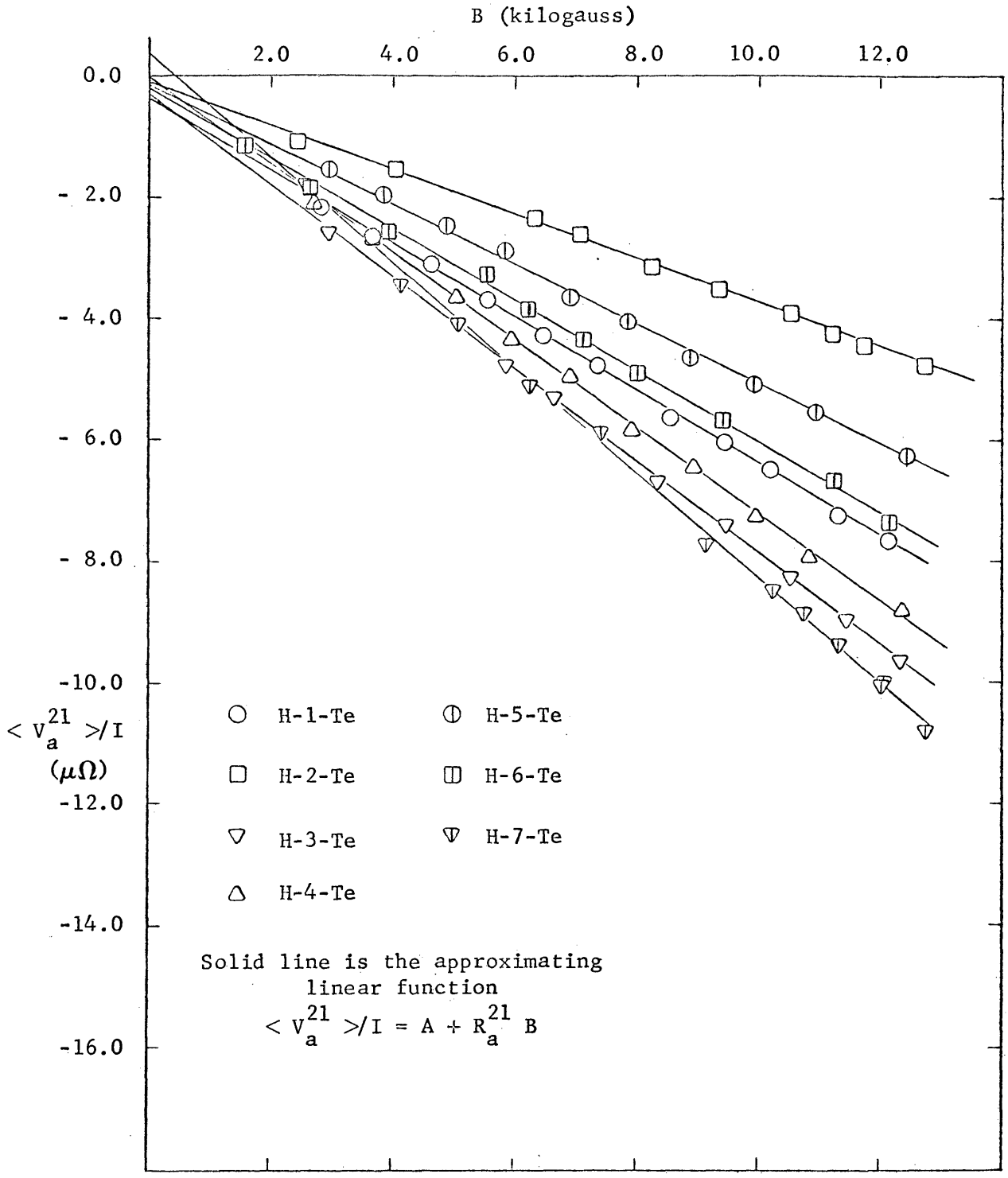

Figure 13. Hall-effect data for the samples containing excess Te.

DISCUSSION OF RESULTS

Possible mechanisms which may account for the complex low-temperature behavior of the components of the zero-magnetic-field resistivity tensor are considered in this section. The results are further examined for changes in electrical conductivity arising from compositional differences (different Au:Te ratios) between the Au- and Te-excess materials.

THE LOW-TEMPERATURE BEHAVIOR OF THE ρ^o_{ik}

Each component, ρ^o_{11}, ρ^o_{22}, ρ^o_{33}, and ρ^o_{12} of the zero-magnetic-field resistivity tensor determined for both types of materials generally increases in magnitude with increasing temperatures in the range $80° \leq T \leq 300°K$. However, for each of the components, the increase in magnitude with temperature is not uniform (Figures 10 and 11). Distinct changes in the temperature dependence, i.e., the temperature derivative, of each ρ^o_{ik} occur in the form of abrupt breaks at 136° and 216°K. Analagous changes are noted in the temperature behavior of the measured resistance values of some of the samples. As shown in Figures 10 and 11, this feature is particularly apparent in those samples having orientations with large direction cosines L^1_1 and L^1_2.

Below 136°K, all components ρ^o_{ik} determined for both the Te- and Au-excess materials increase approximately linearly with temperature.

At 136°K, the temperature derivative of each component, with but one exception, decreases abruptly. The component of exceptional behavior, ρ^o_{33}, determined for the Au- and Te-rich materials, demonstrates an increase in temperature derivative at this temperature. Notably, also,

the slope of the ρ^o_{12} curve determined for the Au-rich material actually becomes negative at the same temperature.

Between 136° and 216°K, the ρ^o_{ik} for each material, save the ρ^o_{33} and ρ^o_{12}, vary with temperature in an approximately linear fashion. For both materials the component ρ^o_{33} changes its initially linear behavior to demonstrate marked negative curvature of temperatures just below 216°K.

At T = 216°K, the components ρ^o_{22} and ρ^o_{12} determined for both materials increase sharply in slope. Conversely, for each component, ρ^o_{11} and ρ^o_{33}, the temperature derivative decreases markedly at this temperature. For temperatures between 216° and 300°K, the component ρ^o_{22} for both materials exhibits linear behavior; the curves of each of the other components demonstrate marked curvature over segments of this temperature range. Although the curvature in each of the components ρ^o_{11} and ρ^o_{33} is marked at the lower temperatures in this range, each approaches linear behavior at temperatures near 300°K. Moreover, for both materials the slope of each of these curves near 300°K appears to approximate that of ρ^o_{22} over the entire range $216° \leq T \leq 300°K$.

In the data of Reference 2 (Figure 9), no changes in temperature behavior of the samples having orientations nominally parallel to the a-, b-, and c-axes were detected at 136° and 216°K. Moreover, the slope changes deduced at 150°K largely from extrapolated data in that work were not detected in measurements on any of the samples of nearly a- and c-orientation used in this study (Table 4 and Figures 10 and 11). These discrepancies between the former and present investigations are attributed

to the rather sparsely taken data in the former work and possible large errors in the low-temperature measurements in that investigation because of inadequate thermal anchoring of the thermocouple leads.

Mechanisms which may act individually or cooperatively to cause the complex temperature behavior of the ρ^{o}_{ik} must account for:

1. Abrupt changes in temperature dependence of the resistivity, and

2. Ranges of approximately linear dependence of the components contrasted with regions of markedly non-linear behavior.

Attempts were made to explain the complex temperature dependence of the ρ^{o}_{ik} in terms of the following:

1. Relative band motion of two or more bands resulting in carrier transfer between bands with changing temperature[40,41],

2. thermal ionization of defects[42], and

3. phase transformations.

Of these mechanisms, the second is not consistent with the marked sharpness of the breaks in the resistivity-temperature curves. However, motion of a conduction or valence band across the Fermi surface and associated appearance or disappearance of a carrier can account for the breaks. Continued motion of the band with increasing temperature could explain the non-linearities in some of the curves. Details of the band structure, which are unavailable for $AuTe_2$, are necessary, however, for quantitative discussion.

The results of the previous low-temperature diffractometer study described in the introduction appear to exclude the presence of transformations resulting in gross changes in the crystal symmetry. However, occurrence of transformations at the two temperatures which involve only

small changes in the monoclinic C2/m symmetry of the compound are possible[2/]. This type of transformation, largely manifested by lattice constant changes, occurs in α-U between 35° and 43°K[43,44,45,46].

[2/] The X-ray structure of monoclinic $AuTe_2$ is discussed in Appendix 1.

The hysteresis of the resistivity measurements noted upon temperature cycling between 300° and 80°K may reflect structural damage introduced by cycling through a phase transformation of the type described above at each of the two temperatures. In this connection, the curves of sample resistance versus temperature for samples R-8-Au and R-3-Te presented in Figure 7; the resistivity data of Reference 2, Figure 9; and the percentage changes in resistivity for all samples used in the present research, which are noted in Table 7, are of interest. Particularly, those samples having orientations near to the crystallographic a- and b-axes (small θ_2^1 and θ_3^1) exhibit greater hysteresis than those corresponding to orientations nearer to the c-axis. This feature may arise from directional differences in the degree of structural damage induced by phase transformation.

However, the data of sample R-9-Au, shown in Figure 8, should be noted. Resistivity hysteresis was found in this sample upon temperature cycling above 216°K. Thus, in some part, the hysteresis in the resistivity appears to be caused by introduction or enhancement of structural imperfections by thermal strains incurred during cooling. Large changes (≈30 percent) in the resistivity ratio $\rho_{298°}/\rho_{1.90°}$ induced by

temperature cycling have been noted in As by Sybert and coworkers[47] in which analagous effects were found in Bi. The resistivity hysteresis in these elemental semimetals probably arises from strain induced (or enhanced) structural imperfection during cooling.

RESULTS AT 290°K

Features of the results of the Hall-effect measurements and zero-magnetic-field resistivity results near room temperature are consistent with characteristics of the phase field of the compound deduced from thermodynamic data. According to discussion in Appendix 1, the width of the phase field at temperatures between 400° and 447°C is only of the order of 10^{-2} atom percent Te. Furthermore, large variations in this value at temperatures nearer to the congruent melting point (464°C) are unlikely. Thus, compositional differences among samples obtained from each ingot, and, moreover, between the samples obtained from both parent ingots (grown from melts containing excess Te and Au, respectively) are probably small. Accordingly, differences in corresponding results calculated from the Hall-effect and resistivity measurements, if present, should be small.

As seen in Table 10, all measured ρ_a^{21} are negative, indicating that at room temperature the dominant conduction band (or bands) is n-type over the compositional range of $AuTe_2$.

Also, at 290°K the values of ρ_{231} and ρ_{132} determined for each material are equal to within the respective uncertainties. Only the determined values of ρ_{123} are clearly different in magnitude; the

signs of the determined components are the same for both materials. Figures 10 and 11 show determined values of ρ^{o}_{11} for these materials to be equal at room temperature. The components ρ^{o}_{22}, ρ^{o}_{33}, and ρ^{o}_{12} are seen to be larger for the Te-excess material than the corresponding components for the Au-excess material. However, only the values of ρ^{o}_{12} are clearly larger because of the uncertainties in the values of the components. These data appear to indicate a slight increase in conductivity with increasing Au:Te ratio.

Further examination of ρ^{o}_{ik} curves in Figures 10 and 11 show differences in the magnitudes of corresponding components of the materials at lower temperatures, particularly near 80°K. However, these data may be influenced by the presence of structural changes or damage associated with the previously discussed phase transformations or with the introduction (or enhancement) of structural imperfections with cooling. Accordingly, the low temperature data are not considered in this discussion.

THE MAGNETORESISTANCE CHANGE

As seen in Table 12, the magnetoresistance change in these samples is a small quantity, of the order of 1 part in 10^7 for B = 13kg. Large uncertainties (calculated by use of Equation 34) make these results of qualitative interest only. The small differences between the results seen in the table are probably because of the different orientations of these samples.

SUGGESTED FUTURE RESEARCH

According to results obtained in this investigation, further research is warranted in determining the band structure of the compound and the charge-carrier densities and mobilities over $0 < T < 464°K$ using samples with known Au:Te ratios. Additional investigation of the suspected phase transformations at 136° and 216°K is also indicated.

DETERMINATION OF THE BAND STRUCTURE

Aside from being of intrinsic interest, knowledge of the band structure is needed for calculating the charge-carrier densities and mobilities. Furthermore, this knowledge would be necessary in discussion of any relative band motion at lower temperatures.

Theoretical calculation of the band structure of this monoclinic compound, with complimentary experimental procedures, is probably the most desirable course of investigation.

DETERMINATION OF CHARGE-CARRIER DENSITIES AND MOBILITIES

Charge-carrier densities and mobilities are not only of intrinsic interest, particularly in multiband construction, which is suspected for this compound, but also of value in determining the mechanism causing the nonlinearities in the ρ^{o}_{ik}. Moreover, determination of the density and mobility of each carrier as functions of known sample compositions would be informative about any effects on conduction associated with small changes in the Au:Te ratio.

A sufficient number of independent equations derived from transport measurements, as well as knowledge of the band structure, are necessary to calculate the carrier densities and mobilities. Particularly, determination of the complete Hall tensor at temperatures, $0° < T < 464°K$, would be of interest in connection with any relative band motion or impurity ionization because of the sensitivity of the ρ_{ikl} to changes in carrier density and mobility.

Other transport measurements of interest may include determining all 12 of the ρ_{iklm} and the five components of the Seebeck-effect tensor from low temperatures to the melting point of the compound.

INVESTIGATION OF THE PHASE TRANSFORMATIONS

These transformations, if present, probably involve only small changes, as in the values of the lattice constants. Thus, techniques sensitive to small changes in lattice constants, such as precision lattice parameter and thermal-expansion measurements, as well as elastic constant determinations, could be of value in attempting to characterize the transformations.

APPENDIX 1

SELECTED PHYSICAL CONSTANTS AND PROPERTIES OF $AuTe_2$

Herein are presented X-ray structure constants and thermodynamic properties important to this work.

The X-Ray Structure Constants

Using samples of the naturally occurring form, Tunnell and Ksanda[49] have determined the structure of monoclinic $AuTe_2$ the mineral calaverite. The data of these workers are summarized in the following:

Space Group	Cell Constants				
C2/m	a(A°)	b(A°)	c(A°)	β	Cell Content
	7.19*	4.40*	5.07*	90°13'**	2($AuTe_2$)

* ±0.01 A°

** ±10'

Atomic Arrangement

Au in (a) 0, 0, 0; 1/2, 1/2, 0;

Te in (i) X, 0, Z; $\bar{X}$, 0, $\bar{Z}$; Z + 1/2, 1/2, Z; 1/2 - X, 1/2, $\bar{Z}$ with

X = 0.689, Z = 0.289

Within the unit cell, which contains 2($AuTe_2$), the Au atoms are on symmetry centers; the Te atoms are located on mirror planes. As shown in Figure A 1.1 each Au atom has six Te atoms as nearest neighbors. Two are located at 2.68±0.05 A° and four at 2.97±0.05 A°.

Each Te atom has three Au and three Te atoms as nearest neighbors. A Te atom is equally close (3.19 A°) to two of its three neighbors, the third lying at a greater distance, 3.47 A°. The Te atoms lying at mutual distances of 3.19 A° comprise puckered chains of Te atoms. Elemental tellurium contains chains of Te atoms in which the Te-Te distance is 2.68 A°. The 3.47 A° distance to the third neighbor lying in an adjacent chain is considerably less than the distance of 3.74 A° between neighbors in adjacent chains in elemental Te.

Thermodynamic Properties

The equilibrium Te vapor pressures over solid gold ditelluride and overliquid alloys near the composition $AuTe_2$ have been determined at various temperatures by Veale and Barrett[3]. The two vapor-pressure isotherms at 400° and 447°C for solid mixtures near the composition $AuTe_2$ are presented in Figure 1 of Reference 3. Compositional limits at the two temperatures inferred from the figure are given in the following table:

Temperature (°C)	Upper Limit (atom % Te)	Lower Limit (atom % Te)
400	66.67	66.63
447	66.70	66.66

These data are uncertain to ±0.02 atom percent Te according to the authors.

Grosser features of the Au-Te phase diagram important to this study are given by Hansen and Anderko[23]. Two eutectic points exist; one, involving the equilibrium $L \rightleftharpoons AuTe_2 + Au$ occurs at 447°C and 42 atomic percent Te and the other, $L \rightleftharpoons AuTe_2 + Te$, is located at 416°C and 88 atomic percent Te. These thermodynamic data indicate that the phase field of $AuTe_2$ is probably quite narrow, approximately 4×10^{-2} atomic percent wide at temperatures between 400° and 447°C. Furthermore, because the two eutectic points, which characterize the phase equilibrium of this system, occur at 416° and 447°C, respectively, the width of the field "$AuTe_2$" deduced from the thermodynamic data probably is a good approximation to the maximum value.

The DTA work on liquid alloys in Reference 3 and the phase diagram presented by Hansen and Anderko[23] indicate that the liquidus is extremely flat in the vicinity of the compound.

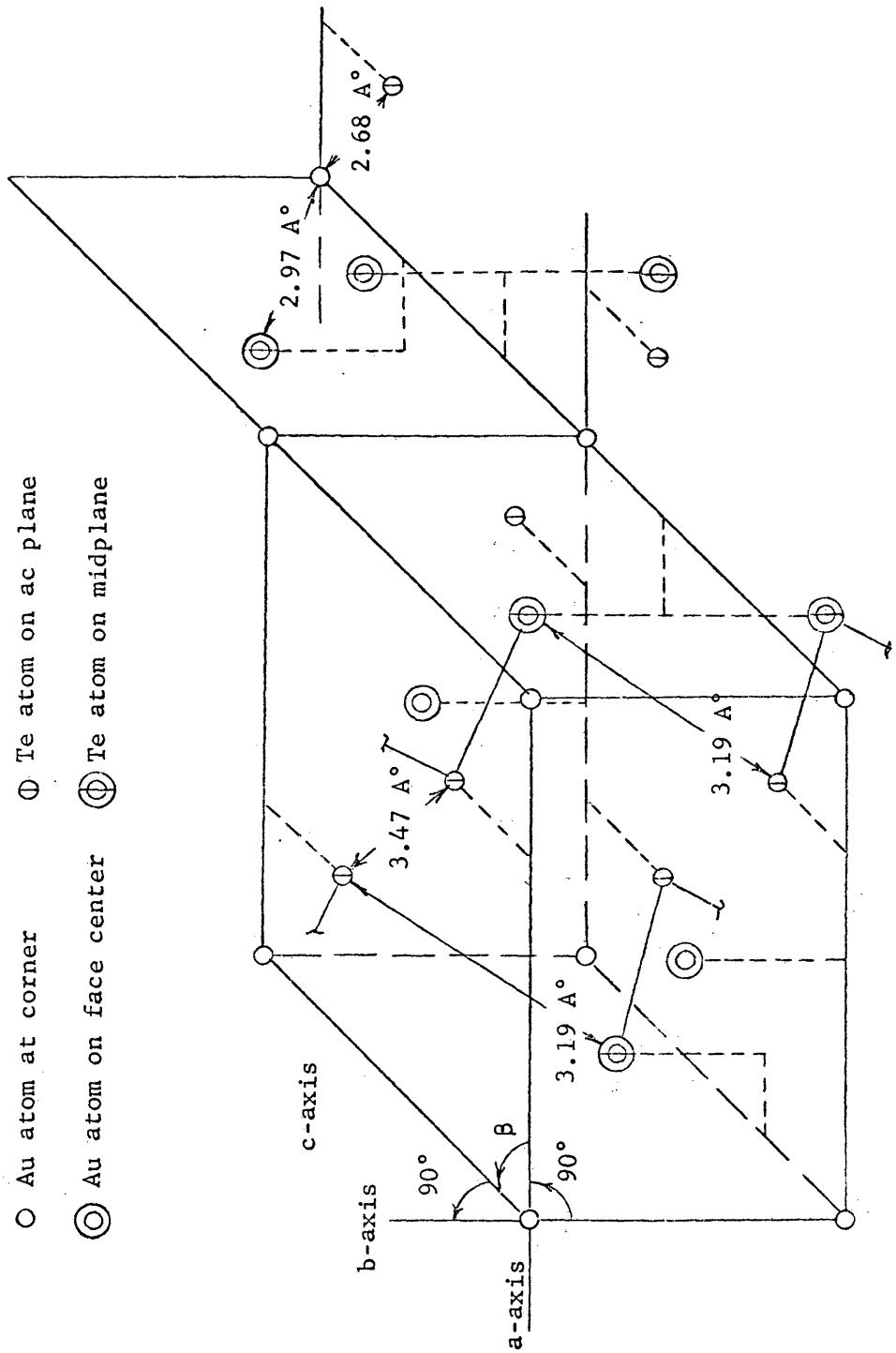

Figure A 1.1. Sketch of adjacent unit cells in $AuTe_2$. Portions of adjacent cells are included to demonstrate the coordination of 6 Te and 1 Au atoms with 2 Te at 2.68 A° and 4 Te at 2.97 A°. The 3.19 A° spacing of the Te atoms within the puckered Te chains and the closest distance of approach, 3.47 A°, of the Te atoms within adjacent chains are also shown. $\beta = 90°13' \pm 10'$.

APPENDIX 2

ANALYSES OF GOLD AND TELLURIUM

The spectrographic analyses provided by the American Smelting and Refining Company of the gold and tellurium, both of 99.999+ percent purity, used in the synthesis of the Te- and Au-excess materials are given here in tabular form. The impurities are reported in parts per million; N.D. denotes "none detected" by standard spectrographic procedures.

TABLE A 2.1

ANALYSIS OF THE ELEMENTS USED IN SYNTHESIS OF THE Te-EXCESS MATERIAL

A. GOLD ANALYSIS			
Element	Impurity Level	Element	Impurity Level
Sb	N.D.	Ca	N.D.
Tl	N.D.	Cu	2
Mg	<1	In	N.D.
Mn	N.D.	Cd	N.D.
Pb	2	Zn	N.D.
Sn	N.D.	Ag	1
Si	<1	Pt	N.D.
Cr	N.D.	Pd	N.D.
Fe	<1	Rh	N.D.
Ni	N.D.	Rm	N.D.
Bi	N.D.	Os	N.D.
Al	N.D.	Ir	N.D.
B. TELLURIUM ANALYSIS			
Sb	N.D.	Bi	N.D.
Tl	N.D.	Al	N.D.
Mg	1	Ca	N.D.
Pb	N.D.	Cu	<1
Mn	N.D.	In	N.D.
Sn	N.D.	Cd	N.D.
Si	<1	Zn	N.D.
Cr	N.D.	Ag	N.D.
Fe	<1	As	N.D.
Ni	N.D.	Hg	N.D.

TABLE A 2.2

ANALYSIS OF THE ELEMENTS USED IN THE SYNTHESIS OF Au-EXCESS MATERIAL

A. GOLD ANALYSIS			
Element	Impurity Level	Element	Impurity Level
Sb	N.D.	Ca	N.D.
Tl	N.D.	Cu	<1
Mg	<1	In	N.D.
Mn	N.D.	Cd	N.D.
Pb	1	Zn	N.D.
Sn	N.D.	Ag	2
Si	<1	Pt	N.D.
Cr	N.D.	Pd	N.D.
Fe	1	Rh	N.D.
Ni	N.D.	Ru	N.D.
Bi	N.D.	Os	N.D.
Al	N.D.	Ir	N.D.
B. TELLURIUM ANALYSIS			
Sb	N.D.	Bi	N.D.
Tl	N.D.	Al	N.D.
Mg	1	Ca	N.D.
Pb	N.D.	Cu	<1
Mn	N.D.	In	N.D.
Sn	N.D.	Cd	N.D.
Si	<1	Zn	N.D.
Cr	N.D.	Ag	N.D.
Fe	<1	As	N.D.
Ni	N.D.	Hg	N.D.

APPENDIX 3

IDENTITY OF THE SYNTHESIZED COMPOUND

The values of θ calculated from Debyegram data obtained for both the Te- and Au-excess materials agree with tabular values cited by Berry and Thompson[25] for the naturally occurring mineral calaverite (Au, Ag) Te_2, as shown in the following tables. The Debyegram data were obtained by use of (1) a 10-cm-diameter camera, (2) Cu radiation with a Ni filter, (3) 12-hour exposure. The data of Berry and Thompson were obtained with Cu radiation and Ni filter.

TABLE A 3.1

COMPARISON OF OBSERVED AND TABULAR VALUES FOR $AuTe_2$

A. Te-EXCESS MATERIAL			
θ (deg.)		Line Intensities	
Observed	Tabular	Observed*	Tabular
14.93	14.8	1	10
15.349	15.25	3	3
20.69	20.5	S	4
21.67	21.6	2	8
21.99	21.95	M	2
22.49	22.5	M	1
26.10	26.0	S	2
27.24	27.15	S	3
30.89	30.8	S	3
34.03	33.9	S	2
35.23	35.1	S	3
35.94	35.9	VS	3
38.19	38.05	M	2

TABLE A 3.1--Cont.

B. Au-EXCESS MATERIAL			
θ (deg.)		Line Intensities	
Observed	Tabular	Observed*	Tabular
14.88	14.8	1	10
15.30	15.25	3	3
19.17	20.5	S	4
20.54	21.6	2	8
21.93	21.95	M	2
22.41	22.5	M	1
25.99	26.0	S	2
27.12	27.15	S	3
30.76	30.8	S	3
33.88	33.9	S	2
35.14	35.1	S	3
35.81	35.9	VS	3
38.01	38.05	M	2

*The numbers indicate visually estimated intensities, with the number 1 corresponding to the maximum visually estimated intensity. The symbols S (Strong), W (Weak), and N.M. (Not Measurable) are also visual estimates.

APPENDIX 4

HALL PROBE CALIBRATION

The Halltron 31 probe used to determine the magnetic field B in the present study was calibrated as follows.

The output emf of the probe $V_p(I, T)$ was determined at known values of B between 3 and 13 kilogauss provided by an electromagnet with 12-inch-diameter flat-faced pole tips and at known probe temperatures. The magnitude of the field was established by the nuclear magnetic resonance of selected isotopes. Measurements were made using the same potentiometer used to measure the probe output during the Hall effect measurements. The probe-input current was determined by measuring the potential difference across a 1×10^{-2}-ohm resistor in series with the probe; the probe temperature was determined by monitoring the output emf of a copper-constantan thermocouple placed in close contact with the probe.

Measured probe emfs at each value of the field were normalized to values at 16-ma input current and a probe temperature of 290°K. Because the Hall emf is linearly related to the input current, the emf at 16 ma operating current and temperature T, $V_p(16, T)$, was calculated from each measured $V_p(I, T)$ by

$$V_p(16, T) = V_p(I, T)(16/I). \qquad \text{(A 4.1)}$$

Normalization was completed by use of

$$V_p(16, T) = V_p(16, 290)\left[1 - 8 \times 10^{-4}(T-290)\right]. \qquad \text{(A 4.2)}$$

where $V(16,290)$ is the output emf normalized to 16-ma input current

and 290°K-probe temperature. Equation A 4.2 was deduced from graphical-temperature derating data provided by the manufacturer.

Lastly, each set of three values of $V_p(16, 290)$, taken at each value of B, were averaged giving $< V_p(16, 290) >$. The calibration data are given in table A 4.1.

The quantities $< V_p(16, 290) >$ and B were used to obtain a polynomial of best fit by least-squares technique. According to the criterion of minimum variance, the polynomial

$$V_p(16, 290) = 5.6236 + 2.2578 \times 10^{-1} B + 2.4139 \times 10^{-2} B^2 - 7.2123 \times 10^{-3} B^3, \quad \text{(A 4.3)}$$

with V_p expressed in mv and B in kilogauss was chosen as the one of best fit over the range $0 \leq B \leq 14$ kilogauss. The r.m.s. error in a measured V_p at any B was calculated to be ±6 microvolts, which is of the order of the ±10 μv uncertainty in any reading on the potentiometer.

Equation A 4.3 was used to calculate tabular values of V_p at values of B from zero to 14 kilogauss using a 10 gauss increment. The calculations were done with a CDC 8090 computer. Use of these tables allowed reduction of Hall-probe voltage readings to values of B during the Hall-effect measurements.

TABLE A 4.1

HALL-PROBE CALIBRATION DATA

Obs. Set No.	V_p (I, T) (mv)	I (ma)	T (°K)	B (kilogauss)	Resonances	
					f (megahertz)	Isotope
1	6.480	16.703	297.18	2.307	9.821	H^1
	6.486	16.715				
2	6.769	16.607	297.18	3.150	13.414	H^1
	6.775	16.658				
3	7.035	16.686	297.41	3.779	16.092	H^1
	7.035	16.696				
4	7.457	16.624	297.65	4.870	20.736	H^1
	7.456	16.621				
5	7.790	16.600	297.92	5.730	7.440	Ga^{71}
	7.809	16.610				
6	8.526	16.595	298.09	7.303	7.462	Ga^{69}
	8.526	16.600				
7	9.954	16.552	297.89	10.213	7.447	As*
	9.952	16.561				
8	10.228	16.553	298.70	10.795	11.030	Ga^{69}
	10.232	16.558				
9	10.858	16.530	298.90	12.027	11.220	In^{115}
	10.860	16.538				
10	11.405	16.524	299.24	13.380	12.482	In^{115}
	11.406	16.520				

*An unspecified As isotope in GaAs

TABLE A 4.1--Cont.

Obs. Set No.	$V_p(16, T)$ (mv)	$V_p(16, 290)$ (mv)	$\langle V_p(16, 290) \rangle$ (mv)	B (kilogauss)
1	6.207	6.243	6.243	2.307
	6.208	6.244		
2	6.522	6.559	6.552	3.150
	6.508	6.544		
3	6.746	6.786	6.784	3.779
	6.742	6.782		
4	7.117	7.221	7.221	4.870
	7.117	7.221		
5	7.508	7.556	7.563	5.730
	7.522	7.570		
6	8.219	8.273	8.270	7.303
	8.218	8.268		
7	9.622	9.683	9.684	10.213
	9.625	9.685		
8	9.886	9.955	9.955	10.791
	9.887	9.956		
9	10.509	10.584	10.583	12.027
	10.507	10.582		
10	11.043	11.125	11.127	13.380
	11.047	11.129		

APPENDIX 5

THE ZERO-MAGNETIC-FIELD RESISTANCE DATA

The data are presented in two groups of tables. The first group, Tables A 5.1 through A 5.5, presents resistance data obtained at various measurement temperatures during descent from room temperature for samples R-1-Te through R-5-Te; corresponding data for R-1-Au through R-8-Au comprise Tables A 5.6 through A 5.13.

The experimentally measured voltages V^{11} and V_s and the resistance values R^{11}, calculated from these quantities by use of Equation 31, are given for each sample. Also given for each sample are the approximating polynomials, generated by least-square techniques, to the resistance-temperature data and the temperature ranges of definition for each polynomial. The uncertainty R^{11} in each R^{11}, calculated from the experimental uncertainty in V_{11}, V_s, and R_s, are presented with the residuals and r.m.s. deviations, S, in the R^{11} calculated during the least-square procedure. For comparison with the experimentally derived values of R^{11}, values of the resistance calculated by use of the approximating polynomials are also given.

TABLE A 5.1

SAMPLE R-1-Te: SAMPLE RESISTANCE AS A FUNCTION OF TEMPERATURE. DATA WERE TAKEN DURING DESCENT FROM ROOM TEMPERATURE.

T (Deg. K)	V^{11} (μv)	V'_s (μv)	R^{11} exp. (10^{-3} Ω)	ΔR^{11} exp. (10^{-6} Ω)	R^{11} calc. (10^{-3} Ω)	Residual (10^{-6} Ω)
291.78	567.10	1049.92	5.402	5.5	5.401	-1
280.70	556.62	1067.48	5.214	5.4	5.215	1
270.42	538.56	1069.58	5.035	5.3	5.034	-1
260.96	521.58	1072.18	4.864	5.2	4.864	0
250.35	502.14	1074.96	4.671	5.2	4.673	2
240.49	484.80	1078.46	4.495	5.1	4.495	0
234.81	475.12	1080.06	4.399	5.1	4.396	-3
230.36	467.08	1081.76	4.318	5.1	4.318*	0*
225.61	458.74	1082.54	4.237	5.0	4.238	1
213.16	440.62	1077.56	4.089	5.0	4.088*	0*
208.02	439.82	1100.06	3.998	4.9	3.995	-3
203.10	430.50	1102.52	3.904	4.9	3.905	1
198.22	421.42	1103.12	3.820	4.9	3.816	-4
193.30	411.22	1105.38	3.720	4.8	3.725	5
187.80	400.72	1106.42	3.622	4.8	3.622	0
182.09	388.76	1107.94	3.509	4.8	3.512	3
177.26	378.50	1109.08	3.413	4.8	3.418	5
170.01	363.66	1110.26	3.275	4.8	3.276	1
159.57	341.70	1115.38	3.064	4.7	3.066	2
150.14	320.70	1117.34	2.870	4.7	2.869	-1
140.11	297.70	1119.50	2.659	4.6	2.655	-4
130.11	274.58	1121.84	2.448	4.6	2.444	-4
105.50	210.95	1126.80	1.782	4.5	1.780	2
94.26	170.15	1127.90	1.508	4.5	1.504	-4

* Denotes average values at common boundary point of two ranges.

TABLE A 5.1--Cont.

APPROXIMATING POLYNOMIALS, R^{11}, AND THE R.M.S. DEVIATION, S, OF R^{11}, BOTH IN UNITS OF $10^{-3}\,\Omega$ AND T IN UNITS OF DEG. K.:

1. $230.4 \leq T \leq 300.0$ °K

$$R^{11} = 3.9400\ (10^{-3}) - 1.0997\ (10^{-5})\ T - 5.42636\ (10^{-9})\ T^2 + 4.6882\ (10^{-10})\ T^3 - 8.9872\ (10^{-13})\ T^4$$

$$S = 1.1\ (10^{-3})$$

2. $213.2 \leq T \leq 230.4$ °K

$$R^{11} = 1.3042\ (10^{-2}) - 9.3149\ (10^{-5})\ T + 2.3994\ (10^{-7})\ T^2$$

$$S = 1.2\ (10^{-3})$$

3. $80.0 \leq T \leq 213.2$ °K

$$R^{11} = -1.2873\ (10^{-3}) + 3.5947\ (10^{-5})\ T - 6.6201\ (10^{-8})\ T^2 + 7.4389\ (10^{-11})\ T^3$$

$$S = 4.0\ (10^{-3})$$

TABLE A 5.2

SAMPLE R-2-Te: SAMPLE RESISTANCE AS A FUNCTION OF TEMPERATURE. DATA WERE TAKEN DURING DESCENT FROM ROOM TEMPERATURE.

T (Deg. K)	V^{11} (μv)	V_s (μv)	R^{11} exp. (10^{-3} Ω)	ΔR^{11} exp. (10^{-6} Ω)	R^{11} calc. (10^{-3} Ω)	Residual (10^{-6} Ω)
297.00	676.32	1079.63	6.264	5.7	6.263	-1
283.55	646.36	1077.46	5.999	5.6	6.000	1
271.16	620.78	1080.50	5.745	5.5	5.747	2
260.45	597.70	1082.72	5.520	5.4	5.523	3
251.05	577.62	1084.18	5.328	5.3	5.326	-2
240.03	553.92	1086.30	5.099	5.3	5.095	-4
235.17	543.12	1086.72	4.998	5.2	4.995	-3
229.90	531.86	1088.24	4.887	5.2	4.888	1
223.36	517.30	1088.48	4.753	5.1	4.755	2
213.64	497.72	1089.40	4.568	5.1	4.565*	-3*
209.12	499.02	1115.08	4.475	4.9	4.470	-5
205.16	489.54	1115.76	4.388	4.9	4.389	2
199.45	476.90	1116.50	4.271	4.9	4.275	4
195.10	467.60	1117.02	4.186	4.8	4.190	4
189.53	455.62	1118.42	4.074	4.8	4.079	5
184.84	444.52	1116.82	3.980	4.8	3.984	4
179.89	434.02	1117.64	3.883	4.8	3.888	5
175.14	424.30	1118.62	3.793	4.7	3.796	3
170.25	414.36	1119.68	3.700	4.7	3.700	0
160.19	393.94	1121.22	3.513	4.7	3.508	-5
148.43	369.90	1124.52	3.289	4.7	3.284	-5
138.66	348.70	1125.94	3.097	4.7	3.093	-4
130.09	326.42	1127.76	2.894	4.6	2.896*	2*
119.96	299.04	1132.44	2.641	4.6	2.638	-3
115.05	283.60	1131.70	2.506	4.6	2.510	4
106.15	257.58	1131.32	2.277	4.6	2.274	-3

TABLE A 5.2--Cont.

T (Deg. K)	V^{11} (μv)	V_s (μv)	R^{11} exp. (10^{-3} Ω)	ΔR^{11} exp. (10^{-6} Ω)	R^{11} calc. (10^{-3} Ω)	Residual (10^{-6} Ω)
100.00	239.78	1136.74	2.109	4.5	2.108	-1
93.49	220.01	1139.12	1.931	4.5	1.931	0
88.73	204.76	1138.50	1.798	4.5	1.798	0
84.58	192.86	1141.12	1.690	4.5	1.690	0

* Denotes average values at common boundary point of two ranges.

TABLE A 5.2--Cont.

APPROXIMATING POLYNOMIALS, R^{11}, AND THE R.M.S. DEVIATION, S, OF R^{11}, BOTH IN UNITS OF $10^{-3}\Omega$ AND T IN UNITS OF DEG. K:

1. $213.6 \leq T \leq 300.0$ °K

$$R^{11} = 6.9099\ (10^{-3}) - 5.9634\ (10^{-5})\ T + 3.1597\ (10^{-7})\ T^2 - 4.1252\ (10^{-10})\ T^3,$$

$$S = 1.8\ (10^{-3})$$

2. $130.1 \leq T \leq 213.6$ °K

$$R^{11} = 4.5237\ (10^{-4}) + 1.8509\ (10^{-5})\ T + 3.3325\ (10^{-9})\ T^2,$$

$$S = 4.2\ (10^{-3})$$

3. $80.0 \leq T \leq 130.1$ °K

$$R^{11} = -3.3714\ (10^{-4}) + 1.76461\ (10^{-5})\ T + 1.1076\ (10^{-7}) - 4.2610\ (10^{-10})\ T^3$$

$$S = 2.2\ (10^{-3})$$

TABLE A 5.3

SAMPLE R-3-Te: SAMPLE RESISTANCE AS A FUNCTION OF TEMPERATURE. DATA WERE TAKEN DURING DESCENT FROM ROOM TEMPERATURE.

T (Deg. K)	V^{11} (μv)	V_s (μv)	R^{11} exp. (10^{-3} Ω)	ΔR^{11} exp. (10^{-6} Ω)	R^{11} calc. (10^{-3} Ω)	Residual (10^{-6} Ω)
299.17	419.06	1059.38	3.956×10^{-3}	5.1×10^{-6}	3.955	-1
284.32	405.20	1078.30	3.758	5.0	3.762	4
267.50	387.28	1081.98	3.579	5.0	3.574	-5
258.05	376.82	1084.28	3.475	4.9	3.475	0
247.44	364.32	1084.32	3.359	4.9	3.361	2
240.53	356.48	1085.80	3.283	4.9	3.287	4
235.63	351.26	1087.06	3.231	4.8	3.231	0
230.58	345.78	1089.72	3.173	4.8	3.172	-1
225.59	339.64	1091.48	3.112	4.8	3.112*	0*
214.43	327.06	1093.10	2.992	4.8	2.987	-5
209.19	326.92	1118.60	2.923	4.7	2.923	0
204.15	319.74	1119.84	2.856	4.7	2.860	4
198.93	312.66	1120.60	2.790	4.6	2.794	4
193.75	305.60	1121.72	2.724	4.6	2.726	2
184.94	293.04	1122.72	2.610	4.6	2.609	-1
175.00	278.28	1124.80	2.474	4.5	2.471	-3
174.66	261.86	1128.26	2.321	4.5	2.322	1
153.73	243.84	1128.08	2.161	4.5	2.160	-2
145.36	229.70	1129.22	2.034	4.5	2.032	-2
133.21	209.48	1134.34	1.846	4.5	1.843	-3
124.62	194.50	1138.06	1.709	4.5	1.707	-2
117.98	180.92	1139.58	1.588	4.5	1.596	-8
106.45	161.42	1137.80	1.419	4.4	1.414	-5
99.00	147.34	1143.92	1.288	4.4	1.290	2

* Denotes average values at common boundary point of two ranges.

TABLE A 5.3--Cont.

APPROXIMATING POLYNOMIALS, R^{11}, AND THE R.M.S. DEVIATION, S, OF R^{11}, BOTH IN UNITS OF $10^{-3}\ \Omega$ AND T IN UNITS OF DEG. K:

1. $225.6 \leq T \leq 300.0$ °K

$$R^{11} = -4.3819\ (10^{-3}) + 4.4459\ (10^{-5})\ T + 6.7652\ (10^{-8})\ T^2 - 8.5605\ (10^{-10})\ T^3 + 1.4859\ (10^{-12})\ T^4$$

$$S = 2.6\ (10^{-3})$$

2. $80.0 \leq T \leq 225.6$ °K

$$R^{11} = -3.3398\ (10^{-4}) + 1.5543\ (10^{-5})\ T + 1.6388\ (10^{-8})\ T^2 - 7.7819\ (10^{-11})\ T^3$$

$$S = 3.6\ (10^{-3})$$

TABLE A 5.4

SAMPLE R-4-Te: SAMPLE RESISTANCE AS A FUNCTION OF TEMPERATURE. DATA WERE TAKEN DURING DESCENT FROM ROOM TEMPERATURE.

T (Deg. K)	V^{11} (μv)	V_s (μv)	R^{11} exp. (10^{-3} Ω)	ΔR^{11} exp. (10^{-6} Ω)	R^{11} calc. (10^{-3} Ω)	Residual (10^{-6} Ω)
296.81	214.66	1641.94	1.307	3.0	1.305	-2
281.20	208.16	1688.12	1.233	3.0	1.236	3
270.13	202.60	1695.20	1.195	3.0	1.194	-1
260.80	197.14	1699.02	1.160	3.0	1.158	-2
250.16	190.58	1703.30	1.119	3.0	1.118	-1
240.00	184.84	1708.64	1.082	3.0	1.081	-1
235.37	181.54	1708.34	1.063	3.0	1.063	0
229.92	178.22	1709.32	1.043	3.0	1.043	0
224.27	174.28	1710.08	1.019	2.9	1.022	3
213.49	169.10	1719.72	0.983	2.8	0.983*	0*
209.06	172.10	1785.14	0.964	2.8	0.964	0
203.13	168.06	1787.08	0.940	2.8	0.941	1
197.77	164.64	1789.20	0.920	2.8	0.920	0
192.39	161.08	1791.84	0.899	2.8	0.899	0
187.93	157.90	1793.94	0.880	2.8	0.880	0
180.21	152.38	1796.78	0.848	2.8	0.849	1
169.00	145.12	1805.18	0.804	2.8	0.803	-1
159.93	138.30	1802.04	0.767	2.8	0.764	-3
150.27	131.06	1808.84	0.725	2.8	0.722	-3
140.00	122.96	1815.70	0.677	2.8	0.675	-2
128.57	113.98	1826.74	0.624	2.8	0.623	-1
119.64	106.26	1832.54	0.580	2.8	0.580	0
106.84	92.05	1833.38	0.502	2.8	0.503	1
89.57	81.38	1834.01	0.444	2.6	0.443	-1

* Denotes average values at common boundary point of two ranges.

TABLE A 5.4--Cont.

APPROXIMATING POLYNOMIALS, R^{11}, AND THE R.M.S. DEVIATION, S, IN R^{11}, BOTH IN UNITS OF $10^{-3}\,\Omega$ AND T IN UNITS OF DEG. K:

1. $213.5 \leq T \leq 300.0$ °K

$$R^{11} = -9.6866\ (10^{-4}) + 1.8209\ (10^{-5})\ T - 6.0418\ (10^{-8}) + 8.3824\ (10^{-11})\ T^3$$

$$S = 2.0\ (10^{-3})$$

2. $80.0 \leq T \leq 213.5$ °K

$$R^{11} = -5.9549\ (10\text{-}5) + 5.9581\ (10^{-6})\ T - 5.0694\ (10^{-9})\ T^2$$

$$S = 1.5\ (10^{-3})$$

TABLE A 5.5

SAMPLE R-5-Te: SAMPLE RESISTANCE AS A FUNCTION OF TEMPERATURE. DATA WERE TAKEN DURING DESCENT FROM ROOM TEMPERATURE.

T (Deg. K)	V^{11} (μv)	V_s (μv)	R^{11} exp. (10^{-3} Ω)	ΔR^{11} exp. (10^{-6} Ω)	R^{11} calc. (10^{-3} Ω)	Residual (10^{-6} Ω)
297.79	603.16	1622.48	3.718	3.3	3.718	0
282.84	592.06	1666.96	3.552	3.3	3.554	2
270.57	572.22	1674.38	3.418	3.2	3.418	0
260.80	556.16	1680.08	3.310	3.2	3.307	-3
250.69	538.88	1687.36	3.194	3.2	3.196	2
240.06	521.68	1693.44	3.081	3.2	3.084	3
235.37	515.78	1697.30	3.039	3.2	3.037	-2
230.00	508.08	1701.30	2.986	3.2	2.984*	-2*
223.74	499.22	1705.10	2.928	3.1	2.932	4
213.85	488.70	1703.68	2.869	3.1	2.867*	-2*
210.06	499.22	1766.54	2.826	3.1	2.825	-1
205.28	490.52	1770.02	2.771	3.1	2.775	4
199.90	482.32	1773.28	2.719	3.0	2.721	2
195.23	474.92	1775.32	2.675	3.0	2.677	2
189.36	467.02	1778.60	2.626	3.0	2.622	-4
180.41	452.16	1784.24	2.534	3.0	2.534	0
170.00	434.58	1789.48	2.428	2.9	2.426	-2
159.37	414.60	1796.48	2.308	2.8	2.307	-1
150.31	394.62	1800.50	2.192	2.8	2.194	2
140.53	374.62	1815.98	2.063	2.8	2.063	0
129.43	345.34	1820.52	1.897	2.8	1.900	3
117.46	313.48	1826.34	1.716	2.8	1.716*	0*
105.70	277.92	1822.34	1.525	2.8	1.525	0
102.31	269.70	1836.14	1.469	2.8	1.466	-3
96.74	251.56	1839.72	1.367	2.8	1.370	3

* Denotes average values at common boundary point of two ranges.

TABLE A 5.5--Cont.

APPROXIMATING POLYNOMIALS, R^{11}, AND THE R.M.S. DEVIATION, S, IN R^{11}, BOTH IN UNITS OF $10^{-3}\ \Omega$ AND T IN UNITS OF DEG. K:

1. $230.0 \leq T \leq 300.0\ ^\circ K$

$$R^{11} = 8.1331\ (10^{-3}) - 7.4627\ (10^{-5})\ T + 3.1661\ (10^{-7})\ T^2 - 3.8888\ (10^{-10})\ T^3$$

$$S = 2.3\ (10^{-3})$$

2. $213.9 \leq T \leq 230.0\ ^\circ K$

$$R^{11} = 6.3350\ (10^{-3}) - 3.7933\ (10^{-5})\ T + 1.0157\ (10^{-7})\ T^2$$

$$S = 2.3\ (10^{-3})$$

3. $117.5 \leq T \leq 213.9\ ^\circ K$

$$R^{11} = 1.8901\ (10^{-3}) - 4.7973\ (10^{-5})\ T + 7.2171\ (10^{-7})\ T^2 - 3.4461\ (10^{-9})\ T^3 + 5.7052\ (10^{-12})\ T^4$$

$$S = 2.6\ (10^{-3})$$

4. $80.0 \leq T \leq 117.5\ ^\circ K$

$$R^{11} = 2.9992\ (10^{-4}) - 2.7083\ (10^{-6})\ T + 2.1973\ (10^{-7})\ T^2 - 7.9958\ (10^{-10})\ T^3$$

$$S = 1.5\ (10^{-3})$$

TABLE A 5.6

SAMPLE R-1-Au: SAMPLE RESISTANCE AS A FUNCTION OF TEMPERATURE. DATA WERE TAKEN DURING DESCENT FROM ROOM TEMPERATURE.

T (Deg. K)	V^{11} (μv)	V_s (μv)	R^{11} exp. (10^{-3} Ω)	ΔR^{11} exp. (10^{-6} Ω)	R^{11} calc. (10^{-3} Ω)	Residual (10^{-6} Ω)
300.61	486.79	973.18	4.808	5.8	4.808	0
278.54	450.35	989.37	4.551	5.6	4.554	3
258.43	430.15	1005.93	4.281	5.4	4.276	-5
241.77	407.02	1008.98	4.034	5.3	4.039	5
227.68	389.22	1011.15	3.852	5.3	3.854*	2*
215.17	366.85	1012.95	3.623	5.3	3.618	-5
192.61	335.80	1037.14	3.238	5.1	3.233	-5
176.36	306.78	1041.44	2.946	5.0	2.952	6
149.87	260.05	1048.02	2.481	4.9	2.477	-4
129.22	215.22	1050.37	2.051	4.8	2.048	-3
115.71	185.12	1053.15	1.758	4.8	1.760	2
102.41	158.17	1055.75	1.499	4.8	1.497	-3
97.19	147.60	1057.70	1.395	4.8	1.397	2

* Denotes average values at common boundary point of two ranges.

TABLE A 5.6--Cont.

APPROXIMATING POLYNOMIALS, R^{11}, AND THE R.M.S. DEVIATION, S, IN R^{11}, BOTH IN UNITS OF $10^{-3}\Omega$ AND T IN UNITS OF DEG. K:

1. $227.7 \leq T \leq 300.0$ °K

$$R^{11} = 6.7545\ (10^{-3}) - 3.2416\ (10^{-5})\ T - 1.7702\ (10^{-8})\ T^2 + 8.0411\ (10^{-10})\ T^3 - 1.5242\ (10^{-12})\ T^4$$

$$S = 3.5\ (10^{-3})$$

2. $80.0 \leq T \leq 227.7$ °K

$$R^{11} = 3.0176\ (10^{-3}) - 8.1661\ (10^{-5})\ T + 1.0467\ (10^{-6})\ T^2 - 4.5888\ (10^{-9})\ T^3 + 7.1915\ (10^{-12})\ T^4$$

$$S = 5.6\ (10^{-3})$$

TABLE A 5.7

SAMPLE R-2-Au: SAMPLE RESISTANCE AS A FUNCTION OF TEMPERATURE. DATA WERE TAKEN DURING DESCENT FROM ROOM TEMPERATURE.

T (Deg. K)	V^{11} (μv)	V_s (μv)	R^{11} exp. (10^{-3} Ω)	ΔR^{11} exp. (10^{-6} Ω)	R^{11} calc. (10^{-3} Ω)	Residual (10^{-6} Ω)
296.64	530.98	998.16	5.359	5.7	5.353	-6
273.61	501.10	1022.22	4.951	5.5	4.958	6
263.03	484.96	1014.16	4.782	5.5	4.780	-2
253.78	469.48	1016.36	4.619	5.4	4.622	3
243.20	452.60	1017.40	4.449	5.4	4.445*	-4*
230.35	432.56	1016.54	4.255	5.4	4.256	1
217.45	426.40	1024.26	4.163	5.3	4.161*	-2*
209.18	419.10	1047.96	3.999	5.1	4.003	4
200.89	404.52	1049.08	3.856	5.1	3.852	-4
187.33	378.82	1053.32	3.596	5.0	3.596	0
170.84	341.74	1055.84	3.237	5.0	3.238*	1*
154.11	302.64	1059.22	2.857	4.9	2.855	2
134.13	255.62	1063.52	2.404	4.8	2.406	2
104.50	187.32	1066.38	1.757	4.7	1.752	-5
94.108	160.62	1072.30	1.497	4.7	1.501	3

* Denotes average values at common boundary points of two ranges.

TABLE A 5.7--Cont.

APPROXIMATING POLYNOMIALS, R^{11} AND THE R.M.S. DEVIATION, S, IN R^{11}, BOTH IN UNITS OF $10^{-3}\ \Omega$ AND T IN UNITS OF DEG. K:

1. $243.2 \leq T \leq 300°K$

$$R^{11} = 1.4733\ (10^{-3}) + 8.3107\ (10^{-6})\ T + 1.6135\ (10^{-8})\ T^2$$

$$S = 3.6\ (10^{-3})$$

2. $217.5 \leq T \leq 243.2\ °K$

$$R^{11} = 1.2040\ (10^{-2}) - 7.8249\ (10^{-5})\ T + 1.9320\ (10^{-7})\ T^2$$

$$S = 4.0\ (10^{-3})$$

3. $170.8 \leq T \leq 217.5\ °K$

$$R^{11} = -7.3320\ (10^{-3}) + 7.5172\ (10^{-5})\ T + 2.5267\ (10^{-7})\ T^2 - 3.0382\ (10^{-9})\ T^3 + 6.4575\ (10^{-12})\ T^4$$

$$S = 2.7\ (10^{-3})$$

4. $80.0 \leq T \leq 170.8\ °K$

$$R^{11} = -1.9463\ (10^{-3}) + 5.3862\ (10^{-5})\ T - 2.3881\ (10^{-7})\ T^2 + 5.9230\ (10^{-10})\ T^3$$

$$S = 3.0\ (10^{-3})$$

TABLE A 5.8

SAMPLE R-3-Au: SAMPLE RESISTANCE AS A FUNCTION OF TEMPERATURE. DATA WERE TAKEN DURING DESCENT FROM ROOM TEMPERATURE.

T (Deg. K)	V^{11} (μv)	V_s (μv)	R^{11} exp. (10^{-3} Ω)	ΔR^{11} exp. (10^{-6} Ω)	R^{11} calc. (10^{-3} Ω)	Residual (10^{-6} Ω)
297.57	662.52	977.82	6.775	6.3	6.775	0
271.09	628.57	996.20	6.310	6.1	6.309	-1
261.56	615.50	1000.93	6.148	6.0	6.150	2
253.49	602.61	1001.14	6.018	6.0	6.018	0
214.86	540.33	1008.03	5.360	5.7	5.358*	-2*
215.92	554.41	1008.51	5.367	5.7	5.371	4
193.84	512.47	1034.08	4.956	5.4	4.956	0
179.18	476.33	1035.02	4.593	5.4	4.590	-3
164.93	434.65	1037.72	4.189	5.3	4.192	+3
140.01	363.37	1045.70	3.475	5.0	3.475*	0*
105.88	253.13	1049.90	2.411	4.9	2.412	0
95.99	179.45	1058.07	2.176	4.8	2.176	0

* Denotes average values at common boundary point of two ranges.

TABLE A 5.8--Cont.

APPROXIMATING POLYNOMIALS, R^{11} AND THE R.M.S. DEVIATION, S, IN R^{11}, BOTH IN UNITS OF $10^{-3}\ \Omega$ AND T IN UNITS OF DEG. K:

1. $214.9 \leq T \leq 300.0\ ^\circ K$

$$R^{11} = 8.6109\ (10^{-5}) + 1.9552\ (10^{-5})\ T + 1.2630\ (10^{-7})\ T^2 - 7.0899\ (10^{-10})\ T^3 + 1.0674\ (10^{-12})\ T^4$$

$$S = 1.0\ (10^{-6})$$

2. $140.0 \leq T \leq 214.9\ ^\circ K$

$$R^{11} = 4.6030\ (10^{-3}) - 7.1385\ (10^{-5})\ T + 6.4622\ (10^{-7})\ T^2 - 1.3854\ (10^{-9})\ T^3$$

$$S = 3.3\ (10^{-6})$$

3. $80.0 \leq T \leq 140.0\ ^\circ K$

$$R^{11} = -1.3896\ (10^{-2}) + 4.0790\ (10^{-4})\ T - 3.5474\ (10^{-6})\ T^2 + 1.0857\ (10^{-8})\ T^3$$

$$S = 0.0\ (10^{-6})$$

TABLE A 5.9

SAMPLE R-4-Au: SAMPLE RESISTANCE AS A FUNCTION OF TEMPERATURE. DATA WERE TAKEN DURING DESCENT FROM ROOM TEMPERATURE.

T (Deg. K)	V^{11} (μv)	V_s (μv)	R^{11} exp. (10^{-3} Ω)	ΔR^{11} exp. (10^{-6} Ω)	R^{11} calc. (10^{-3} Ω)	Residual (10^{-6} Ω)
296.45	403.39	982.09	4.108	5.5	4.109	1
272.69	383.03	1000.04	3.827	5.4	3.827	0
255.65	363.87	1004.23	3.623	5.3	3.618	-5
241.19	343.90	1001.10	3.435	5.3	3.436	1
229.66	328.05	999.80	3.281	5.3	3.286	5
215.82	312.48	1004.67	3.111	5.2	3.109*	-2*
195.91	289.40	1023.94	2.826	5.1	2.825	-1
176.63	263.47	1033.43	2.549	5.0	2.549	0
155.16	231.85	1038.78	2.232	4.9	2.233	1
136.53	202.68	1043.82	1.942	4.9	1.941	-1
105.08	148.33	1051.17	1.411	4.8	1.411	0
94.96	130.22	1053.12	1.236	4.8	1.236	0
81.92	106.82	1056.47	1.011	4.8	1.011	0

* Denotes average values at common boundary points of two ranges.

TABLE A 5.9--Cont.

APPROXIMATING POLYNOMIALS, R^{11} AND THE R.M.S. DEVIATION, S, IN R^{11}, BOTH IN UNITS OF $10^{-3}\ \Omega$ AND T IN UNITS OF DEG. K:

1. $215.8 \leq T \leq 300.0\ °K$

$$R^{11} = -2.1383\ (10^{-4}) + 1.7544\ (10^{-5})\ T - 9.9886\ (10^{-9})\ T^2$$

$$S = 3.9\ (10^{-3})$$

2. $80.0 \leq T \leq 215.8\ °K$

$$R^{11} = 6.6152\ (10^{-5}) + 8.9762\ (10^{-7})\ T + 2.0414\ (10^{-7})\ T^2 - 1.0561\ (10^{-9})\ T^3 + 1.8254\ (10^{-12})\ T^4$$

$$S = 0.6\ (10^{-6})$$

TABLE A 5.10

SAMPLE R-5-Au: SAMPLE RESISTANCE AS A FUNCTION OF TEMPERATURE. DATA WERE TAKEN DURING DESCENT FROM ROOM TEMPERATURE.

T (Deg. K)	V^{11} (μv)	V_s (μv)	R^{11} exp. (10^{-3} Ω)	ΔR^{11} exp. (10^{-6} Ω)	R^{11} calc. (10^{-3} Ω)	Residual (10^{-6} Ω)
298.85	465.93	979.63	4.756	5.7	4.756	0
279.18	445.27	995.63	4.472	5.5	4.475	2
267.24	429.93	995.20	4.320	5.5	4.315	-5
255.28	414.65	998.28	4.154	5.4	4.158	4
244.50	401.62	999.07	4.019	5.4	4.018	-2
232.17	385.58	1000.38	3.854	5.4	3.855*	0*
215.75	365.30	1002.90	3.642	5.3	3.638	-4
199.74	347.98	1028.87	3.382	5.3	3.387	5
180.77	315.62	1032.70	3.056	5.1	3.053	-3
161.17	277.35	1036.90	2.677	5.0	2.677	0
141.70	237.55	1039.25	2.286	4.9	2.286	0
121.72	196.68	1047.57	1.877	4.9	1.876	-1
119.17	194.41	1050.34	1.850	4.8	1.850	0
105.43	161.80	1049.20	1.542	4.8	1.543	1
82.94	115.68	1056.35	1.095	4.8	1.095	0

* Denotes average values at common boundary point of two ranges.

TABLE A 5.10--Cont.

APPROXIMATING POLYNOMIALS, R^{11} AND THE R.M.S. DEVIATION, S, IN R^{11}, BOTH IN UNITS OF $10^{-3}\,\Omega$ AND T IN UNITS OF DEG. K:

1. $232.2 \leq T \leq 300.0$ °K

$$R^{11} = -4.7419\ (10^{-3}) + 7.8966\ (10^{-5})\ T - 2.5987\ (10^{-7})\ T^2 + 3.4124\ (10^{-10})\ T^3$$

$$S = 3.1\ (10^{-3})$$

2. $80.0 \leq T \leq 232.2$ °K

$$R^{11} = -3.2145\ (10^{-4}) + 1.4222\ (10^{-5})\ T + 3.6467\ (10^{-8})\ T^2 + 9.9358\ (10^{-12})\ T^3 - 4.1815\ (10^{-13})\ T^4$$

$$S = 2.4\ (10^{-3})$$

TABLE A 5.11

SAMPLE R-6-Au: SAMPLE RESISTANCE AS A FUNCTION OF TEMPERATURE. DATA WERE TAKEN DURING DESCENT FROM ROOM TEMPERATURE.

T (Deg. K)	V^{11} (μv)	V_s (μv)	R^{11} exp. (10^{-3} Ω)	ΔR^{11} exp. (10^{-6} Ω)	R^{11} calc. (10^{-3} Ω)	Residual (10^{-6} Ω)
297.94	693.73	972.38	7.134	6.3	7.134	0
272.63	655.17	991.43	6.613	6.2	6.615	2
260.76	637.83	991.78	6.431	6.1	6.432	1
250.51	624.65	993.02	6.290	6.1	6.285	-5
241.15	609.78	994.62	6.131	6.0	6.137	6
216.13	564.57	1001.05	5.640	5.8	5.639*	-1*
190.71	508.55	1028.53	4.946	5.5	4.951	5
181.53	483.650	1029.75	4.697	5.4	4.692	-5
172.08	454.82	1030.35	4.414	5.4	4.415	1
156.43	408.02	1034.02	3.946	5.2	3.948	2
141.15	362.42	1038.50	3.490	5.1	3.485	-5
105.62	249.28	1045.20	2.385	5.0	2.390	5
91.76	206.80	1046.57	1.976	4.9	1.974	-2
83.98	182.98	1049.38	1.744	4.8	1.743	-1

* Denotes average values at common boundary point of two ranges.

TABLE A 5.11--Cont.

APPROXIMATING POLYNOMIALS, R^{11} AND THE R.M.S. DEVIATION, S, IN R^{11}, BOTH IN UNITS OF $10^{-3}\ \Omega$ AND T IN UNITS OF DEG. K:

1. $216.1 \leq T \leq 300.0\ ^{\circ}K$

$$R^{11} = -2.1199\ (10^{-2}) + 2.4208\ (10^{-4})\ T - 4.9181\ (10^{-7})\ T^2 - 8.9185\ (10^{-10})\ T^3 + 2.9760\ (10^{-12})\ T^4$$

$$S = 3.3\ (10^{-3})$$

2. $80.0 \leq T \leq 216.1\ ^{\circ}K$

$$R^{11} = -3.9758\ (10^{-4}) + 1.9911\ (10^{-5})\ T + 8.4951\ (10^{-8})\ T^2 - 2.2148\ (10^{-10})\ T^3$$

$$S = 3.5\ (10^{-3})$$

TABLE A 5.12

SAMPLE R-7-Au: SAMPLE RESISTANCE AS A FUNCTION OF TEMPERATURE. DATA WERE TAKEN DURING DESCENT FROM ROOM TEMPERATURE.

T (Deg. K)	V^{11} (μv)	V_s (μv)	R^{11} exp. (10^{-3} Ω)	ΔR^{11} exp. (10^{-6} Ω)	R^{11} calc. (10^{-3} Ω)	Residual (10^{-6} Ω)
294.37	350.28	984.02	3.559	5.4	3.559	0
269.93	333.35	1000.03	3.333	5.3	3.337	4
253.30	321.88	1004.12	3.206	5.2	3.204	-2
239.17	311.55	1008.33	3.090	5.2	3.086	-4
226.58	299.72	1010.73	2.965	5.2	2.970	5
214.07	286.85	1010.88	2.838	5.1	2.836*	-1*
200.29	274.50	1035.78	2.650	5.0	2.654	4
185.82	254.02	1037.13	2.449	5.0	2.448	-1
171.85	233.02	1040.45	2.239	4.9	2.237	-3
154.32	204.75	1043.47	1.962	4.9	1.962	0
140.62	183.02	1047.18	1.748	4.8	1.745	-3
125.54	157.47	1049.70	1.500	4.8	1.504	-4
105.43	125.72	1052.67	1.194	4.8	1.193	-1
94.58	108.68	1054.57	1.031	4.8	1.027	-4
83.18	89.75	1055.22	0.851	4.8	0.853	2

* Denotes average values at common boundary point of two ranges.

TABLE A 5.12--Cont.

APPROXIMATING POLYNOMIALS, R^{11} AND THE R.M.S. DEVIATION, S, IN R^{11}, BOTH IN UNITS OF $10^{-3}\ \Omega$ AND T IN UNITS OF DEG. K:

1. $214.1 \leq T \leq 300.0\ ^\circ K$

$$R^{11} = -9.2639\ (10^{-3}) + 1.29077\ (10^{-4})\ T - 4.6796\ (10^{-7})\ T^2 + 6.0282\ (10^{-10})\ T^3$$

$$S = 3.2\ (10^{-3})$$

2. $80.0 \leq T \leq 214.1\ ^\circ K$

$$R^{11} = -4.0476\ (10^{-4}) + 1.6454\ (10^{-5})\ T - 3.6518\ (10^{-8})\ T^2 + 3.1385\ (10^{-10})\ T^3 - 8.0345\ (10^{-13})\ T^4$$

$$S = 2.7\ (10^{-3})$$

TABLE A 5.13

SAMPLE R-8-Au: SAMPLE RESISTANCE AS A FUNCTION OF TEMPERATURE. DATA WERE TAKEN DURING DESCENT FROM ROOM TEMPERATURE.

T (Deg. K)	V^{11} (μv)	V_s (μv)	R^{11} exp. (10^{-3} Ω)	ΔR^{11} exp. (10^{-6} Ω)	R^{11} calc. (10^{-3} Ω)	Residual (10^{-6} Ω)
297.33	218.76	1497.76	1.461	3.3	1.461	0
272.87	207.50	1539.68	1.347	3.3	1.348	1
259.97	199.28	1542.72	1.291	3.3	1.290	1
247.14	190.70	1547.60	1.232	3.2	1.232	0
233.60	181.62	1553.96	1.169	3.2	1.170	1
227.85	177.32	1553.86	1.141	3.2	1.144	3
219.33	173.34	1563.84	1.108	3.2	1.107*	-1*
207.14	170.46	1627.42	1.047	3.1	1.047	0
197.39	163.42	1631.72	1.001	3.1	1.002	1
183.39	153.80	1638.34	0.938	3.1	0.938	0
165.42	141.36	1649.72	0.857	3.1	0.857	0
142.52	124.30	1662.80	0.748	3.0	0.749	1
133.47	117.26	1663.74	0.705	3.0	0.705	0
119.28	106.82	1676.40	0.637	3.0	0.636	-1
105.25	95.58	1674.42	0.571	3.0	0.574	3
99.73	90.06	1681.02	0.536	3.0	0.540	4
94.64	85.84	1684.92	0.509	3.0	0.508	-1

* Denotes average values at common boundary points of two ranges.

TABLE A 5.13--Cont.

APPROXIMATING POLYNOMIALS, R^{11} AND THE R.M.S. DEVIATION, S, IN R^{11}, BOTH IN UNITS OF 10^{-3} Ω AND T IN UNITS OF DEG. K:

1. $219.3 \leq T \leq 300.0$ °K

$$R^{11} = 1.0755\ (10^{-4}) + 4.5491\ (10^{-6})\ T$$

$$S = 1.7\ (10^{-3})$$

2. $80.0 \leq T \leq 219.3$ °K

$$R^{11} = 8.4066\ (10^{-4}) - 1.6163\ (10^{-5})\ T + 2.0804\ (10^{-7})\ T^2 - 8.9735\ (10^{-10})\ T^3 + 1.4144\ (10^{-12})\ T^4$$

$$S = 0.3\ (10^{-3})$$

APPENDIX 6

CALCULATED VALUES OF ρ^{11} FOR EACH ZERO-MAGNETIC-FIELD RESISTIVITY SAMPLE

The values of ρ^{11} for each sample were calculated by use of the approximating polynomials generated from the resistance data. At the end of each table, upper and lower limiting values (values at 300° and 80°K) of the uncertainty in the values of ρ^{11} are presented. These uncertainties were calculated from values of ΔR^{11}, the experimental uncertainties in R^{11} and errors in the measurement of the area and gauge length of each sample using the theory of the propogation of errors.

TABLE A 6.1

CALCULATED VALUES OF ρ^{11} FOR EACH SAMPLE OF THE SERIES CONTAINING EXCESS Te

T (deg. K)	ρ^{11} ($10^{-4}\ \Omega \cdot$ cm)				
	R-1-Te	R-2-Te	R-3-Te	R-4-Te	R-5-Te
300	2.419	2.638	2.395	1.092	1.746
296	2.392	2.606	2.361	1.077	1.726
292	2.364	2.574	2.329	1.062	1.706
288	2.335	2.542	2.298	1.048	1.686
284	2.306	2.509	2.269	1.034	1.665
280	2.275	2.474	2.241	1.020	1.645
276	2.245	2.441	2.213	1.007	1.624
272	2.214	2.406	2.187	0.994	1.602
268	2.183	2.372	2.161	0.981	1.581
264	2.151	2.337	2.135	0.968	1.560
260	2.119	2.302	2.110	0.955	1.539
256	2.088	2.267	2.085	0.943	1.519
252	2.056	2.232	2.059	0.931	1.498
248	2.025	2.196	2.033	0.918	1.478
244	1.993	2.161	2.007	0.906	1.459
240	1.962	2.127	1.981	0.893	1.439
236	1.931	2.092	1.953	0.882	1.421
232	1.901	2.058	1.925	0.869	1.403
228	1.871	2.024	1.896	0.857	1.385
224	1.844	1.989	1.869	0.845	1.369
220	1.820	1.956	1.842	0.832	1.356
216	1.800	1.923	1.814	0.819	1.344
212	1.778	1.889	1.785	0.807	1.328
208	1.747	1.856	1.756	0.794	1.309
204	1.715	1.823	1.726	0.782	1.289
200	1.683	1.789	1.695	0.769	1.271

TABLE A 6.1--Cont.

T (deg. K)	ρ_{11} (10^{-4} Ω · cm)				
	R-1-Te	R-2-Te	R-3-Te	R-4-Te	R-5-Te
196	1.651	1.757	1.664	0.756	1.253
192	1.618	1.723	1.632	0.742	1.235
188	1.585	1.691	1.600	0.729	1.217
184	1.552	1.657	1.567	0.716	1.199
180	1.518	1.624	1.534	0.702	1.181
176	1.484	1.592	1.500	0.688	1.162
172	1.450	1.559	1.466	0.674	1.142
168	1.415	1.526	1.431	0.660	1.122
164	1.380	1.493	1.396	0.646	1.102
160	1.344	1.461	1.361	0.632	1.080
156	1.308	1.428	1.325	0.618	1.056
152	1.272	1.395	1.288	0.603	1.034
148	1.235	1.363	1.251	0.588	1.010
144	1.197	1.330	1.215	0.574	0.985
140	1.159	1.297	1.177	0.558	0.959
136	1.121	1.265	1.139	0.543	0.933
132	1.082	1.228	1.101	0.528	0.905
128	1.043	1.187	1.063	0.513	0.876
124	1.003	1.144	1.024	0.497	0.849
120	0.963	1.102	0.985	0.482	0.820
116	0.922	1.058	0.947	0.466	0.791
112	0.880	1.014	0.908	0.450	0.761
108	0.838	0.970	0.868	0.434	0.730
104	0.795	0.925	0.828	0.418	0.698
100	0.752	0.880	0.789	0.402	0.666
96	0.708	0.835	0.749	0.385	0.634
92	0.663	0.789	0.709	0.369	0.601
88	0.618	0.744	0.668	0.352	0.569

TABLE A 6.1--Cont.

T (deg. K)	ρ_{11} (10^{-4} Ω · cm)				
	R-1-Te	R-2-Te	R-3-Te	R-4-Te	R-5-Te
84	0.572	0.698	0.629	0.335	0.536
80	0.526	0.653	0.588	0.318	0.504
CALCULATED UNCERTAINTIES, ^{11}, IN THE ^{11}					
T (deg. K)	ρ_{11} (10^{-6} Ω · cm)				
	R-1-Te	R-2-Te	R-3-Te	R-4-Te	R-5-Te
300	1.57	1.8	1.2	0.45	1.1
80	0.50	0.55	0.45	0.35	0.46

TABLE A 6.2

CALCULATED VALUES OF ρ_{11} FOR EACH SAMPLE OF THE SERIES CONTAINING EXCESS Au

T (Deg. K)	ρ_{11} (10^{-4} Ω · cm)							
	R-1-Au	R-2-Au	R-3-Au	R-4-Au	R-5-Au	R-6-Au	R-7-Au	R-8-Au
300	2.716	2.683	2.567	2.650	2.562	2.581	2.518	1.289
296	2.693	2.648	2.539	2.620	2.530	2.543	2.488	1.273
292	2.669	2.613	2.511	2.591	2.498	2.508	2.460	1.257
288	2.643	2.578	2.484	2.561	2.467	2.476	2.433	1.241
284	2.615	2.543	2.457	2.530	2.437	2.447	2.407	1.225
280	2.587	2.508	2.431	2.499	2.408	2.420	2.382	1.209
276	2.557	2.474	2.405	2.469	2.379	2.395	2.358	1.194
272	2.526	2.440	2.379	2.439	2.349	2.371	2.334	1.177
268	2.495	2.406	2.355	2.407	2.321	2.348	2.312	1.162
264	2.463	2.373	2.329	2.376	2.293	2.326	2.289	1.146
260	2.431	2.339	2.305	2.345	2.264	2.305	2.267	1.129
256	2.398	2.307	2.280	2.313	2.237	2.284	2.245	1.114
252	2.366	2.274	2.255	2.281	2.209	2.263	2.222	1.098
248	2.334	2.242	2.231	2.249	2.181	2.242	2.199	1.082
244	2.302	2.209	2.206	2.217	2.153	2.219	2.177	1.066
240	2.270	2.175	2.181	2.185	2.125	2.196	2.153	1.050
236	2.239	2.146	2.155	2.152	2.096	2.172	2.128	1.034
232	2.209	2.122	2.129	2.119	2.067	2.146	2.103	1.018
228	2.180	2.100	2.104	2.085	2.042	2.119	2.077	1.002
224	2.130	2.083	2.078	2.053	2.014	2.089	2.049	0.986
220	2.095	2.068	2.052	2.019	1.985	2.057	2.020	0.970
216	2.053	2.046	2.025	1.986	1.955	2.028	1.989	0.955
212	2.013	2.008	1.999	1.951	1.923	1.986	1.955	0.938
208	1.973	1.972	1.974	1.914	1.889	1.948	1.919	0.921
204	1.935	1.936	1.947	1.877	1.856	1.909	1.883	0.904
200	1.897	1.899	1.916	1.841	1.821	1.871	1.845	0.888

TABLE A 6.2--Cont.

T (Deg. K)	ρ_{11} (10^{-4} Ω · cm)							
	R-1-Au	R-2-Au	R-3-Au	R-4-Au	R-5-Au	R-6-Au	R-7-Au	R-8-Au
196	1.859	1.863	1.884	1.805	1.784	1.831	1.806	0.872
192	1.823	1.826	1.849	1.768	1.747	1.791	1.766	0.856
188	1.785	1.788	1.813	1.732	1.709	1.751	1.726	0.840
184	1.748	1.747	1.775	1.695	1.671	1.709	1.685	0.824
180	1.709	1.706	1.736	1.659	1.631	1.668	1.643	0.808
176	1.671	1.663	1.695	1.623	1.591	1.626	1.600	0.793
172	1.632	1.617	1.653	1.586	1.550	1.584	1.558	0.777
168	1.591	1.570	1.611	1.548	1.509	1.542	1.515	0.761
164	1.550	1.524	1.568	1.511	1.467	1.498	1.472	0.745
160	1.509	1.478	1.524	1.473	1.425	1.456	1.428	0.728
156	1.466	1.433	1.481	1.434	1.382	1.413	1.384	0.712
152	1.422	1.388	1.437	1.395	1.339	1.369	1.340	0.695
148	1.377	1.344	1.393	1.355	1.295	1.325	1.296	0.678
144	1.332	1.301	1.349	1.315	1.252	1.281	1.252	0.662
140	1.285	1.257	1.307	1.275	1.208	1.237	1.208	0.645
136	1.239	1.214	1.265	1.233	1.164	1.193	1.164	0.628
132	1.191	1.171	1.225	1.192	1.120	1.149	1.120	0.611
128	1.144	1.128	1.181	1.150	1.076	1.105	1.076	0.594
124	1.096	1.084	1.135	1.107	1.032	1.061	1.032	0.577
120	1.048	1.041	1.089	1.064	0.988	1.017	0.988	0.559
116	1.000	0.997	1.043	1.021	0.944	0.973	0.944	0.543
112	0.954	0.952	0.997	0.977	0.900	0.929	0.900	0.527
108	0.908	0.907	0.951	0.934	0.856	0.885	0.858	0.511
104	0.863	0.861	0.904	0.889	0.813	0.841	0.815	0.496
100	0.820	0.814	0.857	0.845	0.769	0.797	0.772	0.480
96	0.778	0.766	0.811	0.801	0.726	0.754	0.729	0.466
92	0.739	0.717	0.763	0.757	0.683	0.711	0.687	0.453
88	0.702	0.667	0.716	0.712	0.641	0.668	0.646	0.440

TABLE A 6.2--Cont.

T (Deg. K)	ρ_{11} (10^{-4} Ω · cm)							
	R-1-Au	R-2-Au	R-3-Au	R-4-Au	R-5-Au	R-6-Au	R-7-Au	R-8-Au
84	0.669	0.616	0.669	0.668	0.598	0.626	0.602	0.424
80	0.639	0.563	0.622	0.625	0.557	0.584	0.561	0.408
CALCULATED UNCERTAINTIES, ^{11}, IN THE ^{11}								
T (Deg. K)	ρ_{11} (10^{-6} Ω · cm)							
	R-1-Au	R-2-Au	R-3-Au	R-4-Au	R-5-Au	R-6-Au	R-7-Au	R-8-Au
300	1.4	1.6	1.9	1.2	1.4	2.1	1.1	0.49
80	0.47	0.43	0.63	0.29	0.41	0.55	0.35	0.29

APPENDIX 7

THE HALL EFFECT DATA

Data for samples containing excess Te and for the samples containing excess Au comprise two groups of tables. Tables A 7.1 through A 7.7 and Tables A 7.8 through A 7.15 present data for Te-excess and Au-excess samples, respectively.

Values of $< V_a^{21} >/I$ derived from the experimentally determined Hall voltages at corresponding values of B are given for each sample. The constants in the linear function of best fit,

$$< V_a^{21} >/I = A + R_a^{21} B,$$

and the r.m.s. deviation in $< V_a^{21} >/I$ are given. Also presented are values of $< V_a^{21} >/I$ calculated with the linear function and the associated residuals.

TABLE A 7.1

SAMPLE H-1-Te: HALL EFFECT DATA AND APPROXIMATING LINEAR FUNCTION

$< V_a^{21} >/I$, exp. ($\mu\Omega$)	$< V_a^{21} >/I$, calc. ($\mu\Omega$)	Residual ($\mu\Omega$)	B (kilogauss)
-7.624	-7.681	-0.056	12.159
-7.237	-7.166	0.071	11.298
-6.497	-6.508	-0.011	10.199
-6.039	-6.061	-0.021	9.453
-5.633	-5.541	0.091	8.583
-4.788	-4.806	-0.018	7.355
-4.271	-4.282	-0.011	6.480
-3.703	-3.749	-0.046	5.589
-3.102	-3.172	-0.070	4.626
-2.615	-2.614	0.001	3.694
-2.167	-2.096	0.072	2.827

TABLE A 7.1--Cont.

APPROXIMATING LINEAR FUNCTION $\langle V_a^{21} \rangle / I = A + R_a^{21} B$ AND R.M.S. DEVIATION, S, OF THE EXPERIMENTAL $\langle V_a^{21} \rangle / I$

$A = -0.4037 \pm 0.047$ ($\mu\Omega$)

$R_a^{21} = -0.5985 \pm 0.006$ ($\mu\Omega$/kilogauss)

$S = \pm 0.052$ ($\mu\Omega$)

TABLE A 7.2

SAMPLE H-2-Te: HALL EFFECT DATA AND APPROXIMATING LINEAR FUNCTION

$> V_a^{21} >/I$, exp. ($\mu\ \Omega$)	$< V_a^{21} >/I$, calc. ($\mu\ \Omega$)	Residual ($\mu\ \Omega$)	B (kilogauss)
-4.773	-4.744	0.029	12.780
-4.414	-4.413	0.001	11.868
-4.255	-4.191	0.064	11.253
-3.907	-3.926	-0.019	10.525
-3.499	-3.500	-0.001	9.353
-3.112	-3.098	0.014	8.244
-2.599	-2.681	-0.081	7.094
-2.312	-2.397	-0.085	6.309
-1.531	-1.589	-0.058	4.083
-1.143	-1.008	0.135	2.481

TABLE A 7.2--Cont.

APPROXIMATING LINEAR FUNCTION $\langle V_a^{21} \rangle / I = A + R_a^{21} B$ AND R.M.S. DEVIATION, S, OF THE EXPERIMENTAL $\langle V_a^{21} \rangle / I$

$A = -0.107 \pm 0.063$ ($\mu\Omega$)

$R_a^{21} = -0.3630 \pm 0.007$ ($\mu\Omega$/kilogauss)

$S = \pm 0.064$ ($\mu\Omega$)

TABLE A 7.3

SAMPLE H-3-Te: HALL EFFECT DATA AND APPROXIMATING LINEAR FUNCTION

$< V_a^{21} >/I$, exp. ($\mu\Omega$)	$< V_a^{21} >/I$, calc. ($\mu\Omega$)	Residual ($\mu\Omega$)	B (kilogauss)
-9.623	-9.631	-0.008	12.389
-8.980	-8.939	0.041	11.468
-8.229	-8.230	-0.001	10.524
-7.389	-7.425	-0.036	9.452
-6.679	-6.620	0.058	8.380
-5.859	-5.889	-0.030	7.407
-5.283	-5.322	-0.039	6.650
-4.715	-4.732	-0.017	5.866
-3.434	-3.455	-0.021	4.165
-2.594	-2.541	0.053	2.947

TABLE A 7.3--Cont.

APPROXIMATING LINEAR FUNCTION $\langle V_a^{21} \rangle / I = A + R_a^{21} B$ AND R.M.S. DEVIATION, S, OF THE EXPERIMENTAL $\langle V_a^{21} \rangle / I$

$A = -0.3281 \pm 0.036$ ($\mu\Omega$)

$R_a^{21} = -0.7509 \pm 0.004$ ($\mu\Omega$/kilogauss)

$S = \pm 0.035$ ($\mu\Omega$)

TABLE A 7.4

SAMPLE H-4-Te: HALL EFFECT DATA AND APPROXIMATING LINEAR FUNCTION

$< V_a^{21} >/I$, exp. ($\mu\ \Omega$)	$< V_a^{21} >/I$, calc. ($\mu\ \Omega$)	Residual ($\mu\ \Omega$)	B (kilogauss)
-8.803	-8.907	-0.104	12.391
-7.923	-7.808	0.115	10.844
-7.267	-7.189	0.078	9.972
-6.427	-6.482	-0.055	8.977
-5.860	-5.756	0.104	7.954
-4.950	-5.036	-0.085	6.939
-4.329	-4.358	-0.029	5.984
-3.628	-3.729	-0.101	5.099
-2.699	-2.703	-0.004	3.654
-2.108	-2.028	0.080	2.702

TABLE A 7.4--Cont.

APPROXIMATING LINEAR FUNCTION $\langle V_a^{21} \rangle / I = A + R_a^{21} B$ AND R.M.S. DEVIATION, S, OF THE EXPERIMENTAL $\langle V_a^{21} \rangle / I$

$A = -0.1089 \pm 0.079$ ($\mu\Omega$)

$R_a^{21} = -0.7099 \pm 0.010$ ($\mu\Omega$/kilogauss)

$S = \pm 0.083$ ($\mu\Omega$)

TABLE A 7.5

SAMPLE H-5-Te: HALL EFFECT DATA AND APPROXIMATING LINEAR FUNCTION

$< V_a^{21} >/I$, exp. ($\mu\Omega$)	$< V_a^{21} >/I$, calc. ($\mu\Omega$)	Residual ($\mu\Omega$)	B (kilogauss)
-6.147	-6.278	-0.131	12.405
-5.554	-5.564	-0.010	10.979
-5.096	-5.040	0.056	9.935
-4.624	-4.510	0.114	8.876
-4.053	-4.018	0.034	7.895
-3.649	-3.523	0.125	6.907
-2.890	-2.999	-0.109	5.862
-2.476	-2.516	-0.040	4.896
-1.970	-1.997	-0.027	3.863
-1.517	-1.531	0.014	2.931

TABLE A 7.5--Cont.

APPROXIMATING LINEAR FUNCTION $\langle V_a^{21} \rangle / I = A + R_a^{21} B$ AND R.M.S. DEVIATION, S, OF THE EXPERIMENTAL $\langle V_a^{21} \rangle / I$

$A = -0.0618 \pm 0.077$ ($\mu\Omega$)

$R_a^{21} = -0.5011 \pm 0.010$ ($\mu\Omega$/kilogauss)

$S = \pm 0.081$ ($\mu\Omega$)

TABLE A 7.6

SAMPLE H-6-Te: HALL EFFECT DATA AND APPROXIMATING LINEAR FUNCTION

$< V_a^{21} >/I$, exp. ($\mu\ \Omega$)	$< V_a^{21} >/I$, calc. ($\mu\ \Omega$)	Residual ($\mu\ \Omega$)	B (kilogauss)
-7.356	-7.240	0.116	12.130
-6.652	-6.718	-0.066	11.231
-5.642	-5.682	-0.040	9.445
-4.886	-4.882	0.004	8.068
-4.343	-4.325	0.018	7.109
-3.816	-3.797	0.019	6.201
-3.233	-3.413	-0.180	5.539
-2.562	-2.489	0.073	3.946
-1.810	-1.752	0.058	2.677
-1.116	-1.110	0.006	1.581

TABLE A 7.6--Cont.

APPROXIMATING LINEAR FUNCTION $\langle V_a^{21} \rangle / I = A + R_a^{21} B$ AND R.M.S. DEVIATION, S, OF THE EXPERIMENTAL $\langle V_a^{21} \rangle / I$

$A = -0.1985 \pm 0.082$ ($\mu\Omega$)

$R_a^{21} = -0.5805 \pm 0.010$ ($\mu\Omega$/kilogauss)

$S = \pm 0.083$ ($\mu\Omega$)

TABLE A 7.7

SAMPLE H-7-Te: HALL EFFECT DATA AND APPROXIMATING LINEAR FUNCTION

$< V_a^{21} >/I$, exp. ($\mu\Omega$)	$< V_a^{21} >/I$, calc. ($\mu\Omega$)	Residual ($\mu\Omega$)	B (kilogauss)
- 9.982	-10.069	-0.087	12.075
-10.013	-10.126	0.113	12.010
- 9.359	- 9.405	-0.046	11.308
- 8.821	- 8.937	-0.106	10.769
8.482	- 8.472	-0.100	10.232
- 7.738	- 7.838	-0.100	9.154
- 5.014	- 5.025	-0.011	6.254
- 4.079	- 4.024	0.055	5.098
- 3.164	- 3.131	0.033	4.067
- 1.949	- 2.062	-0.113	2.834

TABLE A 7.7--Cont.

APPROXIMATING LINEAR FUNCTION $\langle V_a^{21} \rangle / I = A + R_a^{21} B$ AND R.M.S. DEVIATION, S, OF THE EXPERIMENTAL $\langle V_a^{21} \rangle / I$

$A = 0.3929 \pm 0.121$ ($\mu\Omega$)

$R_a^{21} = -0.8664 \pm 0.014$ ($\mu\Omega$/kilogauss)

$S = \pm 0.101$ ($\mu\Omega$)

TABLE A 7.8

SAMPLE H-1-Au: HALL EFFECT DATA AND APPROXIMATING LINEAR FUNCTION

$< V_a^{21} >/I$, exp. ($\mu\Omega$)	$< V_a^{21} >/I$, calc. ($\mu\Omega$)	Residual ($\mu\Omega$)	B (kilogauss)
-10.595	-10.707	-0.112	13.125
- 9.920	9.968	-0.048	12.263
- 9.099	- 9.057	0.041	11.202
- 8.076	- 8.028	0.048	10.001
- 7.061	- 7.017	0.044	8.823
- 6.253	- 6.220	0.033	7.892
- 5.251	- 5.219	0.032	6.725
- 4.632	- 4.564	0.067	5.963
- 3.838	- 3.832	0.006	5.108
- 2.802	- 2.703	0.099	3.792
- 2.328	- 2.247	0.081	3.261
- 1.855	- 1.923	-0.067	2.882
- 0.880	- 0.912	-0.032	1.703
- 0.300	- 0.292	0.008	0.980

TABLE A 7.8--Cont.

APPROXIMATING LINEAR FUNCTION $\langle V_a^{21} \rangle / I = A + R_a^{21} B$ AND R.M.S. DEVIATION, S, OF THE EXPERIMENTAL $\langle V_a^{21} \rangle / I$

$A = 0.5484 \pm 0.045$ ($\mu\Omega$)

$R_a^{21} = -0.8576 \pm 0.006$ ($\mu\Omega$/kilogauss)

$S = \pm 0.078$ ($\mu\Omega$)

TABLE A 7.9

SAMPLE H-2-Au: HALL EFFECT DATA AND APPROXIMATING LINEAR FUNCTION

$< V_a^{21} >/I$, exp. ($\mu\Omega$)	$< V_a^{21} >/I$, calc. ($\mu\Omega$)	Residual ($\mu\Omega$)	B (kilogauss)
-4.585	-4.578	0.006	13.126
-4.262	-4.313	-0.052	12.410
-3.840	-3.868	-0.028	11.209
-3.581	-3.565	0.016	10.390
-3.247	-3.201	0.046	9.406
-2.931	-2.897	-0.032	8.588
-2.442	-2.413	0.028	7.280
-2.022	-2.004	0.017	6.175
-1.456	-1.487	-0.032	4.780
-1.009	-1.067	-0.058	3.647
-0.350	-0.328	0.022	1.650

TABLE A 7.9--Cont.

APPROXIMATING LINEAR FUNCTION $< V_a^{21} >/I = A + R_a^{21} B$ AND R.M.S. DEVIATION, S, OF THE EXPERIMENTAL $< V_a^{21} >/I$

$A = 0.2830 \pm 0.029$ ($\mu\Omega$)

$R_a^{21} = -0.3700 \pm 0.003$ ($\mu\Omega$/kilogauss)

$S = \pm 0.036$ ($\mu\Omega$)

TABLE A 7.10

SAMPLE H-3-Au: HALL EFFECT DATA AND APPROXIMATING LINEAR FUNCTION

$< V_a^{21} >/I$, exp. ($\mu\Omega$)	$< V_a^{21} >/I$, calc. ($\mu\Omega$)	Residual ($\mu\Omega$)	B (kilogauss)
-9.567	-9.791	-0.224	13.440
-8.853	-8.800	0.052	12.108
-7.934	-7.833	0.101	10.805
-7.174	-7.171	0.073	9.821
-6.490	-6.396	0.094	8.871
-5.634	-5.606	0.028	7.807
-4.836	-4.822	0.013	6.753
-4.226	-4.300	-0.074	6.050
-3.150	-3.186	-0.036	4.550
-1.312	-1.376	-0.065	2.114

TABLE A 7.10--Cont.

APPROXIMATING LINEAR FUNCTION $\langle V_a^{21} \rangle / I = A + R_a^{21} B$ AND R.M.S. DEVIATION, S, OF THE EXPERIMENTAL $\langle V_a^{21} \rangle / I$

$A = 0.1947 \pm 0.089$ ($\mu\Omega$)

$R_a^{21} = -0.7430 \pm 0.010$ ($\mu\Omega$/kilogauss)

$S = \pm 0.094$ ($\mu\Omega$)

TABLE A 7.11

SAMPLE H-4-Au: HALL EFFECT DATA AND APPROXIMATING LINEAR FUNCTION

$< V_a^{21} >/I$, exp. ($\mu\Omega$)	$< V_a^{21} >/I$, calc. ($\mu\Omega$)	Residual ($\mu\Omega$)	B (kilogauss)
-15.109	-15.136	-0.028	13.011
-14.179	-14.269	-0.089	12.289
-13.069	-13.056	0.013	11.279
-12.435	-12.434	0.001	10.763
-11.436	-11.372	0.063	9.879
-11.009	-10.902	0.018	9.488
-10.061	- 9.967	0.093	8.710
- 8.816	- 8.843	-0.027	7.775
- 7.339	- 7.461	-0.122	6.625
- 6.787	- 6.834	-0.047	6.103
- 4.689	- 4.654	0.035	4.288

TABLE A 7.11--Cont.

APPROXIMATING LINEAR FUNCTION $\langle V_a^{21} \rangle / I = A + R_a^{21} B$ AND R.M.S. DEVIATION, S, OF THE EXPERIMENTAL $\langle V_a^{21} \rangle / I$

$A = 0.4992 \pm 0.084$ ($\mu\Omega$)

$R_a^{21} = -1.207 \pm 0.009$ ($\mu\Omega$/kilogauss)

$S = \pm 0.069$ ($\mu\Omega$)

TABLE A 7.12

SAMPLE H-5-Au: HALL EFFECT DATA AND APPROXIMATING LINEAR FUNCTION

$< V_a^{21} >/I$, exp. ($\mu\Omega$)	$< V_a^{21} >/I$, calc. ($\mu\Omega$)	Residual ($\mu\Omega$)	B (kilogauss)
-21.083	-21.225	-0.142	13.124
-20.120	-20.174	-0.054	12.498
-18.641	-18.617	0.024	11.570
-17.943	-18.018	0.075	11.169
-16.852	-16.863	-0.011	10.526
-15.402	-15.321	0.082	9.607
-13.937	-13.881	0.055	8.750
-12.362	-12.199	0.162	7.748
- 9.389	- 9.413	-0.023	6.089
- 7.224	- 7.365	-0.140	4.868
- 5.432	- 5.504	-0.072	3.760
- 3.725	- 3.680	0.045	2.674

TABLE A 7.12--Cont.

APPROXIMATING LINEAR FUNCTION $\langle V_a^{21} \rangle / I = A + R_a^{21} B$ AND R.M.S. DEVIATION, S, OF THE EXPERIMENTAL $\langle V_a^{21} \rangle / I$

$A = 0.6521 \pm 0.076$ ($\mu\Omega$)

$R_a^{21} = -1.679 \pm 0.008$ ($\mu\Omega$/kilogauss)

$S = \pm 0.088$ ($\mu\Omega$)

TABLE A 7.13

SAMPLE H-6-Au: HALL EFFECT DATA AND APPROXIMATING LINEAR FUNCTION

$< V_a^{21} >/I$, exp. ($\mu\Omega$)	$< V_a^{21} >/I$, calc. ($\mu\Omega$)	Residual ($\mu\Omega$)	B (kilogauss)
-4.423	-4.418	0.005	12.959
-4.230	-4.154	0.076	12.195
-4.025	-3.986	0.038	11.712
-3.947	-3.924	0.023	11.532
-3.708	-3.858	-0.150	11.342
-3.767	-3.635	0.131	10.700
-3.230	-3.385	-0.123	9.899
-3.205	-3.327	-0.122	9.812
-3.057	-3.012	0.044	8.904
-2.729	-2.667	0.061	7.909
-2.366	-2.369	-0.004	7.049
-2.152	-2.097	0.055	6.263
-1.600	-1.662	-0.062	5.010
-1.302	-1.236	0.066	3.781
-0.562	-0.594	-0.032	1.931

TABLE A 7.13--Cont.

APPROXIMATING LINEAR FUNCTION $< V_a^{21} >/I = A + R_a^{21} B$ AND R.M.S. DEVIATION, S, OF THE EXPERIMENTAL $< V_a^{21} >/I$

$A = 0.0749 \pm 0.065$ ($\mu\Omega$)

$R_a^{21} = -0.3467 \pm 0.007$ ($\mu\Omega$/kilogauss)

$S = \pm 0.080$ ($\mu\Omega$)

TABLE A 7.14

SAMPLE H-7-Au: HALL EFFECT DATA AND APPROXIMATING LINEAR FUNCTION

$< V_a^{21} >/I$, exp. ($\mu\Omega$)	$< V_a^{21} >/I$, calc. ($\mu\Omega$)	Residual ($\mu\Omega$)	B (kilogauss)
-8.885	-8.729	0.156	13.012
-8.557	-8.550	-0.007	12.750
-8.248	-8.279	-0.031	12.352
-8.101	-8.207	-0.106	12.247
-7.593	-7.609	-0.016	11.368
-7.264	-7.245	0.019	10.835
-6.274	-6.267	0.007	9.398
-5.489	-5.515	-0.026	8.294
-4.615	-4.646	-0.031	7.017
-4.071	-4.142	-0.071	6.278
-3.416	-3.407	0.009	5.199
-2.426	-2.343	0.083	3.638

TABLE A 7.14--Cont.

APPROXIMATING LINEAR FUNCTION $\langle V_a^{21} \rangle / I = A + R_a^{21} B$ AND R.M.S. DEVIATION, S, OF THE EXPERIMENTAL $\langle V_a^{21} \rangle / I$

$A = 0.1342 \pm 0.066$ ($\mu\Omega$)

$R_a^{21} = -0.6811 \pm 0.007$ ($\mu\Omega$/kilogauss)

$S = \pm 0.065$ ($\mu\Omega$)

TABLE A 7.15

SAMPLE H-8-Au: HALL EFFECT DATA AND APPROXIMATING LINEAR FUNCTION

$< V_a^{21} >/I$, exp. ($\mu\Omega$)	$< V_a^{21} >/I$, calc. ($\mu\Omega$)	Residual ($\mu\Omega$)	B (kilogauss)
-8.724	-8.716	0.008	12.897
-8.486	-8.439	0.046	12.488
-8.004	-8.063	-0.058	11.934
-7.785	-7.646	0.139	11.319
-5.969	-6.029	-0.060	8.935
-5.060	-5.132	-0.072	7.611
-4.379	-4.443	-0.064	6.596
-3.668	-3.659	-0.088	5.439
-2.575	-2.643	-0.067	3.941
-1.914	-1.955	-0.041	2.926
-1.367	-1.205	0.161	1.820

TABLE A 7.15--Cont.

APPROXIMATING LINEAR FUNCTION $\langle V_a^{21} \rangle / I = A + R_a^{21} B$ AND R.M.S. DEVIATION, S, OF THE EXPERIMENTAL $\langle V_a^{21} \rangle / I$

$A = 0.0290 \pm 0.061$ ($\mu\Omega$)

$R_a^{21} = -0.6781 \pm 0.007$ ($\mu\Omega$/kilogauss)

$S = \pm 0.080$ ($\mu\Omega$)

BIBLIOGRAPHY

1. T. C. Harman, private communication.
2. M. M. Judy, M.S. Thesis, Colorado School of Mines, 1964 (unpublished).
3. C. R. Veale and M. F. Barrett, J. Less-Common Metals. 13, 632 (1967).
4. A. C. Beer, Solid State Physics (Academic Press, New York, 1963), Supplement 4, Chap. 1, p. 3.
5. A. C. Beer, ibid, Chap. 1, p. 7.
6. H. B. G. Casimir, Revs. Mod. Phys. 17, 343 (1945).
7. A. C. Beer, ibid, Chap. 3, p. 42.
8. R. R. Birss, Symmetry And Magnetism (North-Holland Publishing Company, Amsterdam, 1964), Chap. 5, p. 226.
9. R. R. Birss, ibid, Chap. 5, p. 227.
10. M. Kohler, Ann. Phys. 20, 879 (1934).
11. J. F. Nye, Physical Properties Of Crystals (Oxford University Press, London, 1957), Chap. 11, p. 195.
12. S. Bhagavantam, Crystal Symmetry And Physical Properties (Academic Press, New York, 1966), Chap. 17, p. 201.
13. H. J. Juretschke, Acta Cryst. 8, 716 (1955).
14. F. G. Fumi, Acta Cryst. 5, 44 (1952).
15. R. R. Birss, ibid, Chap. 2, p. 54.
16. S. Bhagavantam, ibid, Chap. 6, p. 72.
17. R. R. Birss, ibid, Chap. 2, p. 45.
18. R. R. Birss, ibid, Chap. 2, p. 46.
19. R. R. Birss, ibid, Chap. 2, p. 47.
20. R. R. Birss, ibid, Chap. 2, p. 48.

21. A. C. Beer, ibid, Chap. 4, p. 84.

22. M. C. Sneed, J. L. Maynard, R. C. Brasted, Comprehensive Inorganic Chemistry (D. Van Nostrand Company, Inc., New York, 1954), Vol. II, Chap. 3, p. 235.

23. M. Hansen and K. Anderko, Constitution Of Binary Alloys (McGraw-Hill Book Company, Inc., 1958), p. 234.

24. W. D. Lawson and S. Nielsen, Preparation Of Single Crystals (Butterworths Scientific Publications, London, 1958), Chap. 7, p. 127.

25. L. Berry and R. Thompson, X-ray Powder Data For Ore Minerals: The Peacock Atlas (Geological Society of America Memoir 85, 1962), p. 112.

26. W. D. Lawson and S. Nielsen, ibid, Chap. 1, p. 14.

27. W. D. Lawson and S. Nielsen, ibid, Chap. 7, p. 146.

28. R. D. Forest, R. J. Barton, N. C. Schieltz, Advances In X-Ray Analysis (Plenum Press, New York, 1965), Vol. IX, p. 51.

29. Y. S. Touloukian, Editor, Thermophysical Properties Of High Temperature Solid Materials (The Macmillan Company, New York, 1967), Vol. 6, Part 2, p. 986.

30. R. W. Ure, Jr., Rev. Sci. Instr., 28, 836 (1957).

31. R. L. Powell, M. D. Bunch, R. J. Corruccini, Cryogenics, 1, 1 (1961).

32. J. Yahia and J. A. Marcus, Phys. Rev. 113, 137 (1959).

33. W. F. Flanagan, P. A. Flinn, and B. L. Averbach, Rev. Sci. Instr., 25, 593 (1954); 26, 233 (1955).

34. J. K. Logan and J. A. Marcus, Phys. Rev. 88, 1234 (1952).

35. D. C. Baird, Experimentation: An Introduction To Measurement Theory And Experiment Design (Prentice-Hall, Inc., Englewood Cliffs, New Jersey, 1962), Chap. 6, p. 138.

36. J. F. Nye, ibid, Chap. 9, p. 158.

37. B. M. Shchigolev, Mathematical Analysis Of Observations (American Elsevier Publishing Company, Inc., New York, 1965), Chap. 16, p. 236.

38. B. M. Shchigolev, ibid, Chap. 16, p. 260.

39. A. C. Beers, ibid, Chap. 3, p. 76.

40. R. N. Tauber, A. A. Machonis, and I. B. Cadoff, J. Appl. Phys. 37, 4855 (1966).

41. R. N. Tauber and I. B. Cadoff, J. Appl. Phys. 38, 3714 (1967).

42. B. Abeles and S. Meiboom, Phys. Rev. 101, 544 (1956).

43. E. S. Fisher and H. J. McSkimin, Phys. Rev. 124, 67 (1961).

44. C. S. Barrett, M. H. Mueller, and R. L. Hitterman, Phys. Rev. 129, 625 (1963).

45. E. S. Fisher and D. Dever, Phys. Rev. 170, 607 (1968).

46. K. Andres, Phys. Rev. 170, 614 (1968).

47. J. R. Sybert, H. J. MacKey, and K. L. Hathcox, Phys. Rev. 166, 710 (1968).

48. B. J. Vaughn, M.S. Thesis, North Texas State University, 1967 (unpublished).

49. G. Tunell and C. J. Ksanda, J. Wash. Acad. Sci. 25, 32 (1935); 26, 509 (1936).